Water Vapor and Heat Exchange over Lakes

THÈSE N^{O} 4952 (2011)

PRÉSENTÉE LE 18 MARS 2011

À LA FACULTÉ ENVIRONNEMENT NATUREL, ARCHITECTURAL ET CONSTRUIT
LABORATOIRE DE MÉCANIQUE DES FLUIDES DE L'ENVIRONNEMENT
PROGRAMME DOCTORAL EN ENVIRONNEMENT

ÉCOLE POLYTECHNIQUE FÉDÉRALE DE LAUSANNE

POUR L'OBTENTION DU GRADE DE DOCTEUR ÈS SCIENCES

PAR

Nikki VERCAUTEREN

acceptée sur proposition du jury:

Prof. M. Bierlaire, président du jury
Prof. M. Parlange, directeur de thèse
Prof. E. Bou-Zeid, rapporteur
W. H. Brutsaert, rapporteur
Prof. F. Porte Agel, rapporteur

ÉCOLE POLYTECHNIQUE
FÉDÉRALE DE LAUSANNE

Suisse
2011

Résumé

La quantification des interactions entre l'atmosphère et les plans d'eau revêt une importance considérable pour une bonne gestion des ressources en eau, pour les études climatologiques ou encore pour l'étude des échanges entre océan et atmosphère et de la climatologie régionale dans les régions côtières. Les difficultés associées aux campagnes de mesures sur l'eau ont généralement limité l'étude des interactions air-eau. Cette recherche a pour but d'améliorer les paramétrisations physiques des échanges entre un lac et l'atmosphère en intégrant des mesures et des modèles. La campagne de terrain LATEX (sur les échanges turbulents entre un lac et l'atmosphère) est analysée dans le but d'adresser les questions relatives aux interactions air-eau sur le lac Léman. Des simulations des grandes échelles sont employées pour l'étude des flux de chaleurs sensible et latente au-dessus de surfaces humides hétérogènes.

Nous présentons les paramètres d'importance tels que le budget énergétique à la surface et les longueurs de rugosité au transfert de quantité de mouvement, de chaleur et de vapeur d'eau utilisés dans les modèles atmosphériques basés sur la théorie de Monin-Obukhov. Le stockage d'énergie dans le lac se révèle très important, toutefois l'application de la théorie de conduction de chaleur à des profils de température mesurés à l'aide d'une fibre optique ne permet pas de quantifier ce terme. Les méthodes d'estimation de l'évaporation des surfaces saturées en humidité qui incluent ce terme de stockage sont par conséquent revisitées pour dériver une formulation basée sur le flux de chaleur sensible.

Nous portons ensuite notre attention sur des simulations numériques (des grandes échelles) de l'écoulement au-dessus de surfaces d'eau. Les petites échelles de la turbulence qui ne sont pas résolues par les simulations des grandes échelles sont analysées au-dessus du lac. Les mesures de LATEX permettent pour la première fois l'observation du transport turbulent sous maille de la vapeur d'eau au-dessus d'un lac et celui-ci se révèle bien corrélé avec le transport de chaleur. Les résultats de l'analyse *a priori* des flux et dissipations sous maille sont comparés aux observations conduites au-dessus du sol.

Nous employons le code de simulation des grandes échelles de l'EPFL, avec son modèle sous maille Lagrangien dynamique dépendant des échelles, pour simuler des écoulements au-dessus d'une transition entre un sol sec et une surface humide. Nous étudions la distance requise pour un écoulement et une évaporation en équilibre avec la surface humide et la comparons aux résultats de modèles Lagrangiens simplifiés. Nous évaluons l'impact du fetch limité sur l'applicabilité de la théorie de similitude de Monin-Obukhov.

Mots-clés: Interactions lac atmosphère· Turbulence · Simulation des grandes échelles · Dynamiques sous maille · Tests a priori · Evaporation des surfaces saturées en humidité· Transport de vapeur d'eau

Abstract

Quantifying the interaction of the atmosphere and water surfaces is of great importance for water resources management, climate studies of ocean-atmosphere exchange and regional climate in coastal areas. Atmospheric dynamics over water surfaces have generally received less attention than land-atmosphere interactions due to difficulties in operating field studies. In this research we are trying to improve the physical parameterizations of lake-atmosphere processes by integrating measurements and modeling studies. The Lake-Atmosphere Turbulent EXchanges (LATEX) field measurement campaign is analyzed to understand air-water interactions over Lac Léman (Geneva). Large eddy simulations are used to study sensible and latent heat fluxes over heterogeneous wet surfaces.

We present parameters of interest for land-surface modeling, *i.e.* the surface energy budget and the roughness lengths for momentum, heat and water vapor that are embedded in the Monin-Obukhov similarity theory used in atmospheric models. The storage of energy in the lake is a very important term, yet methods used to quantify it, relying on temperature profile measurements from a fiber optic and the theory of conduction of heat, are not successful. We revisit classical wet surface evaporation estimation methods that include this challenging term and derive an evaporation formulation based on sensible heat flux measurements.

We then focus on numerical (large eddy) simulations of the flow above a water surface. Small-scale turbulence (the so-called subgrid scales, SGS) over the lake that cannot be captured in large eddy simulations is investigated. The measurements of LATEX allowed, for the first time, the study of subgrid-scale turbulent transport of water vapor over a lake, which reveals itself well correlated with the transport of heat. Results from an *a priori* analysis of subgrid-scale fluxes and dissipations indicate that the observed subgrid-scale statistics are very similar to those observed over land surfaces.

We use the EPFL-LES code, with its scale-dependent Lagrangian dynamic SGS model, to simulate flows over transition from dry land to wet surfaces. We observe the fetch requirement for evaporation formulations and compare to results from simplified Lagrangian footprint models. We explore the limits of applicability of Monin-Obukhov similarity theory that are due to the finite fetch.

Keywords: Lake-atmosphere interactions · Turbulence · LES · Subgrid-scale dynamics · A priori testing · Wet-surface evaporation · Water vapor transport

Remerciements

A de nombreuses personnes, je tiens à dire un grand merci.

A mon directeur de thèse Marc Parlange tout d'abord ; ce fût un plaisir d'être accueillie au sein de l'EFLUM et d'avoir l'opportunité de découvrir un sujet nouveau pour moi et qui s'est avéré captivant. J'ai toujours bénéficié de sa confiance et je l'en remercie. Elie Bou-Zeid m'a été d'une aide incroyable, et je le remercie de m'avoir orientée dans cette thèse, et de m'avoir toujours encouragée et transmis son enthousiasme. Travailler à ses côtés a toujours été très motivant, il m'a énormément appris et ce travail a bénéficié d'innombrables discussions fructueuses avec lui. Je remercie également Fernando Porté-Agel d'avoir fait preuve de patience en m'initiant à l'analyse des mesures de turbulence atmosphérique lors de mes études de master. Merci aussi à Wilfried Brutsaert dont le point de vue d'hydrologue fût très appréciable dans ce travail, et qui m'a transmis ses encouragements constants. Hartelijk dank voor uw hulp en vruchtbare discussies. Je tiens à remercier également Michel Bierlaire pour avoir accepté de présider ce jury.

Les membres de l'EFLUM qui ont chacun en leur temps été d'une grande aide sont nombreux, et je tiens à tous les remercier. Plus spécialement, Marie-José Pellaud a toujours apporté son aide logistique sans laquelle l'organisation de cette thèse aurait été plus difficile. Marc Calaf, Martin Froidevaux, Chad Higgins, Thomas Mimouni, Ivan Lunati et Charles Meneveau ont contribué à de nombreuses idées présentes dans ce travail, et Natalie Ceperley et Megan Daniels ont effectué un travail de relecture très apprécié. Merci à Natalie d'avoir toujours été prête à me fournir son aide. Elie Bou-Zeid, Hendrik Huwald, John Selker, Jan Overney, Isabelle Kiener et Ulrich Lemmin ont réalisé l'expérience LATEX sans laquelle ce travail n'aurait pas vu le jour.

Le passage de professeurs invités m'a permis d'avoir de nombreux échanges, et j'aimerais remercier particulièrement Eric Pardyjak et Gaby Katul pour des discussions enrichissantes.

Gilles Steiner et Laura Vinckenbosh m'ont apporté leur aide de mathématiciens quand j'en ai eu besoin et je les remercie.

Je tiens aussi à remercier Jesper Oppelstrup et Elisa Fillon pour leurs discussions qui m'ont intéressée aux sciences de l'atmosphère et orientée vers ce chemin.

Enfin, ma famille et mes amis ont toujours été d'un grand soutien, et Martin a été patient, et je les en remercie.

Some of the work in this thesis has been previously published in scientific journals.

Chapter 3

Vercauteren N, Bou-Zeid E, Huwald H, Parlange MB, Brutsaert W (2009)
Estimation of wet surface evaporation from sensible heat flux measurements.
Water resources research 45. doi:W06424

Chapter 4

Vercauteren N, Bou-Zeid E, Parlange MB, Lemmin U, Huwald H, Selker J, Meneveau C (2008)
Subgrid-scale dynamics of water vapour, heat, and momentum over a lake.
Boundary-Layer Meteorology 128 (2):205-228

Table of contents

1 Introduction

Since the first days of farming and hunting until today, humans have been strongly dependent on weather conditions, which forced them to watch atmospheric phenomena for signs that would help foretell future weather. Among the vagaries of weather, the water cycle has always played a central role for life on earth, and humans have learned to understand it better in order to best use the resources of the environment. Mainly, humans perceive the effects of atmospheric hazards in the lowest layer of the atmosphere, where life takes place: this very thin portion of the atmosphere is the atmospheric boundary layer (ABL). Understanding weather patterns and the part of the water cycle affecting human lives requires a good understanding of the dynamics in this layer.

Written traces of the study of the weather and the water cycle date back to the Babylonians, but Greek natural philosophers of antiquity were the first ones to make regular observations and to develop purposeful meteorological theories. Written around 340 B.C, Aristotle's *Meteorologica* is the oldest comprehensive treatise about the subject of meteorology (see (Aristotle 1952) for an English translation). As no instruments were available at that time, observations were limited to the ABL. By experiencing direct contact with the surface of the earth, the ABL responds to its characteristics. The importance of the interactions between the land surface and the atmosphere for the general circulation was first appreciated in the early 18th century, when Edmund Halley identified solar heating as the driving force bringing air and water vapor to rise at low latitude and sink at high latitudes. The ABL is, by this process, the main source of heat and water vapor for the rest of the atmosphere and impacts larger scale weather patterns. Different surface types react differently to solar heating, and assessing the effect of specificities of the land surface is one of the focuses of research in boundary layer meteorology. Comprehensive histories of atmospheric sciences have been provided by among others Lorenz (1983), Brutsaert (1982), Crutzen and Ramanathan (2000) and Frisinger (1977).

Among the many surface types present on the earth surface, lakes and rivers play an important role. Even though they cover less than 1% of the total water on the planet, the amount and

quality of water in each reservoir, natural or man-made, have a significant impact on the well being of life and ecosystems. Loss of water in the reservoirs occurs through evaporation, which is one of the main phases of the hydrological cycle. In many parts of the world, the available water resources are now being used close to their limits (Gleick and Palaniappan 2010; Palmer and Characklis 2009). It is thus of central importance to have an accurate knowledge of the amount of evaporative consumption of the water for a good management of water resources.

Water present in the atmosphere, in its vapor form, also plays a central role in the global climate. Through the change of phase between liquid (or solid) water and vapor, a large amount of energy is consumed. This energy is the primary means by which solar radiation is transmitted to the atmosphere. Indeed, 80% of the solar radiation is absorbed at the land surface, and most of it is subsequently used to evaporation of water (Budyko 1974; Brutsaert 1982). After travelling in the atmosphere, energy known as latent heat can be released when the water vapor condenses to a liquid form. Extreme precipitation events have been shown to be triggered by a convergence of several widely dispersed moisture sources in some cases (Sodemann et al. 2009); knowing how the moisture sources travel up to the high layers of the atmosphere is an important factor for weather forecasting.

Water vapor is also one of the main greenhouse gases. Therefore, climate predictions need to account for how the water content of the atmosphere is changing (Held and Soden 2000). When the air gets warmer, more water vapor can be stored in it. Because temperature in the lower atmosphere decreases with height, most of the water vapor in the atmosphere is generally contained in the lowest few kilometers, in the ABL. This region, separated from the free atmosphere aloft by a strong temperature inversion that limits mixing and damps turbulence, is of crucial importance to the transport of water vapor and heat and thus, of energy above the earth surface.

A specificity of the ABL is that the flow in it is generally turbulent. Turbulence consists of irregular swirls of motion, called eddies. Eddies of different sizes are superimposed in the atmosphere and are the basis of the mixing of heat, momentum, moisture or contaminants from the ground surface to the free atmosphere. These eddies are governed by two

mechanisms, namely mechanical forcing and buoyancy. Mechanical forcing occurs when the flow encounters obstacles, mainly at the land surface, and that the air parcels are forced around the obstacles. Buoyancy on the other hand, is the effect of warm air parcels that have a lower density than colder surrounding air, and therefore tend to travel upwards. Air parcels in contact with the ground often get warmer during the day due to the solar radiation that is absorbed at the land surface.

For these reasons, the land-atmosphere exchange processes are of crucial importance for the state of the atmosphere and for the hydrologic cycle through evaporation of water. Specifically, in the regional hydrologic cycle, lakes and reservoirs represent an important part of the water budget. Many field experiments in the ABL have focused until now on momentum or heat exchanges above land and some on water vapor exchanges. However, measurements are usually confined to a single point and do not bring spatial information. A way to obtain spatial information is to use numerical simulations of the atmosphere. But because of the turbulent nature of the flow and the size of atmospheric investigations, it is an ongoing challenge to simulate realistic atmospheric flows. Simulations need some of the transport processes to be parameterized in order to make computations feasible. In the so-called large eddy simulations, only the smallest scales of motion are parameterized. This parameterization is still a focus of boundary layer research, and field experiments can be designed to investigate specifically the small turbulent scales. Yet, observations of turbulent fluxes of moisture remain sparse, as do observations over water surfaces.

This thesis will focus on turbulence above lakes and evaporation from wet surfaces. A field campaign over Lac Léman (Lake Geneva) provides observations of turbulent fluxes above the lake and thus of the energy transfer across the lake-atmosphere interface. Hydrologic modeling estimates evaporation from the lake surface, and numerical simulations help us understand the effect of water bodies on the surrounding atmosphere.

1.1 The atmospheric boundary layer (ABL) and land-atmosphere interactions

The atmospheric boundary layer (ABL) is the lowest part of the atmosphere that experiences direct contact with the planetary surface. The thickness of the ABL is usually defined as the portion of the atmosphere where the effects of the surface are felt within a timescale of less than a day (Stull 1988; Garratt 1992). Mixing between the ABL and the free atmosphere above is typically prevented by a strong temperature inversion (Fig. 1). When the airflow passes above the ground, characteristics of the surface are transferred to the atmosphere through turbulent mixing. Without this turbulent process, the transfer of air, heat, water vapor but also pollutants would be minimal, occurring at the molecular scale. The surface also exerts frictional resistance to atmospheric motion and acts as a sink of momentum, slowing down the motions. The turbulence present in the ABL does not only consist of mechanical turbulence, but a large part of it is associated with thermal convection. As such, the amount and characteristics of turbulence vary with the time of day, ranging between a turbulent mixing layer of a few tens of meters in calm nocturnal cooling conditions to several kilometers in highly disturbed weather involving deep convection.

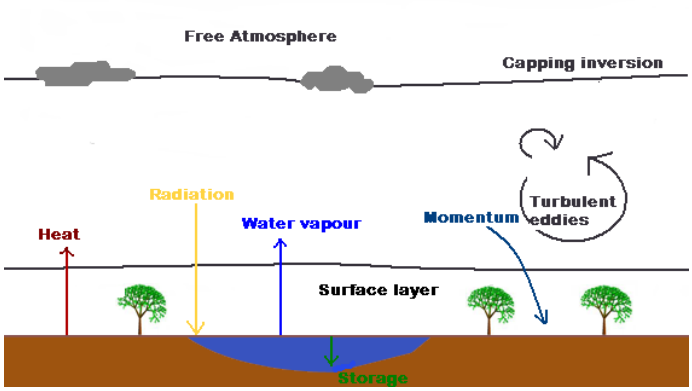

Fig. 1 Schematic view of the atmospheric boundary layer.

Mathematical treatment of fluid flows, including atmospheric flows, is almost always based on the equations of motion. These equations are derived from the fundamental laws of conservation of mass, momentum and energy. Applying Newton's second law of motion in an elemental volume of fluid leads to the Navier-Stokes equation (Pope 2000; Tennekes and

Lumley 1972). As no analytical solutions have been found so far to the complete set of Navier-Stokes equations for viscous flows, combinations of simplified mathematical treatment, experimental and numerical techniques are used for the investigations of ABL flow features. Of the different processes, turbulence is the main feature governing the response of the ABL to surface forcing. The intensity of the turbulence in a flow can be quantified using the Reynolds number, which is a measure of the ratio between the inertial forces of the fluid that tend to produce vortices and instabilities and the viscous forces that damp the motion. This dimensionless number is defined as

$$\mathrm{Re} = \frac{UL}{\nu} \tag{1}$$

where L is a characteristic length scale of the flow, U is a characteristic velocity and ν is the kinematic viscosity of the fluid. The transition to turbulence starts to occur when the Reynolds number is of the order of 10^2 and above. With the typical values of 10^8 in atmospheric flows, turbulence in the ABL is usually fully developed.

An important feature of turbulence is the dissipation of energy and the multiplicity of scales of motion. Important contributions to our understanding of the small scale structure of turbulence and the energy transfer process were made by Kolmogorov, when he described the “cascade” process, through which energy is transferred from the large scale to the smaller scales, in his similarity theory on turbulence (Kolmogorov 1941b; Kolmogorov 1941a; Kolmogorov 1962). Later advances occurred with Monin and Obukhov and their surface layer similarity theory (Monin and Obukhov 1954), in which the role of buoyancy in modifying the wind profile and the flux-gradient relations in general are explained. Our ability to interpret observations was subsequently greatly improved. A series of field experiments took place from then on (Businger et al. 1971; Nieuwstadt 1984; Brutsaert 1992; Parlange and Katul 1995), finding the application of similarity theory to hold on relatively simple homogeneous surfaces. Even over complex terrain Monin-Obukhov similarity theory has been found to hold where the surfaces can be judged statistically homogeneous (Kustas and Brutsaert 1986; Sugita and Brutsaert 1992; Parlange and Brutsaert 1989). Major advances in our understanding of the boundary layer structure have also taken place through the use of numerical modeling where the effects of turbulence are represented more and more

realistically over the years. The large eddy simulation technique has become a tool of choice to investigate micro scale features of ABL flows (Deardorff 1974; Mason 1989; Albertson and Parlange 1999a), and the aggregated effect of heterogeneous land cover on mesoscale parameterizations (Moeng et al. 1999; Bou-Zeid et al. 2004).

However thin the ABL is, most exchanges of heat, momentum, moisture and contaminants start at the land surface. The radiation balance and the heat energy budget at the surface are thereby greatly affected. Surface studies including regional water management or watershed hydrology, but also atmospheric studies such as mesoscale meteorology or general circulation modeling rely on the parameterization of these exchanges. Yet the growing interest for regional climate models is widely recognized to require improvements of the land atmosphere coupling as well as boundary layer treatment (Garratt 1993). In general, several surface types can coexist in a small surface area and the distribution of the sensible and latent heat fluxes can affect the flow on small, regional and global scales (Giorgi and Avissar 1997; Avissar and Pielke 1989; Gao et al. 2008; Lyons and Halldin 2004). In mesoscale models where the exchanges of water, heat and momentum are averaged over one grid cell, the need for improved parameterization of each type of surface is a pressing concern (Pielke and Uliasz 1998; Henderson-Sellers et al. 1996; Henderson-Sellers et al. 2008; Chen et al. 1997; Wu et al. 2009).

1.2 Water vapor transport

In his book *Meteorologica*, Aristotle describes what is known as the “little” hydrologic cycle in the following terms (Aristotle 1952):

Now the sun, moving as it does, sets up processes of change and becoming and decay, and by its agency the finest and sweetest water is every day carried up and is dissolved into vapor and rises to the upper region, where it is condensed again by the cold and so returns to the earth.

These early observations clearly show evaporation as being an important part of the water cycle; no mention is made of the effect of the wind on the water cycle. Evaporation is

however intimately linked to the state of the ABL, the intensity of turbulence and the energy balance at the land surface.

Studying water vapor transport is relevant to several fields, including water resources management, hydrology, agriculture or air quality management. Starting at the surface, evaporation is an important parameter both for hydrology and for atmospheric studies. Planning water resources management involves an accurate quantification of evaporation, especially when demand for water from industry and agriculture must be considered together with drinking water supply. Until now, pan evaporation or standard meteorological measurements from which the drying potential of the air is calculated have been used. These approaches however rely on assumptions that often result in large errors in estimating evaporation and subsequent poorly informed water allocation decision making (Lowe et al. 2009). Recent advances in technology imply that new types of measurements can be available. It is therefore of interest to revise existing evaporation models and make use of up-to-date measurement techniques.

Concerning ABL flows, evaporation at the surface is an important boundary condition. One way of treating the ground surface in atmospheric models is to provide detailed modeling of surface temperature and soil moisture. The alternative is to partition the available energy provided by solar radiation between sensible heat, latent heat and ground storage (Pan and Mahrt 1987; Albertson et al. 2001; Stull 1988). Surface evaporation can substantially reduce the energy available for sensible heat and impact the subsequent daytime boundary layer development. The influence of water vapor does not stop at the surface; the transport of water vapor in the atmosphere is critical for cloud formation and needs to be understood better in order to improve precipitation predictions (Eltahir and Bras 1996; Stohl et al. 2008). For this, one should look at the similarity of transport between water vapor and heat. Indeed, Monin-Obukhov similarity theory (MOST) is used in virtually all atmospheric models and is based on the hypothesis that water vapor and heat are transported by the same turbulent mechanisms. Deviations from MOST have however been reported in the past and must be assessed and explained (Sempreviva and Gryning 2000; De Bruin et al. 1999). For this, detailed numerical simulations including water vapor and heat transport can be a good tool to observe deviations from MOST over different surface conditions. However, some

parameterization is embedded in even the most detailed atmospheric simulation tools and must be accurate. Using a specifically designed dataset, one can test models hypotheses. Then high accuracy simulations can be used to see how the transport of water vapor and heat behave in different conditions.

1.3 Specificities of water bodies

Natural or man-made water bodies such as lakes or reservoirs have a large presence in many landscapes, and their surfaces have very different interactions with the atmosphere than land surfaces. The moisture evaporation, the wind forcing at the surface and energy exchanges have specificities that characterize them from land surface forcing (Rouse et al. 2005). These differences result in a large impact of the presence of lakes on regional weather and water balance (Leon et al. 2007; Rouse et al. 2003; Rouse et al. 2005). However, air-water interactions are complex, and most current mesoscale and global climate models still ignore the specificities of lakes in their surface parameterization (Swayne et al. 2005).

One complexity of water bodies comes from the fact that the thermal capacity of water is much higher than that of many other materials such as soil. A much greater quantity of energy can thus be stored in water bodies than in soils. The energy budget of lakes and the subsequent evaporation patterns are impacted by this characteristic. However, the most commonly used evaporation models require an estimation of the net radiation and the soil heat flux, or the storage of energy by conduction, convection and radiative heating in the case of a water body. Estimation of this term is complicated by the variations of water temperature in depth and space, and data to quantify it are sparse.

A challenge that one encounters in numerical weather prediction schemes is to have accurate boundary conditions at the surface. This includes lake surface temperature and energy exchanges at the surface. An existing method to estimate lake surface temperature is to use a one dimensional lake model like FLake (Mironov et al. 2010). However, such a model also requires a parameterization of the lake-atmosphere energy exchanges. Inherent to the use of MOST is the definition of roughness length. Having a good parameterization of the momentum and scalars roughness lengths is still an open question (Mironov et al. 2010), and

observation of water vapor, heat and momentum fluxes above lake surfaces can help gaining information about these quantities.

Finally, water bodies usually have a limited fetch. Depending on this fetch, the airflow has time or not to adjust to its underlying water surface. The effect of this limited fetch still needs to be assessed.

1.4 Numerical simulations of the atmosphere, large eddy simulations and scalar transport

The Norwegian scientist Vilhelm Bjerknes, in his paper *Weather Forecasting as a Problem in Mechanics and Physics* (Bjerknes 1904), first stated that it should be possible to predict weather phenomena with calculation based on natural laws. Later advances in the understanding of atmospheric sciences combined with advances in computer resources made this possible and led to modern numerical weather prediction.

In the range of turbulent flow prediction tools, Large Eddy Simulations (LES) stand in the middle, between direct numerical simulations (DNS) where all the scales of motion are resolved, and Reynolds Averaged Navier-Stokes (RANS) methods where all the turbulent scales are modeled. LES have been emerging as a leading technique for the simulation of high Reynolds number (Re) turbulent flows in the atmosphere in the last few decades (Moeng 1984; Albertson and Parlange 1999a; Wood 2000; Bou-Zeid et al. 2004). In LES, all the large, energy containing scales that one can computationally afford to capture on a numerical grid (the resolved scales) are simulated, and the dynamics of the small turbulent eddies (subgrid scales) that cannot be captured and their effect on the larger scales are parameterized. Despite the current fast progress of computer resources, if one were to use DNS to resolve all the scales of motion that appear in the atmosphere, one would have to have a spatial resolution of less than one millimeter, and solve for a domain of several kilometers. Even the most advanced computers nowadays would be unable to do so (Voller and Porte-Agel 2002). LES are therefore a good compromise. Furthermore, the large scales, which usually control the behavior of the overall flow, are usually geometry and flow dependant, whereas the small scales have more uniform statistical properties and are therefore easier to model.

The LES have been found to perform well in different stability conditions (Kumar et al. 2006). The dynamics of the atmospheric boundary layer and the transport of mass, momentum and energy are represented using the incompressible Navier-Stokes equations together with the scalar conservation equations (Pope 2000; Tennekes and Lumley 1972). When using Large Eddy Simulations, a filter is applied to the governing flow equations. All scales larger than the grid scale are numerically resolved and the smaller scales are parameterized using a subgrid scale (SGS) model. The set of high Reynolds number (*Re*) incompressible flow equations in the atmospheric boundary layer may be written as follows:

$$\frac{\partial \widetilde{u_i}}{\partial x_i} = 0, \tag{2}$$

$$\frac{\partial \widetilde{u_i}}{\partial t} + \widetilde{u_j}\left(\frac{\partial \widetilde{u_i}}{\partial x_j} - \frac{\partial \widetilde{u_j}}{\partial x_i}\right) = -\frac{1}{\rho}\frac{\partial \widetilde{p}}{\partial x_i} + g\left(\frac{\widetilde{\theta_v} - \langle \widetilde{\theta_v} \rangle}{\langle \widetilde{\theta_v} \rangle}\right)\delta_{i3} - \frac{\partial \widetilde{\tau_{ij}}}{\partial x_i} + f\left(\widetilde{u_2} - V_g\right)\delta_{i1} - f\left(\widetilde{u_1} - U_g\right)\delta_{i2}, \tag{3}$$

$$\frac{\partial \tilde{\theta}}{\partial t} + \widetilde{u_j}\frac{\partial \tilde{\theta}}{\partial x_j} = -\frac{\partial \widetilde{\pi_j^{\theta}}}{\partial x_j}, \tag{4}$$

$$\frac{\partial \tilde{q}}{\partial t} + \widetilde{u_j}\frac{\partial \tilde{q}}{\partial x_j} = -\frac{\partial \widetilde{\pi_j^{q}}}{\partial x_j}, \tag{5}$$

where $\widetilde{u_i}$ is the resolved velocity component in the x_i direction, $\widetilde{p}$ is the resolved dynamic pressure term formulated to satisfy a divergence free condition, δ is the delta of Kronecker, $\widetilde{\theta}$ and $\widetilde{\theta_v}$ are respectively the resolved potential and virtual potential temperature, U_g and V_g are the two components of the geostrophic wind, $\widetilde{\tau_{ij}}$ is the subgrid scale stress tensor, q is the specific humidity, and $\widetilde{\pi_j^{\theta}}$ and $\widetilde{\pi_j^{q}}$ are the subgrid scale fluxes for temperature and specific humidity respectively. Equation (2) is the filtered mass conservation equation, (3) is the filtered momentum transport equation or Navier-Stokes equation in rotational form using the Boussinesq approximation, (4) and (5) are the filtered equations for conservation of a scalar quantity. The potential temperature and specific humidity affect the vertical flow by affecting buoyancy, and this is taken into account in (3) by using the Boussinesq approximation.

The effect of the subgrid scale stress and scalar fluxes on the resolved motions are parameterized in the form of a Smagorinsky model (Smagorinsky 1963), leading to

$$\tau_{ij}^{Smag} = -2\upsilon_T \widetilde{S_{ij}} = -2\left(C_{S,\Delta}\Delta\right)^2 \left|\tilde{S}\right| \widetilde{S_{ij}}, \tag{6}$$

$$\pi_{ij}^{b,Smag} = -Sc^{-1}\left(C_{S,\Delta}\Delta\right)^2 \left|\tilde{S}\right| \frac{\partial \tilde{b}}{\partial x_i}, \tag{7}$$

where *Sc* is the subgrid scale turbulent Schmidt number for the scalar *b* (or the Prandtl number *Pr* for heat) and *Cs* is the Smagorinsky coefficient. Significant progress occurred in LES with the development of dynamic subgrid-scale modeling procedure (Germano et al. 1991). With the dynamic procedure, the Smagorinsky coefficient is automatically computed using information contained in the smallest resolved scales, thereby eliminating the uncertainties coming from the tuning of model parameters. A later development was to make *Cs* scale dependent (Porte-Agel et al. 2000a). This has proven to be useful in the vicinity of the lower boundary where the subgrid scales account for a large portion of the flow and in stable conditions (Kleissl et al. 2003). A Lagrangian approach is used to determine *Cs* from averaging over flow trajectories, leading to the so-called Lagrangian scale dependant dynamic subgrid scale model (Bou-Zeid et al. 2005).

1.5 Field experiments of the ABL

Simulation of the exchange of momentum and heat over land or water bodies in atmospheric models including large eddy simulations relies largely on an accurate parameterization of the turbulent processes near the surface. In order to test the models that are used, measurements are necessary. The Northern Hemisphere climate Processes land-surface Experiment (NOPEX, see (Halldin et al. 1998)) observational campaigns included experiments to investigate the energy exchange over lakes. The field program helped to improve understanding in the exchange of heat and mass over small lakes (Heikinheimo et al. 1999).

Large eddy simulations gather all the unclosed transport terms in the momentum and scalars equation in the residual stress $\tilde{\tau}_{ij}$ and the residual scalar fluxes $\tilde{\pi}_j^{\theta}$ and $\tilde{\pi}_j^{q}$ and rely on the use of a closure model for these terms. Subgrid scale (SGS) variables are thus parameterized and field campaigns can be designed to test the characteristics of SGS variables. Several field experiments have recently been performed in the atmospheric surface layer using various horizontal arrays of sonic anemometers (Tong et al. 1998; Tong et al. 1999; Porte-Agel et al.

2000b; Porte-Agel et al. 2001b; Porte-Agel et al. 2001a; Higgins et al. 2003, 2004; Horst et al. 2004; Kleissl et al. 2003; Kleissl et al. 2004; Sullivan et al. 2003). In these experiments, high frequency measurements of the wind or temperature are filtered to compute the components of the SGS stress tensor.

1.6 Open questions and outline of the thesis

In the present thesis, the focus will be on the state of the atmosphere above a water surface. This will involve, as presented in chapter 2, investigations of the energy exchanges between a lake and the atmosphere. Measurements of the roughness lengths for momentum, heat and water vapor are analyzed there. This chapter also presents observations of the amount of energy that is being stored in a water body – a quantity that is of crucial importance for evaporation modeling but that is very hard to estimate or measure. Chapter 3 however is devoted to the derivation of a method to quantify evaporation above a water body without relying on the energy storage in the water, but relying on measurements of sensible heat flux instead. Results show that this new technique is very promising for evaporation measurements above lakes and reservoirs. Then, simulations of the airflow above wet surfaces are investigated. The subgrid scale transport of water vapor, a scalar whose transport characteristics are less well studied than the characteristics of heat transport, is investigated in chapter 4. Results from a novel field campaign observing the subgrid scale transport of heat and water vapor for the first time above a lake are presented there and a relationship is identified between the two scalar transport terms. Subsequent advice for modelers is given in the conclusions. Chapter 5 will focus on results of simulations over infinite wet surfaces and over wet/dry surface transitions. The implementation of the water vapor transport terms (in equation (2) to (7)) was done in the EPFL-LES code as part of the work of the thesis for this analysis. The effect of a surface transition on the correlation between heat and water vapor transport is investigated. The change in evaporation pattern is observed and the effect of the fetch of the wet surface is assessed. Chapter 6 will compare the footprint of the wet surfaces obtained by the LES to an analytical footprint model. The appendix will show simulations of a moisture transport phenomenon observed over a field site in Seedorf, Switzerland, where a water vapor layer is detached from a wet layer close to the ground.

2 Energy exchanges above a lake surface

2.1 Background on lake parameterization and lake-atmosphere interaction studies

The surface fluxes of momentum, heat and water vapor determine the state of the atmosphere to a large extent. Their accurate parameterization is of crucial importance for short-range forecasts, and has been recognized as a remaining challenge to make LES a more reliable tool for simulation of flows with high Reynolds numbers in engineering and environmental applications (Cabot and Moin 2000; Piomelli and Balaras 2002). Lake surfaces have very different interactions with the atmosphere than land surfaces, particularly in terms of moisture evaporation, wind forcing and energy exchanges. Numerical simulations have shown that the presence of lakes can have significant influence on mesoscale dynamics (Beniston 1986). This is due to the change of roughness, the source of moisture that can enhance cloud formation, and the very high heat capacity of the water versus the land. Lakes are however usually neglected in numerical weather prediction models (Swayne et al. 2005).

Many field experiments above water surfaces have been carried out during extensive sea measurement programs (Edson et al. 2007; Sun et al. 2001; Vickers and Mahrt 2010) that investigated the roughness length parameterization. Fewer field experiments collected comparable data to investigate these parameterizations over lakes.

To use the surface energy fluxes, it is important to gain insight in how the available energy is partitioned between sensible and latent heat.

2.2 The LATEX field campaign

Quantifying the interaction of the atmosphere with its underlying water surface is of importance for many scientific endeavors such as improving lake evaporation models, developing surface parameterizations for atmospheric simulations, studying the ecological implications of climate change on water bodies, and understanding the local-scale atmospheric dynamics in coastal areas (Brutsaert 1982; Parlange et al. 1995; Edson et al.

2007). However, water-atmosphere interaction has generally received less attention than land-atmosphere interaction (DeCosmo et al. 1996), mainly due to logistical difficulties in operating field studies over water surfaces. The Lake-Atmosphere Turbulent EXchange (LATEX) field measurement campaign was designed to help bridge this gap and address some of the issues listed above.

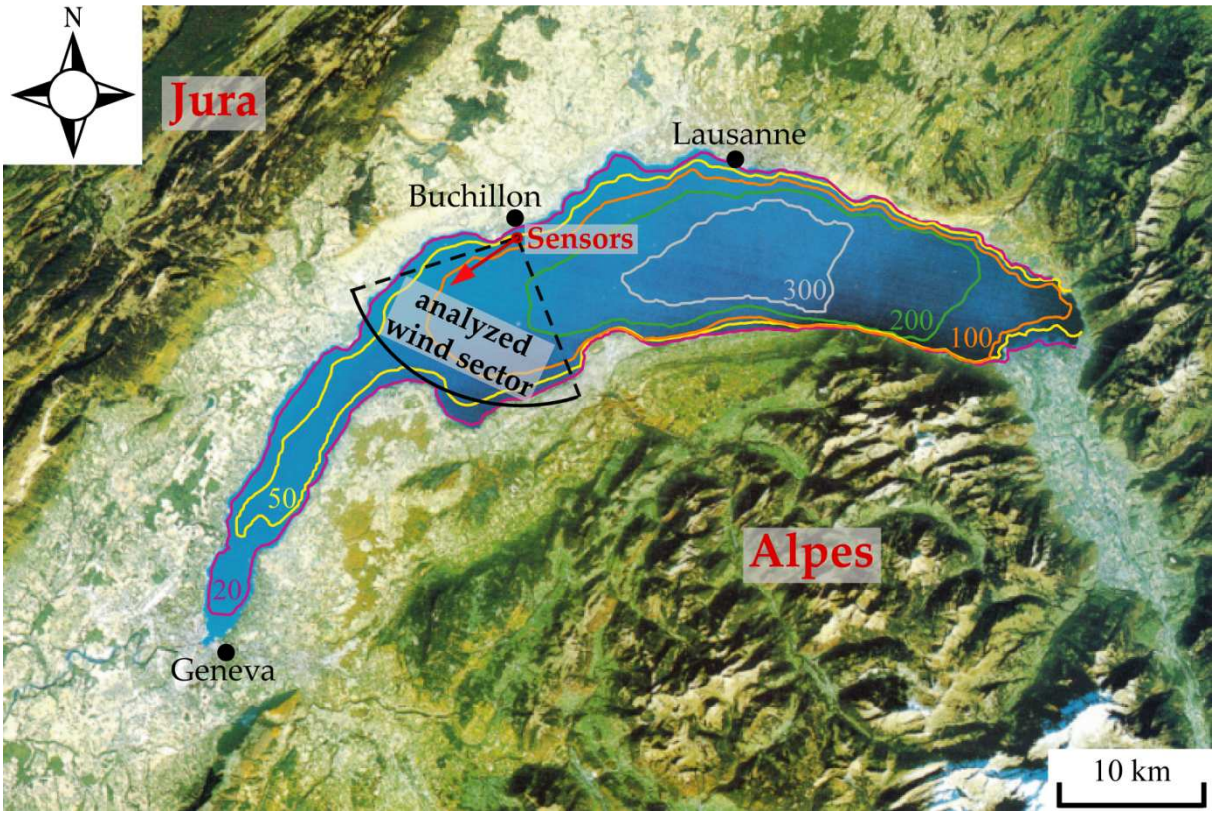

Fig. 2 Location and orientation of sensors, analyzed wind sector, and the bathymetry (m) of Lake Geneva, adapted from public domain satellite image (NASA World Wind) and bathymetry data (SwissTopo).

The experiment took place from mid-August through late October of 2006, 100 meters from the shore, in a 3-meter deep section of Lake Geneva, Switzerland (Fig. 2). The measurements over Lake Geneva in Switzerland were collected on a 10-meter high tower, 100 meters away from the northern shore of the lake. The measuring campaign lasted from mid August till late October of 2006 (DOY 226 to DOY 298). Four sonic anemometers (Campbell Scientific CSAT3) and four open path gas analyzers (LICOR LI-7500) measured wind speed,

temperature, and humidity at 1.65 m, 2.30 m, 2.95 m and 3.60 m above the water surface (Fig. 3). The four pairs of CSAT3/LI-7500 were set-up as a vertical array oriented towards the southwest with a vertical separation of 0.65 m. Only data with wind coming from the south and south-west were used in all analysis to ensure that the minimum fetch remained 10 km and that the tower did not influence the measurements (see analyzed wind sector in Fig. 2). In this sector, the average wind fetch above the water surface is about 15 km. Assuming that the internal equilibrium layer height is roughly equal to 1/100 of the downstream distance (Brutsaert 1998; Bou-Zeid et al. 2004), the minimum fetch of 10 km ensured that the measurements were fully within this internal equilibrium layer of the lake.

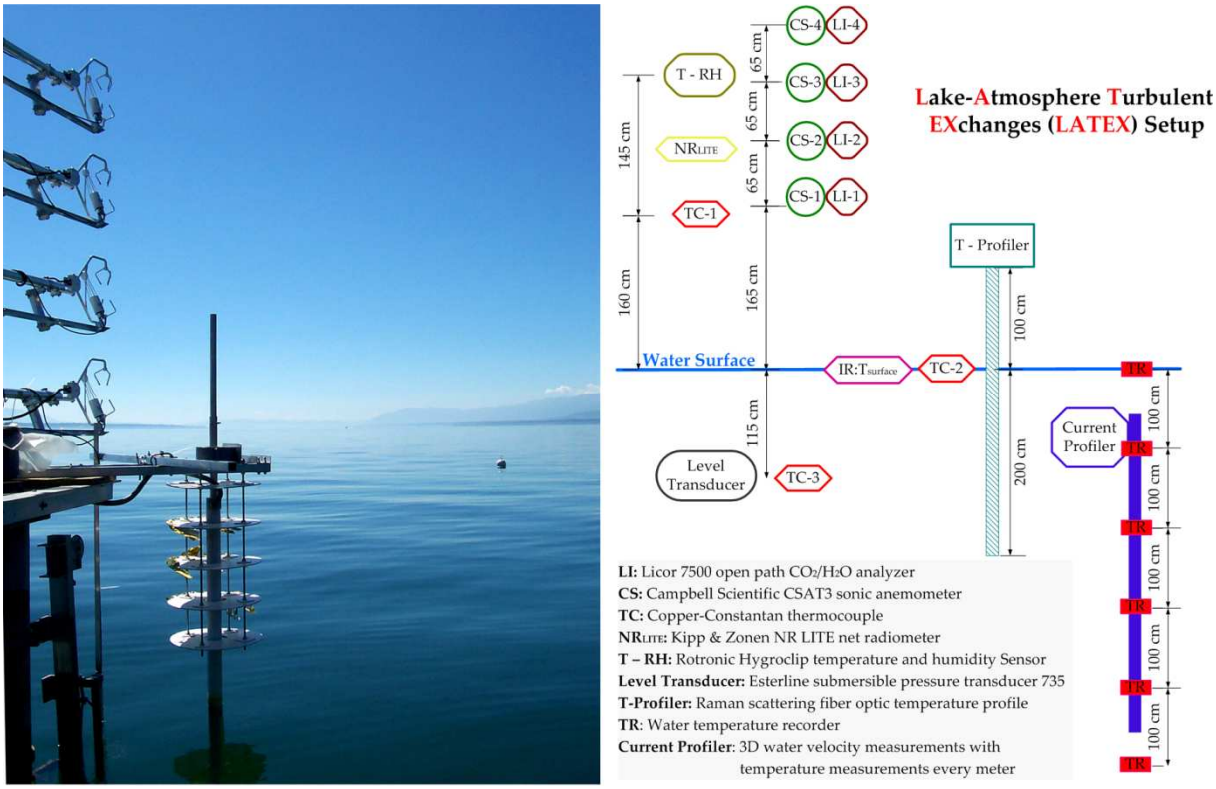

Fig. 3 Upstream view and experimental set-up of LATEX.

Additional measurements, depicted in the diagram of Fig. 3, included (a) lake temperature obtained by a Raman scattering fiber-optic temperature profiler with a 4-mm vertical resolution and up to 0.01 °C temperature resolution (3 m range: 1 m above the water surface and 2 m below), (b) lake current from a profiler (Nortek), (c) net radiation (Kipp & Zonen

NR-Lite), (d) surface water temperature (thermocouple and Apogee Instruments IRTS-P infrared thermocouple sensor), (e) water temperature at 1.15 m depth (thermocouple), (f) relative humidity and temperature of air (Rotronic hygroclip S3 at 3.05 m and a thermocouple at 1.60 m), (g) and wave height and speed (Pressure Systems Inc. submersible level transducer model 735; +/-0.05% accuracy, mounted 1.15 m below the surface). This set of measurements allowed for a deep investigation of the exchanges of momentum, heat and water vapor at the lake surface.

2.3 Roughness length investigation

All numerical weather prediction models, specifically LES codes, make use of the Monin-Obukhov similarity theory (MOST, (Monin and Obukhov 1954)) in some way. For LES, it is used to define values for the wind speed or scalar concentrations at the first grid point above the surface. In this theory the following equations for the wind speed, water vapor concentration and virtual temperature are expected to be valid in the surface layer,

$$u = \frac{u_*}{k}\left[\ln\left(\frac{z-d_0}{z_{0m}}\right) - \psi_{sm}\left(\zeta\right)\right], \tag{8}$$

$$q_s - q = \frac{E}{a_v k u_* \rho}\left[\ln\left(\frac{z-d_0}{z_{0v}}\right) - \psi_{sv}\left(\zeta\right)\right], \tag{9}$$

$$\theta_s - \theta = \frac{H}{a_h k u_* \rho c_p}\left[\ln\left(\frac{z-d_0}{z_{0h}}\right) - \psi_{sh}\left(\zeta\right)\right], \tag{10}$$

where q is the mean specific humidity, θ is the mean potential temperature (the subscript s denotes the surface value), u is the wind speed, a_h and a_v are constants of value one, d_0 is the surface displacement height and the Ψ are universal functions of the stability parameter ζ. The roughness lengths for momentum, heat and water vapor (z_0, z_{0h} and z_{0v}) are therefore important parameters that are still determined in a crude way. While the roughness length is usually specified as a constant for each surface or vegetation type over land, it is a dynamic value over sea, depending on the evolution of the wave field that strongly influences the momentum transfer between the water and the atmosphere (Donelan et al. 1993). One of the questions that the LATEX field campaign tried to investigate was: should the wave field over

the lake be taken into account in the roughness length parameterization? How does the water vapor roughness length evolve compared to heat?

Sensible and latent heat fluxes during LATEX were obtained using the eddy covariance measurements, following:

$$H = \rho c_p \overline{w'T'}, \tag{11}$$

$$E = \rho \overline{w'q'}, \tag{12}$$

where the prime represents the fluctuating (turbulent) component for the vertical wind (w) and temperature (T) and the specific humidity (q); ρ is the mean density of the air, and the overbar denotes Reynolds averaging, which was performed in time over data records of 30 minutes. The different roughness lengths are computed following equations (8) to (10) based on the 30 minute averaged data. The surface displacement d_0 is taken as zero since we are above a water surface. The other parameters are given by the measurements from LATEX. We compare the results with and without the stability correction functions Ψ. The definition of the functions Ψ that are used here can be found in Brutsaert (2005) (page 50). The results are shown in Fig. 4. We can see a lot of scatter in the results, which makes a choice of a value difficult. The value of z_{0v} and z_{0h} are expected to be related to z_0, but in the vicinity of the surface, momentum and scalars are not following the same transport mechanisms since molecular viscosity affects the transport of scalars. The results show indeed that the scalar roughness length take different values from that of the momentum roughness length. Fig. 5 shows the variation of momentum roughness length with wind speed. It appears that the scatter increases at lower wind speed. In the low wind speed regime, the momentum exchange is probably affected by the swell on the water surface, which depends on many non-atmospheric factors. However a roughness length $z_0=10^{-4}$ m seems to be appropriate on this water surface.

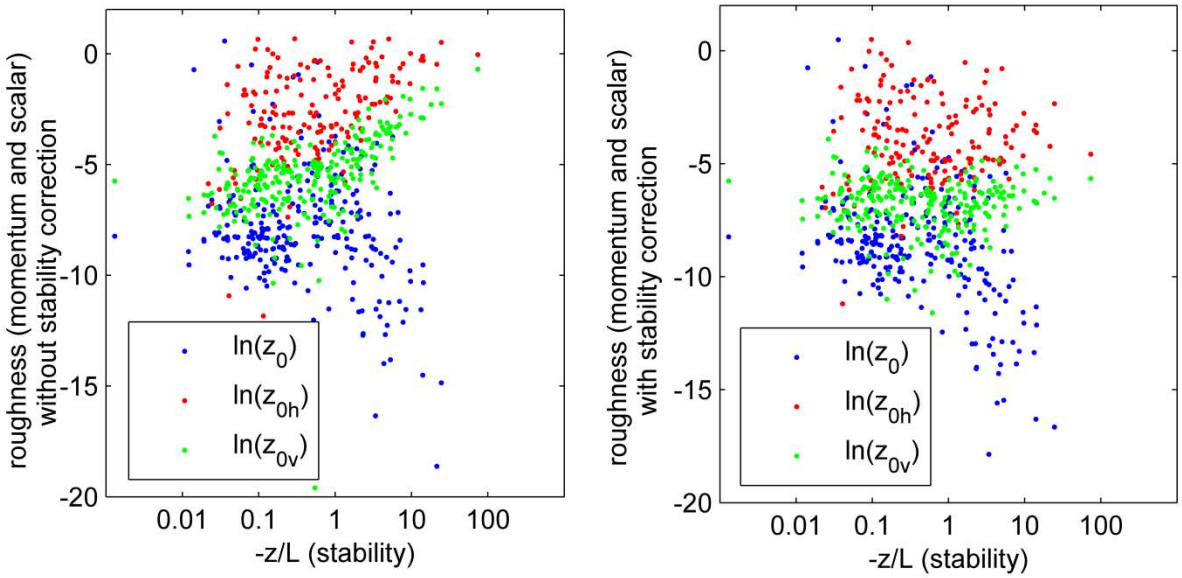

Fig. 4 Surface roughness length for water vapor, heat and momentum over Lake Geneva (m).

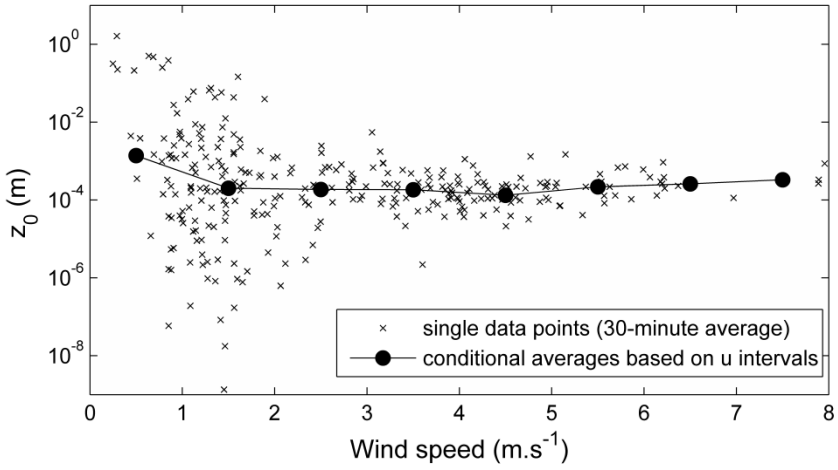

Fig. 5 Observed momentum roughness length as a function of wind speed.

The wave dependence of the momentum roughness length is investigated in Fig. 6, following the theory of Charnock (1955). Charnock argued on dimensional ground that for well developed waves the roughness length should be proportional to the wind stress, leading to

$$z_0 = \alpha \frac{u_*^2}{g} \tag{13}$$

where α is a constant, u_* is the friction velocity and g is gravity. Results from LATEX do not show this proportionality, except in the very low stress cases where the scatter is however the largest. As will be shown later though, the wave field during LATEX was very weak (section 4.1).

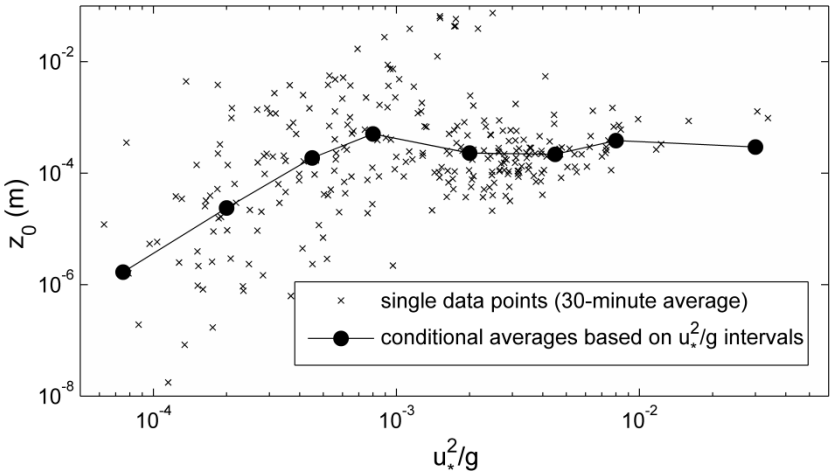

Fig. 6 Variation of momentum roughness length with Charnock parameter $u_*^2 g^{-1}$.

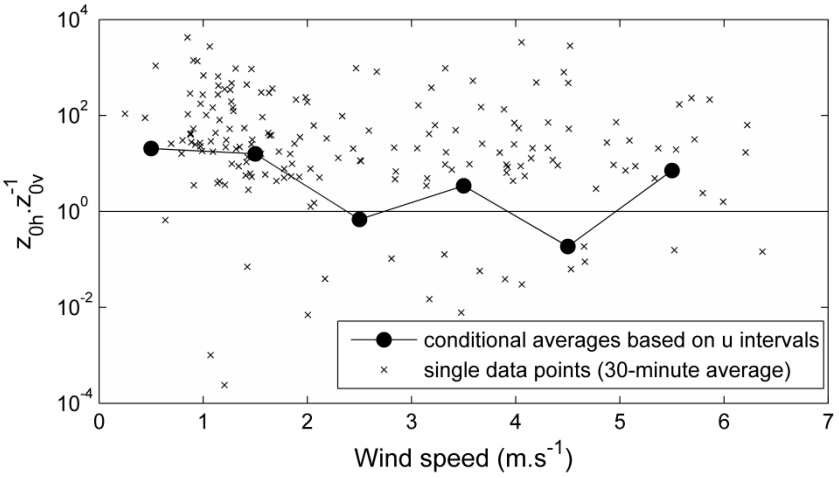

Fig. 7 Observed scalar roughness length ratio as a function of wind speed.

The roughness length for heat is consistently higher than that of water vapor. Models currently often use an equal value for both scalar roughness lengths. The higher value found

for heat compared to moisture has been observed and explained by the dynamic nature of temperature that generates more buoyancy than vapor by Vickers and Mahrt (2010).

2.4 Energy budget investigation

In atmospheric boundary layer research, the surface is essentially treated as the lower boundary condition to the atmosphere. For the land surface, the balance of fluxes is an important factor too. The primary energy input at the surface occurs through solar radiation absorption at the ground, and generally results in a diurnal variation in temperature and turbulent heat and vapor fluxes. The surface temperature also responds to the balance of all energy fluxes at the earth's surface. In the absence of vegetation, conservation of energy at the ground surface implies that

$$L_e E + H = R_n - G \tag{14}$$

which is the energy balance equation. $R_n - G$ represents the available energy and is often used in evaporation modeling.

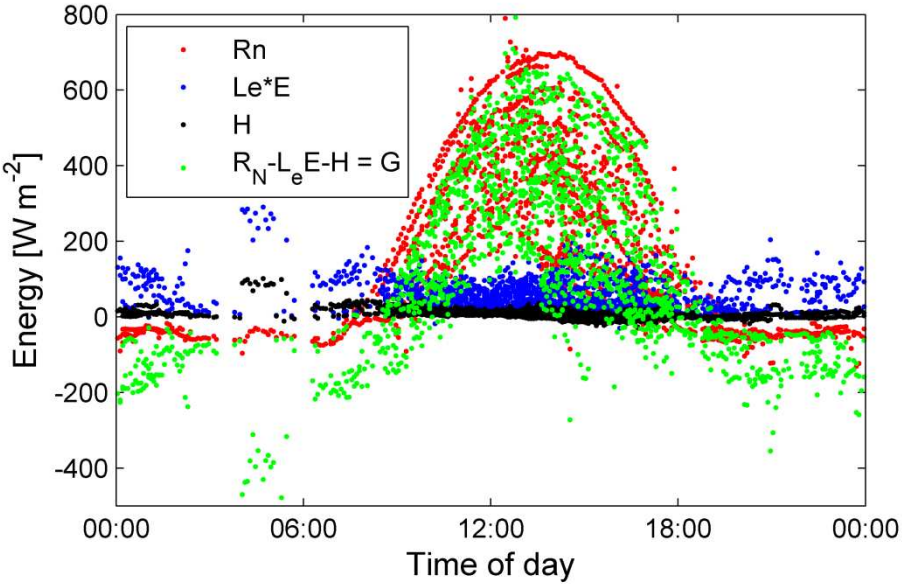

Fig. 8 Daily energy budget during LATEX.

We investigate the diurnal variations in all fluxes in Fig. 8. The net radiation shows a clear diurnal cycle, but latent and sensible heat fluxes do not. The latent heat flux is always positive, and much larger than the sensible heat flux. More important, the latent and sensible heat fluxes represent only 10% of the total net radiation and show no diurnal cycle. The storage term on this figure is taken as the remaining energy, *i.e.* $G = R_n - H - L_eE$. Most of the available energy is used to warm the lake. This is different from ground surfaces where the storage term is small and often neglected in practice. We therefore tried to quantify this term more accurately, using temperature profiles in the water body. However our methods revealed unsuccessful, and results are not presented here. The reader is referred to a paper currently under review for results of this analysis (Vercauteren et al 2011).

3 The estimation of wet-surface evaporation from sensible heat flux measurements

3.1 Review of evaporation models

Accurate estimates of evaporation are crucial to project future water availability (Rind et al. 1997; Bou-Zeid 2002; Ortega-Farias et al. 1995; Kustas 1990) and to study the potential effects of climate change on ecosystems (Szilagyi et al. 2001; ter Heerdt 2007). In regional hydrological systems, open water bodies such as lakes or wetlands are often important components of the landscape. Therefore, methods to estimate evaporation from wet surfaces are essential. Moreover, this type of evaporation, also known as potential evaporation, is used in many operational methods as a basic component in the estimation of evaporation from non-wet surfaces (Brutsaert 1982; Stagnitti et al. 1989).

A widely used approach to estimate evaporation, including evaporation from wet or other surfaces where the water vapor concentration at the surface can be presumed to be at saturation, is based on energy budget considerations (Priestley and Taylor 1972; Brutsaert 2005; Shuttleworth 2007; Rosenberry et al. 2007; Parlange and Katul 1992). The energy available for evaporation can be written as $Q_n = R_n - G$, where R_n is the net radiation and G is the downward positive surface or ground heat flux (consisting of conductive, convective and radiative heating of the water body and the underlying bed). The flux G is sometimes neglected in the available energy flux density, such that $Q_n = R_n$ is assumed. Nevertheless, the contribution of this term for water bodies can be considerable (Tanny et al. 2008). Its omission from Q_n was already pointed out almost fifty years ago as an important source of error by Tanner and Pelton [1960]. Measurements of G are thus necessary in energy balance methods to accurately estimate evaporation from any surface. But, even when available, the use of measurements of G has also been shown to be a large potential source of error in lake evaporation calculations (Stannard and Rosenberry 1991).

Another problem that arises with the application and verification of energy budget related methods is that the individual footprints of the necessary measurements can be very different

and often mutually incompatible. For example, a typical radiometer will have a footprint area located directly underneath the instrument on the order of 10 m^2; ground heat flux measurements (G) will be very local with a footprint on the order of 0.1 m^2; and air properties (temperature, humidity, …) will represent upstream surface conditions of several square kilometers (Parlange et al. 1995; Brutsaert 1998; Albertson and Parlange 1999a; Eichinger et al. 1996; Bou-Zeid et al. 2004). Thus, when these measurements are combined to compute evaporation with formulations such as Penman's, the footprint of the resulting evaporation rate will be ambiguous. In addition, when the model is verified against direct eddy-covariance measurements of evaporation (with a variable footprint that can be on the order of several kilometers for unstable atmospheric stability conditions with strong winds), the discrepancy in the footprints of the various measurements will cause differences between the measured and modeled evaporation rates that cannot be distinguished from the differences caused by instrument and model errors.

In light of the limitations inherent in methods using the energy budget with net radiation R_n and surface heat flux G, it is the purpose of this paper to present an alternative approach using measures of the turbulent sensible heat flux H. The derivation of the proposed formulation relies on an approximation of the Bowen ratio used in Penman's [1948] model, which has been shown to be accurate in many studies in the past [e.g. Stannard and Rosenberry, 1991; Katul and Parlange, 1992]. By using estimates of H, discrepancies between footprint scales of the different measurements can be greatly reduced, if not totally avoided. Moreover, even when no such discrepancies exist, measurements of G and R_n are not always easy; in contrast, measurements of the H from the surface into the atmosphere have become more ubiquitous through rapid advances in suitable instrumentation, such as for example, sonic anemometers and, more recently, scintillometers [(Andreas 1991; Kleissl et al. 2008; Meijninger et al. 2006) and references therein]. Estimates of H have been reliably obtained among others from a free convective second order model (Tillman 1972; Kader and Yaglom 1990; Weaver 1990; Albertson et al. 1995; Assouline et al. 2008) using very simple high-frequency measurements of the air temperature alone. In what follows, the proposed method will be presented and tested with experimental data obtained over Lake Geneva, Switzerland, and will be shown to produce results that are at least as accurate as other methods currently available.

3.2 Formulation of the method

The derivation starts with an estimate of the Bowen ratio,

$$Bo = \frac{H}{LeE} \tag{15}$$

where E is the rate of evaporation from the surface and L_e the latent heat of vaporization of water. If the turbulent transfer coefficients of heat and water vapor are assumed equal above a wet surface (e.g. lake surface, well irrigated field, surface after precipitation…), this ratio can be estimated as

$$Bo_P = \gamma \frac{T_s - T_a}{e_s^* - e_a}, \tag{16}$$

where T_S is the surface temperature (K), $e_S^* = e^*(T_S)$ the surface water vapor pressure (hPa) (i.e. saturation value at the temperature T_S), the asterisk denotes saturation values, the subscript *a* denotes the same variables in the air, at the measurement level,

$$\gamma = \frac{c_p\, p}{0.622\, L_e}$$

is the psychrometric constant, where c_p is the specific heat of air at constant pressure (J kg^{-1} K^{-1}), p is the pressure (hPa). At 20°C and atmospheric pressure at sea level, $L_e = 2.453\times10^6$ J kg^{-1} and γ = 0.67 hPa K^{-1}. The subscript *P* in (16) denotes that this Bowen ratio estimate is derived from a profile method.

Note with Penman that $\Delta = (e_s^* - e_a^*)/(T_s - T_a)$ can be used to estimate the slope of the saturation vapor pressure curve $\Delta = de^*/dT$ at air temperature. For the wet surface under consideration, (16) then can be rewritten as

$$Bo_L = \frac{\gamma}{\Delta}\left(1 - \frac{e_a^* - e_a}{e_s^* - e_a}\right), \tag{17}$$

where the subscript *L* indicates that this ratio is a linearized approximation.

The ratio $\left(e_a^* - e_a\right)/\left(e_s^* - e_a\right)$ in (17) can be readily determined, after Penman, by use of a bulk transfer equation for evaporation $E = f(u)(e_s^* - e_a)$ and by defining a drying power of the air, $E_A = f(u)(e_a^* - e_a)$, where $f(u)$ is a function of the wind speed u (m s^{-1}). Thus, one can write

$$\frac{e_a^* - e_a}{e_s^* - e_a} = \frac{E_A}{E}, \tag{18}$$

which, by virtue of (15) yields immediately from (17) the final result

$$E = \frac{\Delta}{\gamma}\frac{H}{L_e} + E_A \ . \tag{19}$$

In practice, the slope of the saturation vapor pressure curve Δ can be readily estimated from the air temperature using available equations of e^* versus T such as, for example, the polynomial derived by Lowe [1977]. Equation (19) thus needs only measurements of H, the mean wind speed u, the vapor pressure of water in the air e_a and the air temperature T_a, all of which will have very similar footprints if measured at the same height. No measurements of surface temperature, net radiation, or surface heat flux are needed.

The simplest form of the wind function is an empirical formulation of the type $f(u) = a + bu$, where a (s/m) and b (s^2/m^2) are dimensional constants; in practical applications over land surfaces, $f(u)$ as proposed by Doorenbos and Pruitt [1975] can be used or it can be determined on the basis of similarity or by calibration [Brutsaert, 2005]. For reasons to be explained below, in the present study dealing with Lake Geneva, we used the formulation $f(u) = 1.25.10^{-8}u$, (with $a = 0$) in which all the variables are in S.I. units. Note in the case of a water surface, that as wind speed increases, waves may start to have an important effect on the fluxes (see (Veron et al. 2008)) that is not taken into account in this particular $f(u)$ formulation; therefore the wind function used here is valid only for small to moderate wind speeds. Note also that if H in (19) is replaced by ($R_n - G - L_eE$) one obtains exactly the formulation first derived by Penman,

$$E = \frac{\Delta}{\Delta + \gamma}\frac{Q_n}{L_e} + \frac{\gamma}{\Delta + \gamma}E_A . \qquad (20)$$

3.3 Experimental data

The proposed formulation was tested with data collected during the Lake-Atmosphere Turbulent EXchange (LATEX) field campaign (August – October, 2006) over Lake Geneva, Switzerland. Wind velocity, temperature and humidity profiles were measured at 20Hz using a 5 m tower with a vertical array of four sonic anemometers (Campbell Scientific CSAT3) and open path gas analyzers (LICOR-7500). The heights of the four measurement levels above the lake surface were 1.65 m, 2.3 m, 2.95 m and 3.6 m, but only measurements at 2.95 m were used in the following results. The analysis was actually done for the four heights, giving very similar results (the average of the root mean square differences between the heat flux measurements from the four sonics was only about 1 W m^{-2}). For the benefit of later tests the water surface temperature was also measured by two independent systems (though these measurements are not needed in the formulation proposed). One was a thermocouple that was placed just below the average water surface, rigidly attached to the tower structure. The second system consisted of an Apogee Instruments IRTS-P infrared temperature sensor. Note that all subsequent comparative analyses requiring surface temperature made use of the thermocouple.

The area of the lake is 582 km^2, and the measurement site was located 100 m from the northern shore of the lake. Only data collected with the wind coming from over the lake (south-west) were used, ensuring a minimal fetch of 10 km, with the measurements fully within the internal equilibrium layer of the lake. The wind speed never exceeded 10 m s^{-1} and waves rarely exceeded 20 cm. The details of the experiment are presented in Vercauteren et al. [2008] and in Bou-Zeid et al. [2008], and the setup is depicted in Fig. 3.

Sensible and latent heat fluxes during LATEX were also obtained using eddy covariance measurements, following:

$$H = \rho c_p \overline{w'T'}, \tag{21}$$

$$E = \rho \overline{w'q'}, \tag{22}$$

where the prime represents the fluctuating (turbulent) component for the vertical wind (w) and temperature (T) and the specific humidity (q); ρ is the mean density of the air, and the overbar denotes Reynolds averaging, which was performed in time over data records of 30 minutes. The evaporative flux obtained by eddy correlation was used to test the evaporation formulation (19) proposed in this paper.

3.4 Results

The assumptions made in the proposed formulation (and also in the Penman model) are embedded partially in the approximation of the Bowen ratio. The first one, used in (16), states that the transfer coefficients of heat and water vapor are equal. The subsequent estimate of the Bowen ratio (Bo_P, (16)) is shown in Fig. 9, and compared to the measured Bowen ratio (15) computed using the eddy-covariance measurements for H and L_eE as described above. The correlation between the two is 76%, but the root-mean square error is 109% due to the presence of a bias due to difficulties in measuring surface temperature that is discussed in more detail at the end of the paper. The second assumption used in the proposed formulation appears in (17) and states that the Bowen ratio can be computed using the linearized slope of the saturation vapor pressure curve (in addition to the equal turbulent transfer coefficients assumption). The quality of this estimate (Bo_L, of (17)) can be judged in Fig. 10, where it is tested again versus the measured Bowen ratio computed using the eddy-covariance flux measurements. The correlation coefficient is 77%, and the root-mean square error is 113%, again because of a bias. The averaging period used for the results is 30 minutes. Since the measurements used to compute Bo_L and Bo_P are the same, the fact that both have practically the same correlation and error may suggest that the assumptions underlying (16) and (17) are nearly equally valid, and that the errors result primarily from the measurements themselves. Actually, this should be no surprise, because both assumptions have already been validated in numerous studies in the past.

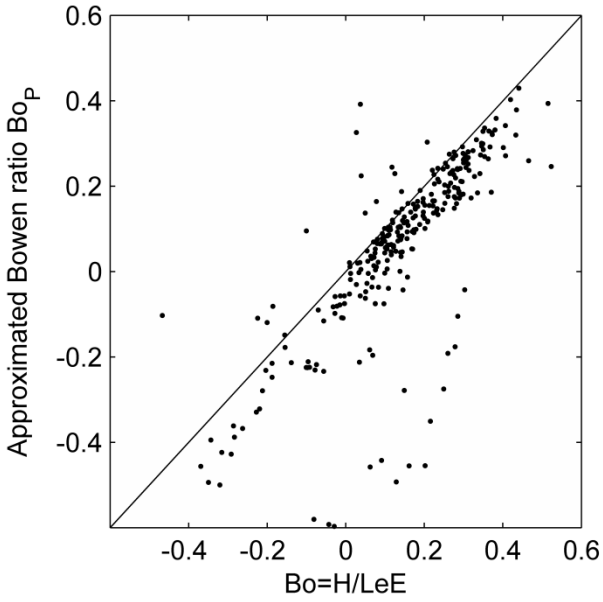

Fig. 9 Approximated Bowen ratio assuming equal heat and water vapor turbulent diffusivities versus Bowen ratio estimated by eddy covariance measurements.

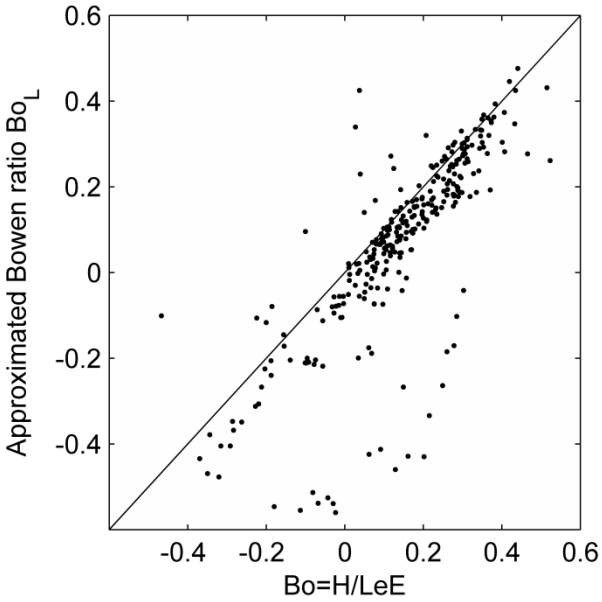

Fig. 10 Linearized Bowen ratio versus Bowen ratio estimated by eddy covariance measurements.

Beside the Bowen ratio approximation, the other assumption used in (19), as well as in the Penman model, states that the evaporation can also be expressed as a bulk transfer equation, namely as a wind function multiplied by the difference between the water vapor pressures at two heights. As can be seen in (18), this leads to the second term in the equation with the drying power of the air. The wind function used here is the one mentioned above, *i.e.* $f(u) = 1.25.10^{-8}u$, which was obtained by using (19) together with the eddy correlation measurements of *H* and *E*. Note that this is thus derived on the basis of the drying power of the air and not from the mass transfer equation. One could determine $f(u)$ on the basis of similarity (Brutsaert 1982; Katul and Parlange 1992) but for simplicity we rely on the simple wind function as it can be more easily applied in field applications. Finally note that this wind function is similar to the original form given by Penman.

After describing the different steps and separate components of the derivation, the proposed model performance can be directly tested by comparing the evaporation obtained with (19)

with the evaporation measured using the eddy covariance technique. The results are shown in Fig. 11, and the correlation coefficient is 95%, with a root-mean square error of 23%. Thus the method certainly appears quite promising for regular applications. It is interesting to observe that evaporation values derived with the Bowen ratio (17) combined with the eddy covariance technique is much less reliable. The correlation of the measured evaporation and the evaporation obtained from a pure Bowen ratio model (namely (15) with (17) and (21), or $L_e E = \rho c_p \overline{w'T'} / Bo_L$) can be inspected in Fig. 12. This comparison shows significant scatter, with a correlation coefficient of 50% and root mean square error of 67%. This difference in performance may be explained as follows. In the computation of the estimated Bowen ratios Bo_P and Bo_L, the measured water surface temperature is needed to determine the difference between air and water properties (temperature and water vapor pressure). This is likely to include significant measurement errors when different temperature sensors are used. In addition, water surface temperature is not a straightforward variable to measure. Recall that during LATEX, two independent measurements of water surface temperature were made: one using a thermocouple that was kept as much as possible at most just a few centimeters below the surface (attempts to mount it on a float were not successful) and the other using the Apogee Instruments IRTS-P infrared temperature sensor. The two instruments did not agree all the time (see Fig. 13). The thermocouple measurements were almost always higher. The thermocouple could have had errors related to its immersion or to radiative heating. The IR surface temperature measurements tend to have errors associated with the sensor body temperature correction needed and recommended by the manufacturer (Bugbee et al. 1999) and with the IR transmissivity of liquid water (although liquid water is largely opaque to the wavelengths used by the Apogee instrument: 6 - 14 μm corresponding to frequencies of 275 – 715 cm $^{-1}$). With the significant errors in measuring the water surface temperature, and with the higher order dependence of e^* on temperature T which will amplify any errors, the computations of the differences between T_a and T_s and e_a and e_s in (16) and (17) to estimate the Bowen ratios can be expected to produce significant errors. Hence the relatively low correlation between the measured and modeled Bowen ratios is not unexpected. On the other hand, when (15) and (18) are combined to yield (19), the parameters related to the water surface are canceled out (approximated by the linearized Δ) and the measurement errors related to water surface temperature are removed in the estimation of the surface evaporation.

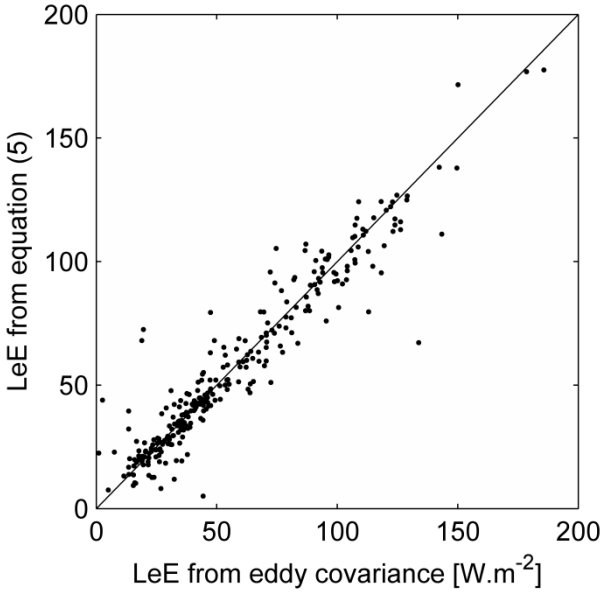

Fig. 11 Evaporation from equation (19) versus measured evaporation.

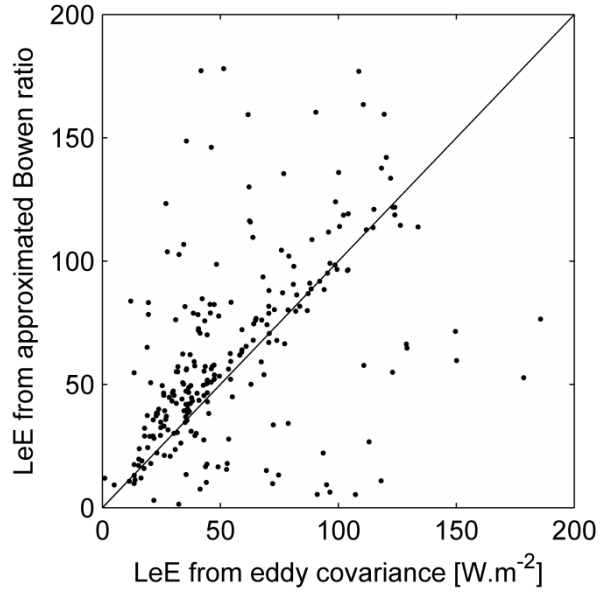

Fig. 12 Evaporation from the Bowen ratio (equation (15) with (17) and (21)) versus measured evaporation.

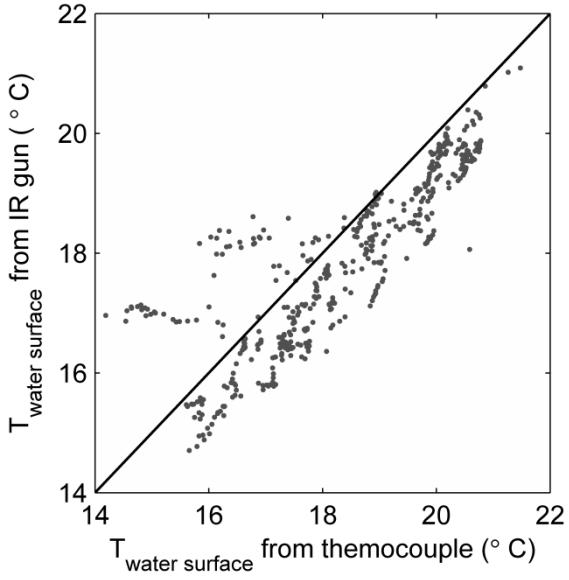

Fig. 13 Comparison of different water surface temperature measurements.

The important difference of performance between the Bowen ratio estimated evaporation and the one obtained via (19) can partly be explained by the difference of error propagation in each method. The propagation of errors is very different in the Bowen ratio estimation and in our proposed evaporation estimation method. Errors in the measurements of the vapor pressure of water and temperature in the air and at the surface will appear directly in the Bowen ratio estimate from (17), whereas measurement errors in air temperature and vapor pressure of water in the air will be balanced and somehow buffered by the first term in (19). A discussion about error propagation for Bowen ratio evaporation estimations can be found in (Crago and Brutsaert 1996). However, the difference of performance is probably mostly due to the use of the error-prone surface temperature measurement in the Bowen ratio approximation. The above analysis reveals one of the main strengths of the new approach proposed here: no surface measurements are needed so that the model will hence not suffer from the errors associated with such measurements.

3.5 Conclusions and Implications

A method to estimate evaporation from wet surfaces, requiring estimation of the sensible heat flux and standard atmospheric variables (temperature, humidity and wind speed), is derived

following the method of linearization of the Bowen ratio in the manner of *Penman* [1948]. The new approach does not require measurements of the ground heat flux and the net radiation and is especially useful where measurements of the sensible heat flux are more easily and cheaply available. This is often the case, since such data can be obtained, for example, by measurements relying on flux-variance relations using fine-wire thermocouples (Albertson et al. 1995) or from estimates of the average rate of dissipation of the temperature fluctuations among other approaches (Kiely et al. 1996; Albertson et al. 1995; De Bruin et al. 1993; Katul et al. 1994). Also other methods based on optical scintillometers, direct eddy covariance measurements from a sonic anemometer can be used. Though often not discussed, evaporation methods that require measurements of heat flux both into a water body and into a moist land surface involve many challenges (Tanny et al. 2008). The proposed method could also be useful in applications with satellite remote sensing products that allow the estimation of the sensible heat flux.

The performance of the proposed formulation (19) was assessed using data from the Lake-Atmosphere Turbulent EXchange (LATEX) experiment over Lake Geneva, Switzerland and excellent agreement was obtained between predicted and measured evaporation rates.

Formulations like the one proposed here, which are based on assumptions that allow the use of measurements at one level only instead of two, actually appear to improve the model performance. This is due to the typically large errors involved in measuring temperature and humidity differences between two or more levels over wet surfaces (especially surface temperatures). Finally, in any model of evaporation requiring variables measured with different types of instruments, the characteristic spatial scales of all observed variables and the upwind fetches, that is the footprints captured by the instruments, should ideally be mutually compatible. The proposed formulation also satisfies this requirement. Indeed, the air properties (wind speed, humidity, temperature …) and sensible heat flux measurements that are needed in (19) will have roughly the same footprint, and the resulting evaporation estimate will consequently have the same footprint as well. It is suggested then that the next generation weather stations for hydrologic applications (including wireless weather sensor networks, e.g. (Barrenetxea et al. 2008) include simple extensions to estimate sensible heat flux.

4 Subgrid-scale dynamics of water vapor, heat, and momentum over a lake

4.1 Motivation

The main goal of the Lake-Atmosphere Turbulent EXchange (LATEX) field measurement campaign presented in section 2.2 was to study the dynamics of small-scale turbulence over the lake. The increasing interest in small-scale turbulence over the past decade is directly linked to the emergence of large eddy simulation (LES) as a leading technique for the simulation of high Reynolds number (*Re*) turbulent flows in the atmosphere (Moeng 1984; Albertson and Parlange 1999a, b; Wood 2000; Bou-Zeid et al. 2004; Bou-Zeid et al. 2007; Patton et al. 2005; Stoll and Porte-Agel 2006), oceans (Shen and Yue 2001; Sullivan et al. 2007), rivers (Bradbrook et al. 2000; Keylock et al. 2005), as well as in engineering systems (Piomelli 1999; Sagaut 2003). In LES, all the large scales that one can computationally afford to capture on a numerical grid (the resolved scales) are simulated. The dynamics of the small turbulent eddies cannot be captured and have to be parameterized using subgrid-scale (SGS) turbulence models. The results of LES are sensitive to the SGS model formulation and hence significant research efforts have focused on understanding the dynamics of small-scale turbulence and on developing and testing various SGS models for applicability under different conditions.

The focus of this chapter is on the dynamics of these small turbulent scales in the air over the water surface of the lake. Specifically, the aim is to answer the following two questions: 1) How are SGS dynamics over the lake different from SGS dynamics over relatively flat land surfaces? 2) How correlated are SGS fluxes and dissipations of water vapor (a nearly passive scalar) and heat (an active scalar) (Katul and Parlange 1995; Assouline et al. 2008), and if well correlated, could their modeling be coupled/combined in LES.

To answer the first question, one has to look at the effect of water surface dynamics on atmospheric turbulence at the measurement height. LATEX had an average upwind fetch of about 15 km (Fig. 2). The lake is only 3 m deep at the measurement site and turbulence in the

water body is relatively weak and mainly generated by the shear at the air-water interface. During active winds (with a velocity between 1 $m.s^{-1}$ and 10 $m.s^{-1}$), the heights of the waves had a median of about 0.03 m and rarely exceed 0.2 m (note that atmospheric measurements start at a height of 1.65 m); wavelengths were about 8 m on average. Fig. 14 shows the significant wave height $H_{1/3}$, defined as the average of the highest third of the waves, versus wavelength. The wave speed was about 70 % of the wind speed. The wind speed and the friction velocity u_* reached up to 8 $m.s^{-1}$ and 0.3 $m.s^{-1}$ respectively. During low winds (lower branch in Fig. 14), swell (and occasionally boats) generates much longer waves but their heights never exceed 0.05 m. These features suggest that the dynamics of the water surface are relatively weak, mainly local, and atmosphere-driven. Therefore, the LATEX experimental site allows the study of a relatively simple case of atmosphere-water interaction where the effect of the waves on atmospheric turbulence is minimal.

This sets LATEX apart from the only other field experiment designed to study SGS dynamics over water surfaces, the Ocean Horizontal Array Turbulence Study (OHATS, (Sullivan et al. 2006)) which took place over the Atlantic Ocean, off the coast of Massachusetts. The OHATS set-up consisted of two vertically separated horizontal arrays, each having 9 sonic anemometers. Results from that study indicate that the interaction of the atmosphere with the underlying ocean waves in OHATS is an important factor to consider mainly due to low wind conditions and the presence of swell generated far from the measurement site (Sullivan et al. 2006). Under such conditions, the ocean dynamics are not a response to, or in equilibrium with, the local atmospheric dynamics and the effect of the high ocean waves on atmospheric turbulence is important (DeCosmo et al. 1996; Sullivan et al. 2000). Proper understanding and modeling of air-water interactions obviously require a thorough investigation of the two limiting dynamics illustrated by LATEX and OHATS, as well as intermediate regimes. A discussion of different water surface dynamic regimes subjected to the disrupting effects of turbulence and the stabilizing effects of gravity and surface tension can be found in Brocchini and Peregrine (2001a, b).

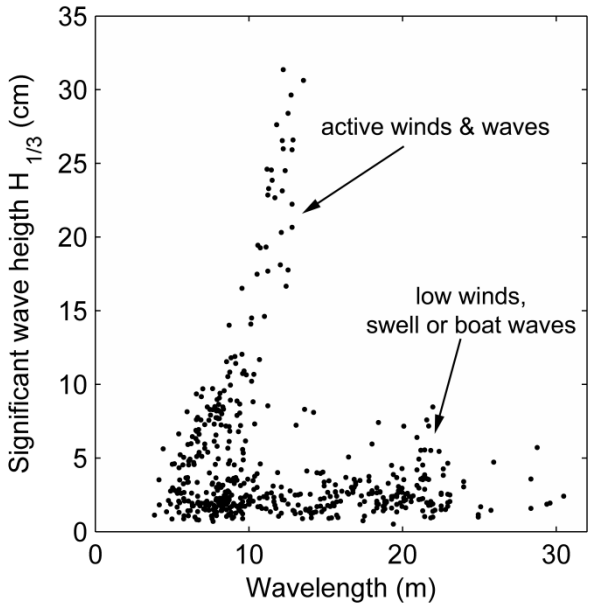

Fig. 14 Significant wave height versus wavelength during the experiment as measured by a submersible level transducer (Pressure systems Inc. model 735; 0.05% accuracy) mounted 1.15 m below water surface.

A novel aspect of LATEX was the high-frequency measurements of water vapor concentrations in the air allowing computation of SGS parameters, testing of SGS models, and derivation of optimal model coefficients for water vapor. The second open question of the chapter can then be addressed by comparing them with the results for heat. The findings are of particular importance since little has been reported in the literature on the SGS dynamics of water vapor, as opposed to numerous studies on heat and momentum dynamics.

A short review of SGS equations and models is presented in the following section, including the formulations of the two SGS models tested in this chapter, the Smagorinsky model and the non-linear model. Section 2.2 describes the experimental site and set-up. The data sets and the processing needed to compute SGS parameters are detailed in section 4.3. Section 4.4 presents transects through the flow (at the resolution afforded by the set-up) illustrating the turbulent structures and their relation to the filter size. The optimal coefficients for the two models and their dependence on filter size and stability are discussed in section 4.5. In section 4.6, we test the ability of the models to reproduce the measured fluxes and dissipations. A comparative analysis of heat and water vapor SGS physics is included in section 4.7. The

chapter concludes with a synthesis of the results addressing the two questions we raised above.

4.2 Subgrid-scale physics

LES of high Reynolds number flows is computationally possible because it resolves only the large eddies that contain most of the energy and perform most of the turbulent transport of momentum and scalars. The large eddies are explicitly captured by solving prognostic equations for their motion. These equations are obtained by applying a filtering operation to the full Navier-Stokes equations to remove the contribution of the unresolved eddies that are smaller than the grid size. The dynamics of these small eddies cannot be captured; however, their effect on the resolved eddies cannot be totally removed by the filtering operation due to non-linear scale interactions. This effect appears in the filtered Navier-Stokes equations as the divergence of the subgrid-scale (SGS) stress defined as:

$$\sigma_{ij} = \widetilde{u_i u_j} - \tilde{u}_i \tilde{u}_j , \tag{23}$$

where u_i , u_j , u_k are the velocity components in three directions and the tilde ($\tilde{}$) denotes the filtering operation. In practice, the isotropic (hydrostatic) part of σ_{ij} is lumped with the pressure term and the equations are written with the divergence of the anisotropic (deviatoric) part

$$\tau_{ij} = \sigma_{ij} - \frac{1}{3}\sigma_{kk}\delta_{ij} . \tag{24}$$

Similar issues arise with the filtered scalar transport equations where the effect of the unresolved scales appears as the divergence of the subgrid-scale fluxes defined as:

$$q_i = \widetilde{u_i b} - \tilde{u}_i \tilde{b} , \tag{25}$$

b being the concentration of a generic scalar such as potential temperature, humidity, etc...

To close the system of filtered equations, a model for the subgrid-scale stress or flux is required. The results of large-eddy simulations are quite sensitive to this model especially in the vicinity of solid boundaries where the subgrid-scale fluxes are the most important and

their physics are harder to model due to the anisotropy of the flow (Meneveau and Katz 2000; Bou-Zeid et al. 2005). A large variety of subgrid-scale models have been proposed in the literature; however, the performance of a given model depends on the flow being simulated, grid resolution, performance assessment criteria, etc. Usually, model validation is performed *a posteriori*, i.e. results from an LES are compared to results for the same flow obtained through experimental measurements or through direct numeric simulation (DNS, which solves the full Navier-Stokes equations for all turbulence scales). Although this *a posteriori* assessment is the most pertinent test for LES and should be performed in model validation, it often does not reveal why a given SGS model works well or not for a given flow.

A complimentary approach for assessing SGS models is *a priori* testing. In this approach, highly-resolved turbulent fields from laboratory or field observations or DNS are filtered to split the turbulent fields into resolved and SGS fields (Meneveau 1994; Tong et al. 1999). The resolved fields are used to model SGS statistics as is done in an LES simulation (for example to compute the resolved strain rate tensor or the model coefficients as in (Germano et al. 1991). These modeled statistics are then compared to the measured statistics obtained from the experimental or DNS SGS fields (Meneveau and Katz 2000; Porte-Agel et al. 2001b).

The most widely used model for the subgrid scales remains the Smagorinsky (1963) model or variants of that model. The model relates the subgrid-scale stress to the resolved strain rate tensor $\tilde{S}_{ij} = 0.5\,(\partial\tilde{u}_i / \partial x_j + \partial\tilde{u}_j / \partial x_i)$ via an eddy viscosity (hence the use of *eddy model* acronym later in this chapter):

$$\tau_{ij}^{eddy} = -2c_S^2\Delta^2 \left|\tilde{S}\right| \tilde{S}_{ij}\,, \tag{26}$$

where $|\tilde{S}| = (2\,\tilde{S}_{ij}\,\tilde{S}_{ij}\,)^{1/2}$ is the magnitude of resolved strain rate tensor, c_s the Smagorinsky coefficient, and Δ is the filter scale. Similarly, the SGS flux of a scalar can be related to the gradient of that scalar via an eddy diffusivity,

$$q_i^{eddy} = -Sc^{-1}c_S^2\Delta^2 \left|\tilde{S}\right| \frac{\partial\tilde{b}}{\partial x_i}\,, \tag{27}$$

where *Sc* is the subgrid-scale turbulent Schmidt number for the scalar *b* (or the Prandtl number, *Pr*, for heat).

Another widely used set of SGS models is derived from the so-called similarity model (Bardina et al. 1980). This approach postulates that the SGS stress is proportional to the turbulent stresses from the smallest resolved scales (between the grid scale Δ and a second test filter scale αΔ). A simpler implementation of the similarity model can be derived by performing a Taylor-series expansion of $\boldsymbol{u}$ yielding the non-linear model (Clark et al. 1979; Liu et al. 1994)

$$\tau_{ij}^{nl} = C_{nl}\Delta^2 \frac{\partial \tilde{u}_i}{\partial x_k}\frac{\partial \tilde{u}_j}{\partial x_k}. \tag{28}$$

For the SGS flux of a scalar *b*, the non linear model yields

$$q_i^{nl} = C_{nl}^{b}\Delta^2 \frac{\partial \tilde{u}_i}{\partial x_k}\frac{\partial \tilde{b}}{\partial x_k}. \tag{29}$$

The coefficients of the Smagorinsky and nonlinear models appearing in equations 26-29 can be computed from LATEX data so that the mean measured SGS dissipation rates of turbulent kinetic energy (TKE, $\langle\Pi\rangle = -\langle\tau_{ij}\tilde{S}_{ij}\rangle$) or scalar variances ($\langle\chi\rangle = -\langle q_i\, \partial\tilde{b}/\partial x_i\rangle$) match the modeled ones (as done in (Porte-Agel et al. 2000b) and (Kleissl et al. 2003) for example). We thus obtain the most suitable coefficients for the Smagorinsky model,

$$c_s^2 = \frac{-\left\langle \tau_{ij}\tilde{S}_{ij}\right\rangle}{2(\Delta)^2\left\langle |\tilde{S}|\tilde{S}_{ij}\tilde{S}_{ij}\right\rangle}, \qquad Pr^{-1}c_s^2 = \frac{-\left\langle q_i^{heat}\frac{\partial\tilde{T}}{\partial x_i}\right\rangle}{\left\langle \Delta^2|\tilde{S}|\frac{\partial\tilde{T}}{\partial x_i}\frac{\partial\tilde{T}}{\partial x_i}\right\rangle}, \qquad Sc^{-1}c_s^2 = \frac{-\left\langle q_i^{H_2O}\frac{\partial\widetilde{\rho_v}}{\partial x_i}\right\rangle}{\left\langle \Delta^2|\tilde{S}|\frac{\partial\widetilde{\rho_v}}{\partial x_i}\frac{\partial\widetilde{\rho_v}}{\partial x_i}\right\rangle}, \tag{30}$$

and for the nonlinear model,

$$C_{nl} = \frac{\left\langle \tau_{ij}\tilde{S}_{ij}\right\rangle}{\Delta^2\left\langle \frac{\partial\widetilde{u_i}}{\partial x_k}\frac{\partial\widetilde{u_j}}{\partial x_k}\tilde{S}_{ij}\right\rangle}, \qquad C_{nl}^{heat} = \frac{\left\langle q_i^{heat}\frac{\partial\tilde{T}}{\partial x_i}\right\rangle}{\left\langle \Delta^2\frac{\partial\widetilde{u_i}}{\partial x_k}\frac{\partial\tilde{T}}{\partial x_k}\frac{\partial\tilde{T}}{\partial x_i}\right\rangle}, \qquad C_{nl}^{H_2O} = \frac{\left\langle q_i^{H_2O}\frac{\partial\widetilde{\rho_v}}{\partial x_i}\right\rangle}{\left\langle \Delta^2\frac{\partial\widetilde{u_i}}{\partial x_k}\frac{\partial\widetilde{\rho_v}}{\partial x_k}\frac{\partial\widetilde{\rho_v}}{\partial x_i}\right\rangle}, \tag{31}$$

where T is the temperature and ρ_v is the water vapor. Even a coefficient that matches the dissipation rates on average cannot guarantee good results, since it only influences the average magnitude of the modeled rates of energy or scalar variance flux/cascade to smaller

scales (in homogeneous isotropic turbulence, the mean SGS fluxes are zero; close to walls, the coefficient will also influence the mean fluxes which are non-zero). Another important aspect is the alignment of the measured and modeled flux tensors (Clark et al. 1979; Meneveau and Katz 2000; Higgins et al. 2003; Higgins et al. 2007) and the mean magnitude and the correlation of their individual components. The correlations of the measured and modeled fluxes and dissipations will be studied for both the Smagorinsky and the non-linear models; however, the focus of the chapter remains on understanding the SGS physics and answering the two questions introduced earlier, rather than testing the limits of a particular model.

4.3 Computation of gradients, fluxes, and dissipations

The site and the setup of the experiment are described in section 2.2. The raw data were collected at 20 Hz using a Campbell Scientific CR5000 data logger and all computations were done afterwards. Pre-processing and data conditioning mainly included triple rotation to correct the yaw, pitch, and roll misalignments of the sonic anemometers, linear detrending, and the Webb correction for fluxes (Webb et al. 1980). All instruments were purchased directly before the experiment and intercompared in the laboratory to ensure good calibration.

We first note that the mean of the temperature and humidity over an averaging period (typically 15 minutes) are subtracted from the signals before computing the subgrid fluxes and gradients of these scalars. This is needed because the accuracy of the means measured by the sonic anemometers (for temperature) and gas analyzers is not always satisfactory; these instruments are much better suited for the measurements of the turbulent deviations. This approach is in accordance with previous field studies of SGS physics (e.g. (Porte-Agel et al. 2001b) and (Kleissl et al. 2003)) and implies that the effects of mean gradients and interactions with the mean flow (for scalars) will not be captured; these effects should not be very critical at the turbulence scales we are studying. The components of the SGS stresses and fluxes are computed according to their definitions in equations 23 to 25. The filtering operation needed in these equations was performed in two dimensions (which was found to be equivalent to filtering in three dimensions with a filter size reduced by about 16 % by (Higgins et al. 2007). The 20 Hz data were first filtered in the vertical direction using a box

filter of size 2*dz* = 1.3m. This operation was applied separately to the upper three sonic-Licor pairs and to the lower ones as depicted in Fig. 15 (left side). Taylor's frozen turbulence hypothesis was then employed to transform the two box-filtered time series into streamwise spatial series. This transformation allowed the application of a Gaussian filter (of any size Δ) in the streamwise direction, yielding two spatial data series labelled as P1 (for the lower three sonic-Licor pairs) and P2 (for the upper three pairs) in Fig. 15 (right side). The gradients of filtered quantities were needed in all three directions. The points around which these gradients were computed are points P1 in Fig. 15 coinciding with sonic-Licor pair number 2 at a height *z* = 2.3 m. The vertical gradients were computed using first order one-sided finite differences (FD) between points P1 and P2. The streamwise gradients were computed using a fourth-order centered differences (CD) scheme applied to the data stream P1, assuming Taylor's hypothesis. The *dx* step was taken to be equal to *dz* (see (Kleissl et al. 2003)). Tests performed for this study show that using second-order CD in the streamwise direction made no significant difference in the results.

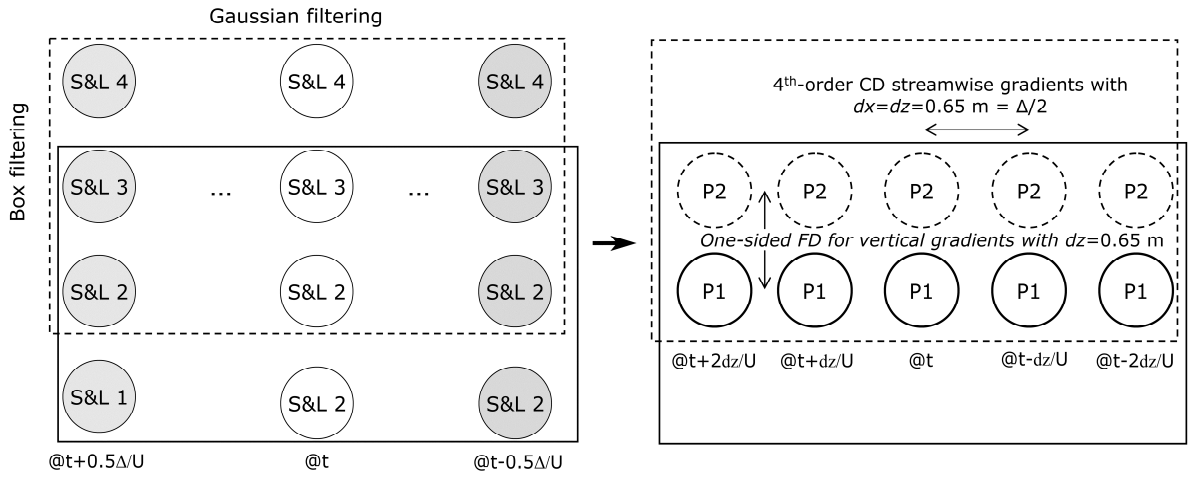

Fig. 15 Filtering and gradient computations in LATEX.

The cross-stream gradients could not be computed from the experimental settings since that would require at least two vertical arrays at two cross stream locations. We can however approximate the computations by assuming turbulence isotropy or by ignoring the missing terms and effectively computing the two dimensional (2D) surrogates (in the x-z plane) of the fluxes and gradients. The first approach (isotropy assumption) is usually preferable but it is

problematic to apply for this data set since, for momentum, it involves assuming turbulence isotropy in all three directions which implies setting the missing contractions $\overline{\tilde{S}_{12}\tilde{S}_{12}}$ and $\overline{\tilde{S}_{23}\tilde{S}_{23}}$ equal to $\overline{\tilde{S}_{13}\tilde{S}_{13}}$ and $\overline{\tau_{12}\tilde{S}_{12}}$ and $\overline{\tau_{23}\tilde{S}_{23}}$ equal to $\overline{\tau_{13}\tilde{S}_{13}}$. These assumptions are not very realistic in a wall bounded flow at such a small distance from the surface since the computed vertical gradient $\tilde{S}_{13}$ and flux τ_{13} will be higher than the (1,2) and (2,3) components. Subtraction of the means of $\tilde{S}_{13}$ and τ_{13} could be performed but will not solve the problem since the turbulent part will not be isotropic either. For scalars, isotropy can be assumed in the horizontal directions only but for the non-linear model this would transform some cross-product terms into streamwise quadratic terms (in the denominators of equation 9). To avoid these issues, the 2D surrogates of the fluxes and gradients are computed, i.e. only the x and z components are included in the analysis. This approach is justifiable on the basis that the vertical components are expected to be much larger close to the surface and the cross-stream terms contribution to the tensor contractions in equations 30 and 31 will be small. The only cross-stream term that we include is dv/dy appearing in the strain rate tensor $\tilde{S}_{ij}$, this term can be accurately estimated from the continuity equation as: $dv/dy = -(du/dx+dw/dz)$ and its inclusion is expected to improve the estimate $\tilde{S}_{ij}$.

To check the effect of these assumptions, various tests were done (only feasible with the Smagorinsky model) and the effect of the treatment of the missing cross-stream gradients on the results was found to be minimal. When the isotropy assumption was tested, we noticed slight changes in the values of the optimal model coefficients for momentum and scalars and a small decrease in the effect of stability on these coefficients compared to those obtained with the adopted 2D surrogate approach. This indicates either that the contribution of the missing terms is not important or that their trends are the same as the other terms that are computed and included (vertical and streamwise). The approach we selected is however the most realistic and gives the results that best match previous *a priori* studies. It gave indeed the same value of c_s at neutral atmospheric stability as (Kleissl et al. 2003) and (2004), whereas assuming isotropy and removing the means of $\tilde{S}_{13}$ and τ_{13} gave slightly lower values. In addition, it allows the comparison of the two SGS models.

The averaging operation (or the computation of correlations later in the chapter) is always performed over 15-minute time intervals. This was the base period for all runs and each run yields one data point (model coefficient, correlation, …). For some aspects of the analysis, data from the 15-minute runs were subsequently conditionally averaged based on atmospheric stability.

4.4 Flow structures

To compare the filter scale to the size of the eddies at the measurement heights, we first look at vertical slices of the streamwise and vertical turbulent wind velocities, as well as the turbulent components of temperature and moisture depicted in Fig. 16. A low-pass filter of size 0.65 m is applied in the streamwise direction to match its frequency content with the vertical direction (following (Porte-Agel et al. 2000b)); however, note that the actual resolution in the streamwise direction is typically much higher than the grid displayed in Fig. 16 (resolution = wind speed / sampling frequency). Well defined flow structures can be identified. The strong correlation between w', T' and q' and their anti-correlation with u' are also visible indicating that these slices correspond to a period of upward heat flux $\langle w'T' \rangle$, moisture flux $\langle w'q' \rangle$ and downward momentum flux $\langle w'u' \rangle$. Most of the measurements of LATEX correspond to periods of unstable stratification as measured by the stability parameter

$$\frac{z}{L} = \frac{z\kappa g\, \overline{w'\theta_v'}}{-u_*^3 \overline{\theta_v}}, \tag{32}$$

where z is the measurement height, L is the Obukhov length scale, u_* is the friction velocity, θ_v is the virtual temperature, and κ is the von Karman constant, g is the gravitational constant, and the overbar denotes averaging, which in this chapter is performed in time over 15 minutes. Unstable stratification corresponds to negative values of z/L. We note that even when the sensible heat flux was downward suggesting stable stratification, the latent heat flux was upward and frequently balanced the stabilizing effect of the sensible heat flux. Values recorded for the sensible heat flux H during the experiment ranged approximately between -15 W.m^{-2} and 40 W.m^{-2}, while the latent heat flux LE was always positive and higher than the sensible heat flux but rarely exceeded 150 W.m^{-2}. The combined effect of temperature and moisture on density and stability is given by the virtual temperature in the formulation of z/L.

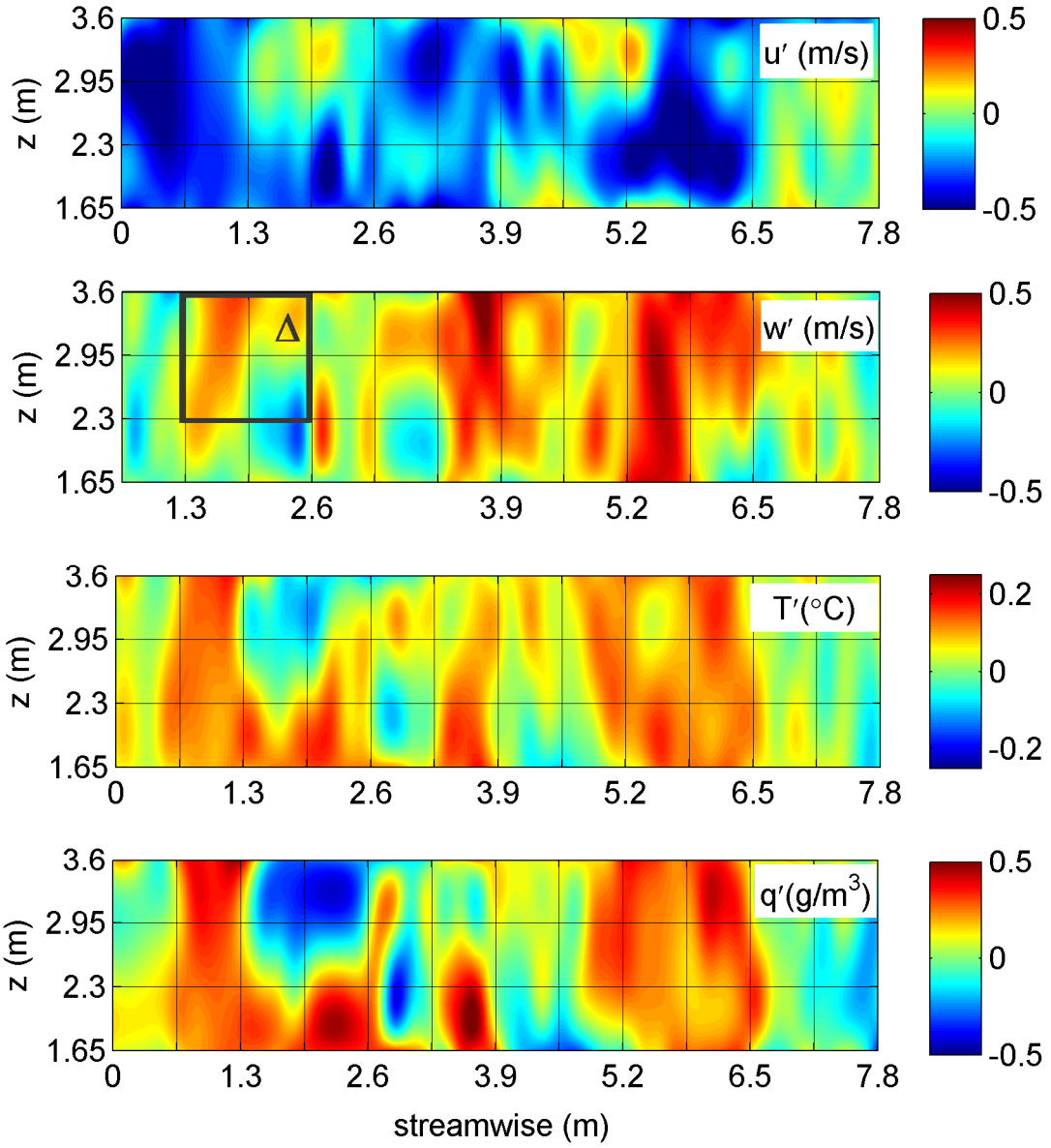

Fig. 16 Contour plots in a vertical plane of the turbulent components of the streamwise and vertical velocities, temperature, and moisture. The bold black square depicts the size of the filter. The horizontal grid lines show the vertical locations of the 4 sensors. The vertical grid lines show "virtual" streamwise locations of the sensors after applying Taylor's hypothesis and filtering out scales smaller than *dx* = *dz* = 0.65 m from the streamwise signal. The intersections of the grid lines can be interpreted as grid nodes where the flow is sampled to produce these slices. The turbulent components for this figure are computed based on 1-minute averages to filter out the very large scales.

Fig. 16 also illustrates that eddies with sizes on the order of 1 m are quite active in carrying vertical fluxes. This size can be compared to the basic filter size Δ = 1.3 m used in this chapter and depicted by the bold square in Fig. 16. The relative size of the structures is often comparable to or smaller than the filter size. This underscores the importance of SGS fluxes and dynamics in the vicinity of boundaries (in the friction layer) in LES of high Reynolds-number flows where the viscous sublayer cannot be resolved (Pope 2004). In this limit, the SGS fluxes contribute a significant amount to the total fluxes, more than only dissipating TKE from the resolved scales. We found that the SGS contribution could be up to 40% of the total vertical fluxes of momentum and scalars.

4.5 Dependence of SGS model coefficients on filter size, height, and stability

The values for the model coefficients obtained from equations 30 and 31 were computed and their variation with the stability parameter z/L was investigated for various filter sizes Δ. As previously discussed, most LATEX data were taken under unstable conditions and we hence restrict our analysis to variations of the coefficients with $z/L<0$. Furthermore, we note that the box filter size in the vertical direction is limited to 1.3 m by the set-up of the experiment, whereas the horizontal Gaussian filter size can be varied. The filter size reported here is the effective size $\Delta = (\Delta_{vertical} \, . \, \Delta_{horizonal})^{1/2}$. The anisotropy of the filter resulting from this approach can affect the results, as will be discussed.

The Smagorinsky coefficient c_s is expected to increase with increasing height to filter size ratio z/Δ to reflect the increasing mixing length $c_s\Delta$ (see for example (Mason and Thomson 1992)). On the other hand, it is often assumed that the effect of atmospheric stability on the Smagorinsky coefficient is negligible under unstable conditions (whereas the coefficient decreases sharply under stable conditions, (Kleissl et al. 2004)). This assumption of a constant c_s (for a given z/Δ) under unstable conditions implies that increased mixing due to buoyancy in unstable boundary layers has little effect on the turbulence structure. A review of previous studies ((Porte-Agel et al. 2001a); (Kleissl et al. 2004) for example) that did not report any sensitivity to increasing instability reveals that these studies were mostly restricted to mildly unstable ABLs ($-z/L$ lower than 1). Other experimental studies (Chamecki et al. 2007)

reported a continuous increase in c_s as the instability (measured by using the Richardson number) increased.

During LATEX, higher values of $-z/L$ were observed due to the smoothness of the water surface (under low wind conditions) keeping u_* low, while allowing the heat fluxes to reach values similar to what is observed over land (latent and sensible heat fluxes sometimes exceeded 150 $W.m^{-2}$ and 40 $W.m^{-2}$, respectively). The resulting data indicate that c_s values are significantly affected by stability. Fig. 17 depicts the profile of c_s as a function of z/Δ for different classes of stability: near neutral ($0< -z/L <0.1$), unstable ($0.1< -z/L <1$), and very unstable ($1 < -z/L$). We note that for $z/\Delta =1.77$, the filter is square; as we depart from this value, the filter becomes rectangular. To discriminate between the effect of the filter anisotropy and the filter size, we apply a correction for the anisotropy as proposed by (Scotti et al.)(1993). The same results, but with c_s values corrected for filter anisotropy, are presented in Fig. 18 (all previous studies usually only use square filters). The values of c_s increase with the height-to-filter ratio z/Δ for all stabilities, as expected. The effect of increasing instability is to increase the integral scale and vertical mixing. This seems to flatten the profile of c_s as the shear is reduced and the variations of SGS dissipation with filter scale decrease. Depending on the value of z/Δ, c_s might increase or decrease with stability.

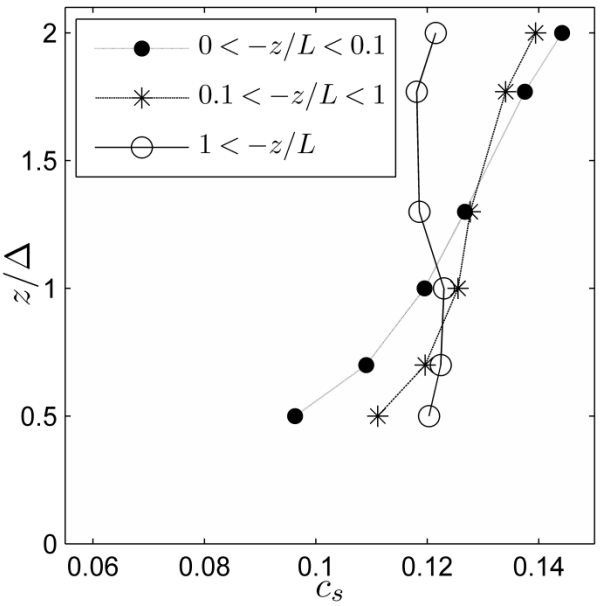

Fig. 17 Conditional averages of c_s, for 3 different classes of stability, versus z/Δ.

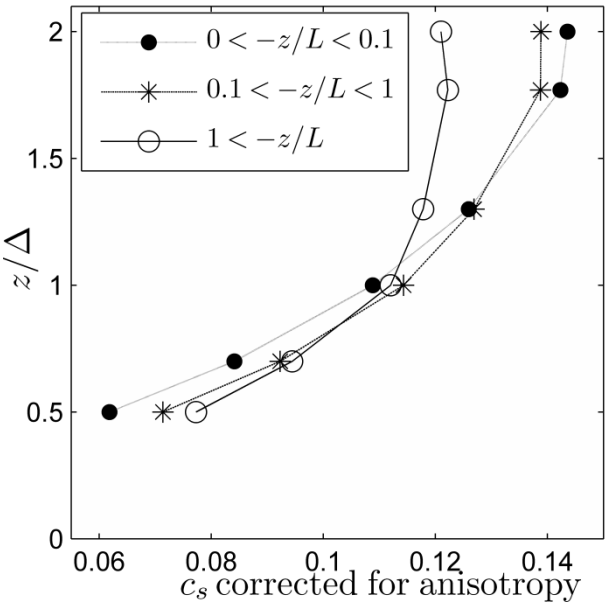

Fig. 18 c_s corrected for anisotropy ((Scotti et al. 1993)), versus z/Δ for 3 classes of stability.

The measured SGS Schmidt number is shown in Fig. 19 for Δ = 1.3 m (square filter). The approximate value of *Sc* is around 0.3 and shows a decrease from around 0.37 at near neutral stabilities to around 0.27 under highly unstable conditions. Note that here we quantify stability in terms of Δ/L which is proportional to z/L since we have a constant ratio z/Δ = 1.77. The value of 0.3 is very close to values reported in the few other studies that investigated the subgrid-scale Schmidt number through the dynamic SGS approach of Germano et al. (1991). Pitsch and Steiner (2000) found a value of *Sc* around 0.4 in (compressible) LES of a methane-air flame. Stoll and Porte-Agel (2006) obtained a value of about 0.3 away from the wall for a passive scalar in a neutral boundary layer, increasing as the wall approached to around 0.4 at z/Δ=1 (further increase was noticed at lower z/Δ but those points are likely to be significantly affected by the wall-model). A value of about 0.3 was again obtained through a dynamic model by Mitsuishi et al. (2003) for mass transfer across an air-water interface. While to the best knowledge of the authors, no previous *a priori* determination of the SGS Schmidt number for a passive scalar has been performed, the available evidence suggests that a value of subgrid-scale *Sc* in the range of 0.3 to 0.4 holds well for a wide variety of flows. This is

remarkable and underlines a basic strength of large eddy simulation: the subgrid-scales have universal properties and are easier to model than the full turbulence spectrum required in Reynolds-averaged Navier-Stokes (RANS) simulations. Note also that the value of the SGS Schmidt number of 0.3 is significantly lower than the 0.7 typically used in RANS to account for all turbulent scales, although the optimal value for RANS is known to be more flow dependent (see for example (Yimer et al. 2002)).

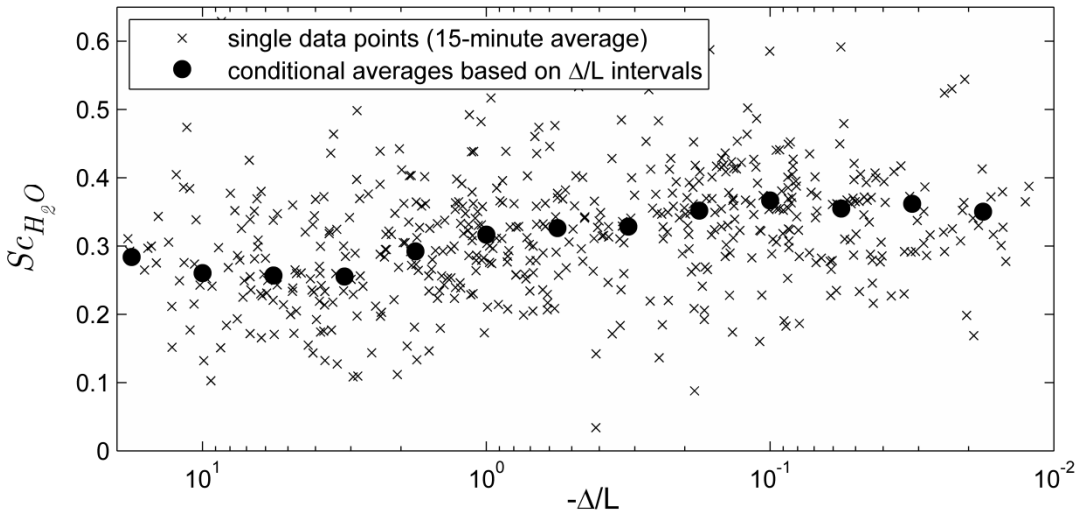

Fig. 19 The measured SGS Schmidt number for water vapor as a function of stability.

The measured SGS Prandtl number depicted in Fig. 20 shows a trend similar to that of the Schmidt number with a more significant sensitivity to stability. *Pr* displays a clear decrease with increasing buoyancy going from around 0.38 at neutral stability to around 0.2 under highly unstable conditions. This indicates that the relative efficiency of heat transport increases in comparison with the efficiency of momentum transport as the surface layer becomes more unstable. The trend of increasing *Pr* as we approach neutral conditions is in agreement with the model used by Brown et al. (1994) and Mason and Brown (1999); however, the values do not match. That model predicts a value of $Pr \approx 0.7$ at neutral stability decreasing to 0.44 under highly unstable conditions. The 0.38 value that we obtain at neutral stability is closer to the estimate of 0.47 by Mason (1989), who matched the subgrid-scale dissipation and its estimate based on the Kolmogorov theory in the inertial subrange (similar

to the approach of Lilly, (1967), for c_s). We again note that the SGS Prandtl number is lower than the 0.7 typically used in RANS (Pope 2000) although, as we noted for the RANS Schmidt number, the RANS Prandtl number is highly flow dependent (see review in (Kays 1994)).

The variation of *Pr* with stability seems to be related to the active role of temperature since smaller variations are observed for the *Sc* of water vapor, a passive scalar. However, as the stability tends to neutral, the temperature field becomes almost homogeneous and the accuracy of the measurements of temperature variations tends to decrease. This explains the increased scatter of *Pr* values for single data points at low -Δ/*L* (Fig. 20) and indicates that more analysis is needed to confirm and explain the physical basis of the increase of *Pr* as the stability tends to neutral. This however will be left to future investigations based on results from LATEX and other field experiments.

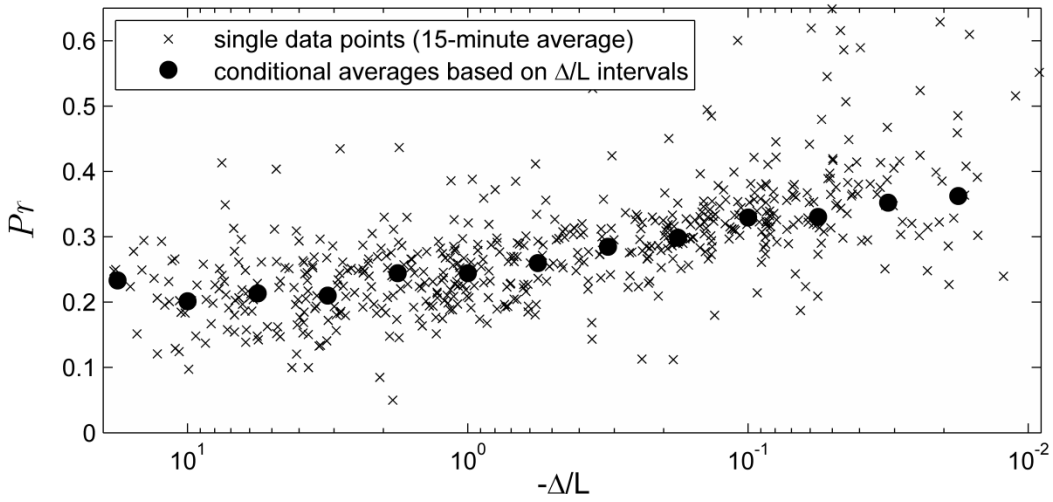

Fig. 20 The measured SGS Prandtl number for heat as a function of stability.

The variations of Prandtl and Schmidt numbers with the height to filter size ratio z/Δ are shown in Fig. 21 and Fig. 22, for different stability ranges. A decrease of about 30% is observed for both numbers as the filter size decreases (z/Δ increases). The effect of the filter size is hence considerably smaller than for the Smagorinsky coefficient which doubled as z/Δ increased from 0.5 to 2 (Fig. 18). A very similar effect of z/Δ on *Pr* was observed by (Porte-

Agel et al. 2001b) (where all three dimensional components were available and the filter size varied by actually changing the experimental set-up), although their values were 5 to 10% higher than the values reported here. This decrease of *Pr* and *Sc* and the coinciding increase of c_s as the filter size decreases indicates that the effect of the filter size on the SGS diffusivities of heat and water vapor ($\approx c_s^2/Pr$) is smaller than its effect on the eddy viscosity for momentum ($\approx c_s^2$).

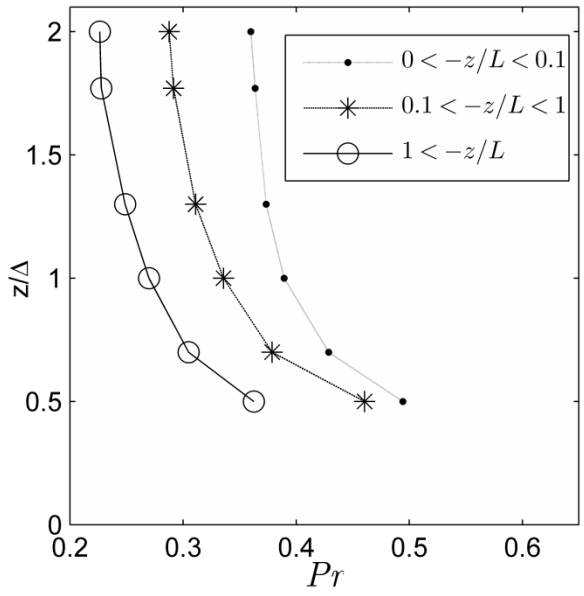

Fig. 21 Conditional averages of *Pr*, for 3 different classes of stability, versus *z*/Δ.

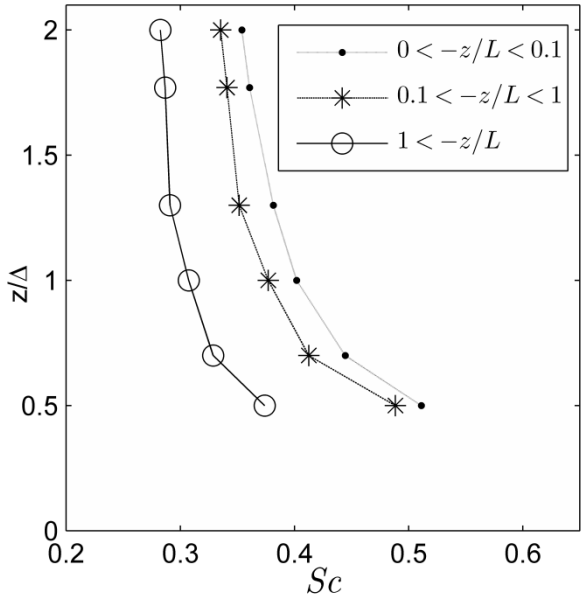

Fig. 22 Conditional averages of *Sc*, for 3 different classes of stability, versus *z*/Δ.

The variation of the nonlinear model coefficients with filter size and stability was also investigated and we observed an increase of the coefficients with increasing *z*/Δ. However, unlike with the Smagorinsky coefficients, there is no analytic correction for filter anisotropy; this makes it difficult to distinguish between the effect of the filter size and aspect ratio. Therefore we only report results obtained with the square filter, with a subsequent height to filter size ratio of *z*/Δ = 1.77. For this ratio, the nonlinear model coefficients were found to be not very sensitive to variations in stability. The values of C_{nl} for heat and water vapor were very close, both around 0.35. This value is close to the value observed by Porte-Agel et al. (2001b, Fig.11) for neutral conditions (they report an increase under stable conditions which

we cannot check here). For momentum, the value of C_{nl} was found to vary between 0.2 and 0.4.

4.6 Effect of filter size on modeled fluxes and SGS coefficients

Even if the optimal coefficient is used in LES, the modeled fluxes will not be identical to the measured SGS fluxes. The models imply that the SGS stress tensor is aligned with the strain rate tensor (Smagorinsky model) or with the resolved stress tensor (similarity models) and that the model coefficients are constant over the averaging period or direction. In reality, the alignment assumption is not accurate (Liu et al. 1994; Tao et al. 2002; Higgins et al. 2003) and the optimal model coefficients vary considerably in space and time. The realistic aim of an SGS model is therefore to yield accurate SGS and resolved statistics, rather than to reproduce exact SGS fluxes locally in time and space. In spite of these arguments, an often used indicator of the realism of an SGS model is the correlation coefficient between individual components of the measured and modeled stress or flux tensors/vectors. As discussed in many references dealing with LES and SGS models (e.g. Meneveau & Katz, 2000), good correlation coefficients may be observed for SGS models that still do not perform well in LES (such as the similarity model on its own). Therefore, results from such a-priori correlation analysis must be interpreted carefully and we use them here to probe the alignment trends and physics of SGS fluxes rather than to validate the models. In addition, correlations have been reported in many other references dealing with SGS modeling and LES (e.g. (O'Sullivan et al. 2001; Sullivan et al. 2003)) and here we have the opportunity to compare the correlation coefficients trends for water vapor with previously observed trends for heat and momentum.

Another interesting parameter to analyze is the correlation of measured and modeled dissipations. Matching these dissipations averaged over 15 minutes allowed us to compute the optimal coefficients; however, the correlation coefficients of the instantaneous modeled and measured dissipations (within the 15 minute run) will indicate how well the model captures the unsteady dynamics of SGS dissipation. This correlation will hence reflect the variability of the model coefficient and is insensitive to the tensor misalignment.

All correlation coefficients are computed from the instantaneous values of fluxes or dissipations during a period of 15 minutes (yielding one correlation value per run). This computation is repeated for all runs yielding a data set of correlation coefficients. The following results in this section present probability density functions of these correlation data sets or report their medians and standard deviations.

The probability distribution of the correlations between measured and modeled vertical fluxes of water vapor is depicted in Fig. 23 (for both models), for the square filter yielding $z/\Delta = 1.77$. As frequently reported in the literature, the non-linear model performs better than the Smagorinsky model. The same results but for the correlations of variance dissipations are presented in Fig. 24. Again we observe that the non-linear model is better correlated with the measurements. Note that the correlations of the dissipations are significantly higher than the correlations of the fluxes.

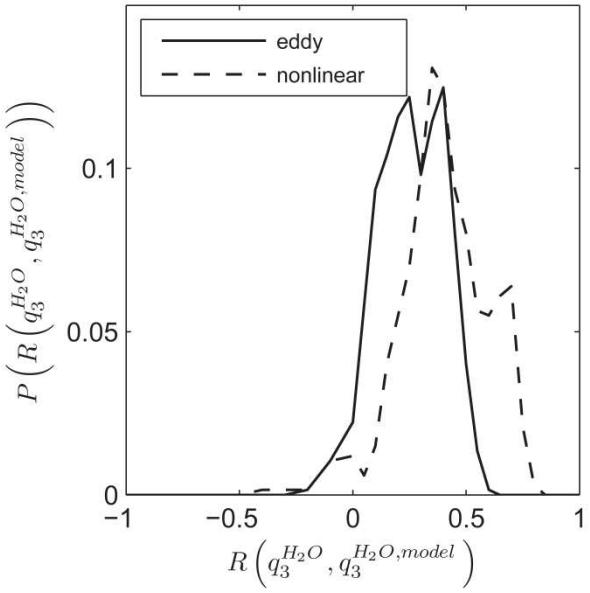

Fig. 23 Distribution of the correlations between measured and modeled vertical water vapor fluxes.

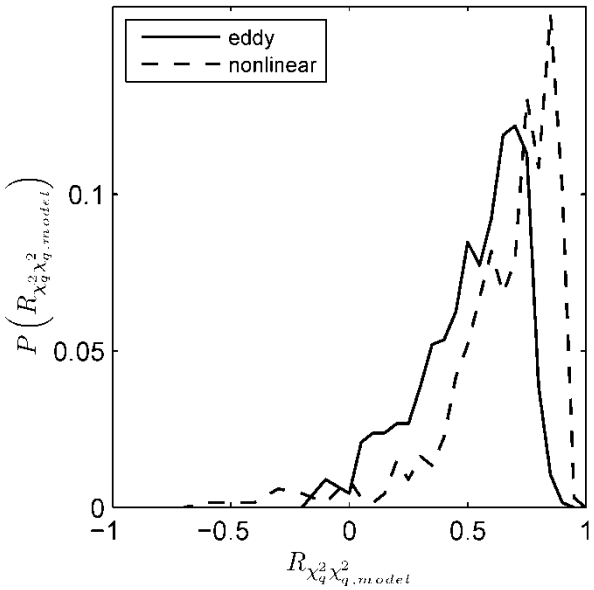

Fig. 24 Distribution of the correlations between measured and modeled dissipations of water vapor variance.

Since the SGS dynamics depend strongly on the filter size Δ ((Pope 2004)), it is interesting to compare how the correlations vary with Δ. However, the relative magnitude of Δ compared to the characteristic size of turbulent eddies is more important than the absolute value of the

filter size. A surrogate of the integral scale of turbulence in wall bounded flows is the height above the ground z. Hence, we analyze the correlations as a function of z/Δ. As previously noted, the stability parameter z/L is also important and will affect the integral scale of turbulence; however, in this work, we do not assess the sensitivity of the correlations to stability.

The medians and standard deviations of the distributions depicted in the figures above are listed for different z/Δ ratios in Table 1. Also included in the table are the correlations for the streamwise fluxes and for heat, for both models. The first part (4 lines) of the table reports the correlations for streamwise and vertical heat fluxes. All correlations seem to peak around $z/\Delta \approx 1$ and decrease for any changes in z/Δ thereafter. In the streamwise direction, the non-linear model performs much better than the eddy model; however, its advantage decreases at low z/Δ. In the vertical direction, the performance of the two models is close and, surprisingly, the eddy model gives much higher correlation at low z/Δ.

This comparative change in correlation behavior as z/Δ decreases indicates that, as the grid size Δ increases and the LES filtering tends to the Reynolds average (close to walls), the validity of eddy viscosity hypothesis for relating fluxes and strains improves (at least in comparison to the scale similarity hypothesis, which is more appropriate for inertial range turbulence, far from walls). As discussed above, these near wall regions are typically the most critical for an SGS model (highest SGS fluxes and dissipations); the relatively higher correlations of the Smagorinsky model in these regions is a very significant result.

The second part of the table (lines 5-8) presents the same results but for water vapor. We observe the same peak in the correlations at about $z/\Delta \approx 1$ with correlations higher for the streamwise than the vertical flux component. The non linear model again displays higher correlations in general except for low z/Δ values. Overall, the correlations for moisture are slightly lower than for heat; this could be due to lower accuracy in moisture measurements.

The last part of the table reports the correlation between modeled and measured dissipations for heat and water vapor. As for fluxes, a peak of correlations is again clear at $z/\Delta \approx 1$, and temperature yields higher correlation than moisture. The overall correlations are higher than

the correlation for fluxes; such increased correlations for "scalar-level" a-priori tests based on dissipation instead of fluxes was already observed in the first a-priori tests in turbulence (Clark et al. 1979). The non-linear model correlates better with measurements but the difference with the eddy model decreases at low z/Δ.

Table 1 Median (standard deviations in parentheses) of the correlations between the measured and modeled fluxes for different height to filter ratios

	$z/\Delta = 0.5$	$z/\Delta = 0.7$	$z/\Delta = 1$	$z/\Delta = 1.3$	$z/\Delta = 1.77$	$z/\Delta = 2$
$q_1^{heat}, q_1^{heat,eddy}$	0.40 (0.18)	0.42 (0.17)	0.39 (0.15)	0.35 (0.13)	0.28 (0.11)	0.26 (0.10)
$q_1^{heat}, q_1^{heat,NL}$	0.54 (0.31)	0.65 (0.26)	0.74 (0.22)	0.75 (0.22)	0.69 (0.22)	0.66 (0.21)
$q_3^{heat}, q_3^{heat,eddy}$	0.43 (0.14)	0.47 (0.13)	0.49 (0.13)	0.48 (0.14)	0.44 (0.14)	0.42 (0.13)
$q_3^{heat}, q_3^{heat,NL}$	0.24 (0.17)	0.39 (0.16)	0.58 (0.17)	0.68 (0.18)	0.61 (0.18)	0.54 (0.17)
$q_1^{H2O}, q_1^{H2O,eddy}$	0.36 (0.17)	0.34 (0.15)	0.28 (0.14)	0.22 (0.12)	0.17 (0.10)	0.15 (0.10)
$q_1^{H2O}, q_1^{H2O,NL}$	0.47 (0.31)	0.53 (0.28)	0.57 (0.25)	0.52 (0.25)	0.44 (0.24)	0.41 (0.24)
$q_3^{H2O}, q_3^{H2O,eddy}$	0.38 (0.16)	0.39 (0.15)	0.38 (0.15)	0.34 (0.15)	0.26 (0.14)	0.23 (0.14)
$q_3^{H2O}, q_3^{H2O,NL}$	0.21 (0.17)	0.33 (0.18)	0.49 (0.18)	0.51 (0.20)	0.4 (0.19)	0.34 (0.17)
$\chi^{heat}, \chi^{heat,eddy}$	0.58 (0.21)	0.64 (0.18)	0.72 (0.19)	0.75 (0.20)	0.70 (0.19)	0.66 (0.19)
$\chi^{heat}, \chi^{heat,NL}$	0.64 (0.32)	0.75 (0.26)	0.86 (0.21)	0.90 (0.20)	0.84 (0.22)	0.80 (0.20)
$\chi^{H2O}, \chi^{H2O,eddy}$	0.53 (0.23)	0.59 (0.21)	0.64 (0.21)	0.65 (0.21)	0.57 (0.21)	0.52 (0.20)
$\chi^{H2O}, \chi^{H2O,NL}$	0.59 (0.32)	0.70 (0.29)	0.80 (0.25)	0.82 (0.23)	0.73 (0.23)	0.66 (0.23)

4.7 Comparison between heat and moisture SGS dynamics

Several studies of subgrid-scales heat fluxes can be found in the literature ((Porte-Agel et al. 1998) for example), but little has been published about moisture fluxes, as noted earlier. LATEX is the first experimental set-up that allows the computation of SGS fluxes and dissipation for water vapor and it is therefore of interest to compare the dynamics of moisture fluxes and dissipations to heat fluxes and dissipation. The goal is to investigate under what conditions the dynamics are sufficiently correlated to realistically combine the modeling of the two SGS dynamics in LES. The gradients of the heat and water vapor would still be

calculated separately of course but dynamic determination of the model coefficients (Germano et al. 1991) could be combined if the two components are well correlated.

Fig. 25 depicts strong correlation between the vertical SGS heat and water vapor fluxes (similar correlations, not shown here, are obtained for streamwise fluxes). Fig. 26 shows even higher correlations between the dissipation of heat and of water vapor variances (peaks above 85%). Again, the effect of the filter size is investigated for sizes that do not entail significant filter anisotropy (recall that the square filter yields $z/\Delta = 1.77$). One observes an increase in the correlation when the size of the filter increases. This indicates that at larger scales, where the dynamics are more averaged, the correlation between the two scalars is stronger. Conceptually, at the largest scale (the mean), the two fluxes are either upwards or downwards and the correlation tends to 1 (or -1 if the mean fluxes are opposite). The large coherent structures maintain high correlations at large scales since they almost act like convection. Further down in the turbulence cascade process, in the inertial subrange, the two scalars de-correlate. This trend was clearly visible in a coherence spectrum (which can be viewed as a frequency dependent correlation coefficient) of temperature and humidity (not shown here). The spectrum was above 0.9 for all the low frequencies and started to decrease only in the highest frequency decade (i.e. for scales smaller than 0.5 seconds).

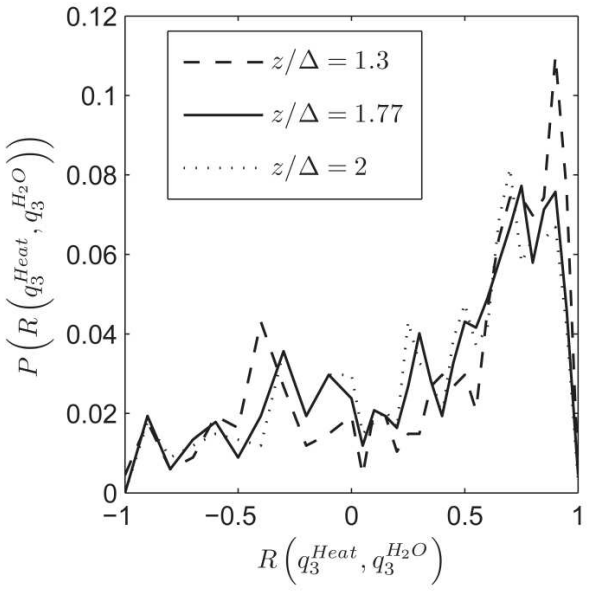

Fig. 25 Distribution of the correlations (based on 15-minute periods) of vertical heat and moisture fluxes and variation with *z*/Δ.

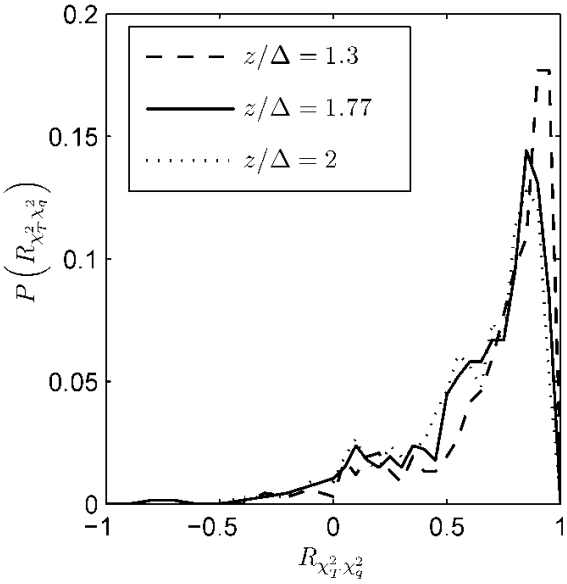

Fig. 26 Distribution of the correlations (based on 15-minute periods) of heat and moisture variance dissipations and variation with *z*/Δ.

The strong correlations observed above encouraged us to look at the correlation between the model coefficients for water vapor and heat. As previously illustrated, these coefficients vary with stability and filter size and the question hence is whether their variations with these parameters are similar (only for unstable conditions with $z/L < 0$). For the Smagorinsky model, the plot of *Pr* versus *Sc* on the left hand side of Fig. 27 shows a very robust linear relation between the two numbers that is not sensitive to stability or filter size. A bisquare linear fit for all the data yields a Schmidt number about 7% higher than the Prandtl number. The right hand side of Fig. 27 depicts the relation of the two coefficients of the non-linear model and a bisquare linear fit (solid line in figure). We again observe good correlation between the two coefficients with C_{NL}^{heat} roughly 11% higher than C_{NL}^{H2O} according to the fit. For both models, one can note that the correlation improves considerably when the size of the filter increases; this is attributed to the increase in the correlation of humidity and temperature fields with scale, which we observed in a coherence spectrum as discussed above. We also observed (trend not illustrated in Fig. 27) that the correlation tends to improve as the atmospheric instability ($-z/L$) increases. The total correlation coefficient for all filter sizes is

about 65% for both models (ranging, for the coefficients of the non-linear model, from 33% for $z/\Delta = 1.77$ to 73% for $z/\Delta = 0.5$, and for the Smagorinsky model, from 38% at $z/\Delta = 1.77$ to 75% at $z/\Delta = 0.5$).

The good linear relations of the coefficients for heat and water vapor in both models suggest that a dynamic determination of only one of the coefficients could be sufficient. The other coefficient can then be imposed based on the fits proposed here. This would save significant computational time and complexity in large eddy simulation. Moreover, this suggests that dynamic coefficients for other passive tracers can also be computed from the coefficients of heat or water vapor via simple linear relations.

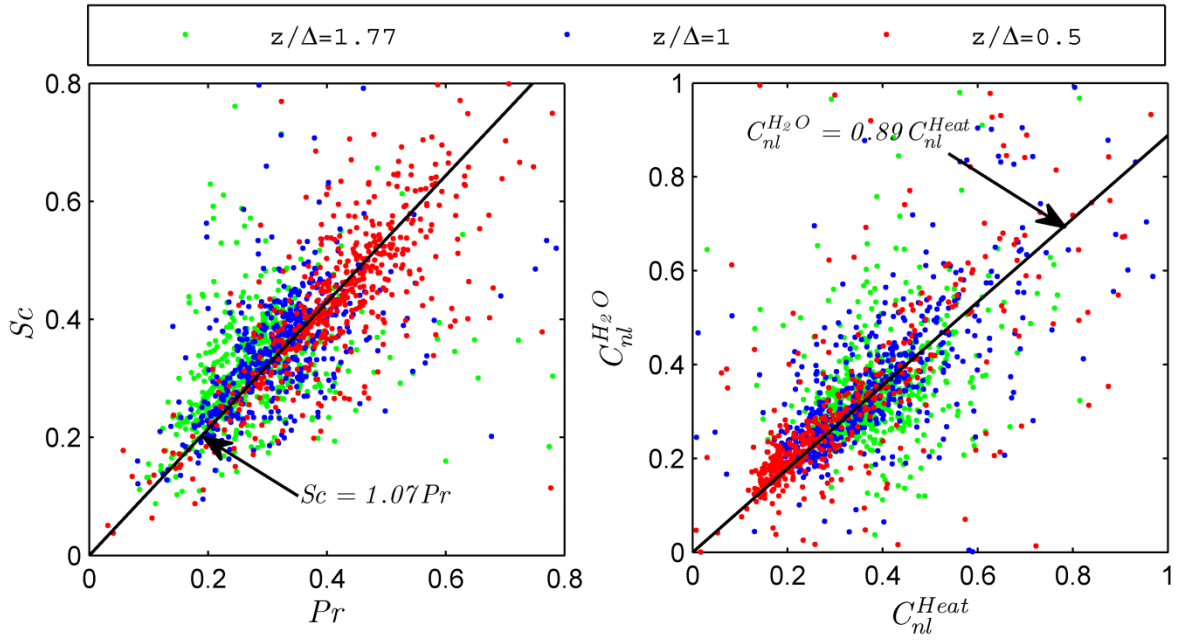

Fig. 27 Relations between model coefficients for heat and water vapor for three different filter sizes, on the left for the Smagorinsky model (*Sc* versus *Pr*) and on the right for the nonlinear model.

4.8 Conclusions

Measurements from the Lake-Atmosphere Turbulent Exchanges Experiment (LATEX) were analyzed to study specific aspects of subgrid-scale modeling for large eddy simulation. The data analyzed here mainly consisted of high frequency measurements of wind, temperature

and humidity that can be used to study actual SGS dynamics and compare them to modeled ones; we tested the Smagorinsky (eddy) model and the nonlinear model. The main goals of the chapter were to: 1) compare SGS dynamics over the lake to the dynamics over flat land surfaces, 2) study SGS fluxes and dissipations of water vapor (a passive scalar) and compare them to fluxes and dissipations for heat (an active scalar). The following observations help us address the first goal of the chapter:

1. The variations and values of the Smagorinsky model coefficient obtained over the lake (Fig. 18) were similar to the ones observed over land (Porte-Agel et al. 2001b; Kleissl et al. 2003). However, we detected more sensitivity of the model coefficients to stability mainly due to the fact that LATEX was able to reach much higher values of $-z/L$ than previous studies over land.

2. The SGS Prandtl and Schmidt numbers showed relatively mild variations with filter scale and stability (*Pr* being more sensitive to stability than *Sc*). These variations and the values of the two coefficients were similar to those obtained in other field experiments and through dynamic models for many types of flow.

3. The non-linear SGS model coefficients showed little sensitivity to stability and the values were comparable to values obtained at neutral stabilities over land (Porte-Agel et al. 2001a)

4. The correlations between measured and modeled SGS fluxes and dissipations (Table 1) were slightly lower than the values reported over land surfaces (Porte-Agel et al. 2001b); though this is likely due to the details of the analysis (mainly the vertical filtering and use of 2D surrogates in this chapter).

From the above, we conclude that the turbulent subgrid-scales over the lake obey the same dynamics observed over land. No significant effect of the moving interface could be detected. Of course, the momentum and heat fluxes over the lake are different from those over land; however, variations in these parameters affect SGS dynamics in the same way over land and water. These findings can only be confirmed for water surfaces where the wave heights are low compared to the measurement height as is the case during LATEX (Fig. 14) and where the dynamics of the surface exchanges are mainly controlled by the atmospheric flow.

To address the question relating to the similarities between water vapor and heat SGS dynamics we note that:

1. The fluxes and dissipation of heat and water vapor show high correlations (Fig. 25 and Fig. 26)

2. The model coefficients for heat and water vapor are closely related for both the eddy and non-linear model and the relations are not sensitive to stability or filter size (Fig. 27).

3. The variations of the correlations, as a function of filter size, between measured and modeled fluxes and dissipation (Table 1) have the same trends for heat and water vapor, though the correlations are generally slightly higher for heat.

This suggests that the subgrid-scale dynamics for heat and water vapor are strongly correlated and dynamic SGS model implementations could compute the coefficient of one of the two scalars and impose the other coefficient based on the first one through the linear fits in Fig. 27 (dynamic coefficient determinations are rather expensive computationally). This result has been validated here only for unstable conditions and for surfaces where the temperature and moisture are well correlated at the large scales (sensible and latent heat exchanges at the lake surface are well correlated). It is not clear if the good correlation between heat and moisture SGS dynamics will hold under stable conditions or over heterogeneous terrain with alternating hot-dry and cold-wet patches.

5 Large Eddy Simulation investigation of wet surface evaporation in the presence of advection

5.1 Introduction

Evaporation usually represents the largest loss of water for open water bodies such as lakes or reservoirs, but is a theoretical and practical challenge for hydrology. Methods to quantify it, as presented in the previous chapter, usually rely on similarity theory and energy budget methods and are developed for homogeneous surface conditions and high Reynolds number flow (Brutsaert 1982). The widely used energy budget methods rely on the assumption that the turbulent diffusivities of temperature and water vapor are equal, which has been shown to be valid under non-advective conditions. However most of the time, non-homogeneous conditions and advection are encountered with water bodies of small to medium size. Typically, alternating wet and dry patches are found in many landscapes, and in some cases such as reservoirs in deserts or wetlands in northern landscapes in the summertime, alternating wet and cold patches and warm and dry patches are present. Such strong spatial differences in temperature and wetness of the surface are likely to affect the transfer processes of heat and water vapor, specifically the evaporation rates and the Bowen ratio (ratio of sensible to latent heat). In the presence of a wind velocity, some of the dry air is advected from the dry surface to the wet surface, causing evaporation to be enhanced over the wet surface. An internal boundary layer develops that characterizes the region influenced by the wet surface.

The transition from dry to wet surfaces has been studied extensively, as reviewed partially by Brutsaert (1982) and Garatt (1990). Results have been applied among others to grassland discontinuities (Rider et al. 1963; Baldocchi and Rao 1995), small water surfaces (Brutsaert and Yeh 1969) and discontinuous irrigation (Yuge et al. 2005; McNaughton 1981; Figuerola and Berliner 2005). Methods of investigation include the use of Reynolds analogy and simplified power law assumptions for the wind velocity and eddy diffusivity profiles (Philip 1959; Brutsaert and Yeh 1970), first order closure (Taylor 1970), second order closure (Rao et

al. 1974). For all the methods, a key point is to represent the surface exchange of momentum, heat and water vapor accurately. Indeed the interactions between the land surface and the atmosphere are dynamic and complex, and the quality of numerical predictions have been shown to be very sensitive to the details of models of the land-atmosphere exchanges (Tjernstrom et al. 2005; Garratt 1993). The computation of the surface fluxes is usually done on the basis of Monin-Obukhov similarity theory (Monin and Obukhov 1954). The applicability of the theory has been investigated widely for the case of homogeneous boundary layers for which it was developed, by means of numerous field investigations of the land-atmosphere interactions (Brutsaert et al. 1989; Parlange and Brutsaert 1989). In the context of surface heterogeneities, its applicability remains questionable. However in order to test this and improve the parameterization embedded in numerical models of ABL flows, detailed information on the spatial variation of turbulent fluxes must be obtained. Measurements of spatial variations in the ABL are challenging and require the use of several turbulent flux towers, tethered balloons and aircraft (Mahrt et al. 1994) or Lidar systems (Froidevaux et al. 2009).

An increase in computer resources and the improvement of computational fluid dynamics methods enable numerical methods to be a good alternative tool for investigations of ABL flow features. Modeled physics and dynamics must be adequately resolved to have realistic simulations. The improved treatment of both in current Large Eddy Simulation models have led a number of prior studies of the effect of surface heterogeneity to use LES (Hechtel et al. 1990; Albertson et al. 2001; Esau and Lyons 2002; Kustas and Albertson 2003; Bou-Zeid et al. 2004). In the following, large eddy simulations will be used to study the development of an internal boundary layer above a wet surface in an advective situation, and to explore how the transport characteristics of heat and water vapor that are relevant to lake evaporation modeling can be perturbed from conditions where MOST can be applied with no restriction. A review of numerical studies of flow over wet surfaces can be found for example in Crosman and Horel (2010).

At the edge of the internal boundary layer that develops above the transition from a dry to a wet surface, both upstream and downstream sources influence the fluxes and gradients of scalars and eddy diffusivities for latent and sensible heat flux are not equal (McNaughton and

Laubach 1998). Close enough to the surface, the horizontal fluxes can be neglected and a dynamic equilibrium develops with the underlying surface, in which the fluxes conform to the MOST and the diffusivities are identical. This assumption is the basis of the definition of surface fluxes that serve as boundary conditions in numerical models, including LES models (Bou-Zeid et al. 2004; Rao et al. 1974). As Hill pointed out in 1989, one of the consequences of MOST is that similarity relationships should be identical for all scalars transported in the atmosphere, and the correlation between scalars should be either +1 or -1 (Hill 1989). MOST relationships for mean gradients and higher order statistics are also the main tools used for the computation of surface fluxes from measurements in the atmospheric surface layer (Parlange et al. 1995; Albertson et al. 1995). For this reason, global scalar similarity between temperature and humidity has been investigated widely in the unstable atmospheric surface layer (Albertson et al. 1995; Wesely 1988). Dissimilarities have been observed previously and attributed to several causes. Among them are the entrainment at the top of the boundary layer (Asanuma et al. 2007; De Bruin et al. 1999), heterogeneity at the surface (Lamaud and Irvine 2006; Asanuma and Brutsaert 1999; Choi et al. 2004), advective conditions (Assouline et al. 2008), or the different nature of the two scalars (active temperature creating buoyancy versus passive water vapor being simply transported) (Katul and Parlange 1994; Katul and Hsieh 1999). Many field experiments so far reported that the relative sensible heat to latent heat transport efficiencies exceed unity (Lamaud and Irvine 2006). Latent heat fluxes, either relying on the sensible heat flux energy budget method presented in the previous chapter or on the flux variance method, are subsequently overestimated. Some authors have suggested to connect the relative transport efficiencies to the correlation between heat and water vapor (De Bruin et al. 1999). In this paper, De Bruin suggested to use the correlation between T and q as a tool to see if similarity holds. But if the wet limit and the dry limit are clear cases with regard to the correlation between temperature and humidity, this correlation above the transition zone between a dry and a wet surface is unclear and needs to be investigated.

Some field campaigns have observed specifically the effect of local advection on applicability of MOST. An example of a field campaign looking at the effect of the size and climate characteristics of water bodies is shown by Assouline et al. (2008). The authors used three very different water bodies to investigate the relationship between the fluxes of heat and water vapor under varying advective conditions. Their findings show that deviations from the

MOST are to be expected under advective conditions. Bink (1996) used a combination of field data and second order closure model to study the eddy diffusivities of sensible heat and water vapor in conditions of local advection. The main finding is that the eddy diffusivity for sensible heat is smaller than that of water vapor in the stable internal boundary layer (IBL) and larger in the unstable IBL. Figuerola and Berliner (2005) carried out measurements above an irrigated tomato field in a desert area and found that Penman-Monteith estimation of evaporation could be applied only in the lowest layer close to the ground. The objective of the following study is to use high-resolution LES to gain more insight in the region of applicability of MOST and subsequent evaporation estimation methods.

5.2 Validation of LES and simulations details

Large Eddy Simulations as described in section 1.4 are used to investigate the airflow as it passes from a dry surface to a wet surface. Parameterization in this model is brought to the minimum by use of a Lagrangian scale-dependent dynamic subgrid-scale model (Porte-Agel 2004; Bou-Zeid et al. 2005). The SGS components are described by equation (6) and (7). Originally, the SGS coefficient *Cs* was given a fixed value of approximately 0.17, which was based on analyses made for homogeneous isotropic turbulence (Lilly 1967). Far away from the ground surface, this value works well; however in the vicinity of the lower, solid boundary of the ground surface, the integral scale of turbulence is of the order of the distance to the ground and the SGS represent a significantly larger portion of turbulence (Kleissl et al. 2003; Mason 1994). Over heterogeneous terrain, the application of a priori fixed values of *Cs* does not take into account the spatial variability of the subgrid scale dynamics. The application of the scale-dependent, Lagrangian dynamic SGS model was shown to correct this flaw. Reviews of the evolution of the SGS parameterization can be found in Bou-Zeid (2005) and Kumar (2007). The use of this LES model was validated against measurements in case of diurnal cycles with different stability conditions (Kumar et al. 2006; Kumar et al. 2010).

The simulated domain is 8000 m in the streamwise direction, 2000 m in the cross-stream direction and 1000 m in the vertical. The numerical resolution used is 512x128x512, leading to a spatial resolution of approximately 16 m in the streamwise and 2 m in the vertical direction, with the first vertical node at 1 m. The bottom boundary is fixed at a constant

temperature and a constant specific humidity, and a constant roughness height of is specified. Monin-Obukhov similarity theory is then used to compute the gradients and stress at the first vertical level. A rate of entrainment is imposed for temperature and humidity at the top boundary. Periodic boundary conditions are used in the horizontal plane.

Three different simulations are used in the following. One simulation is a control simulation in which the temperature and humidity boundary conditions are homogeneous. The temperature at the surface is kept constant at 292 K, and the specific humidity is set at 13 $g.kg^{-1}$. The second simulation has a homogeneous temperature, but the first half of the domain in the streamwise direction (4000 m) has a specific humidity set to 13 $g.kg^{-1}$ whereas the second half has a specific humidity set to 0 $g.kg^{-1}$. In the third simulation, the first half of the domain has a temperature of 283 K and a specific humidity of 13 $g.kg^{-1}$ whereas the second half has a temperature of 292 K and a specific humidity set to 0 $g.kg^{-1}$. This last case would represent a situation of a reservoir in a dry and hot climate, where the wet surface leads to stable atmospheric conditions. In all simulations, the roughness length is set to 1 cm.

5.3 Development of the internal boundary layer

In going over heterogeneous terrain, the flow encounters sudden or gradual changes in surface roughness, temperature or wetness. The mean wind, temperature or humidity profiles are modified in a layer confined near the surface whose thickness increases with downwind distance from the surface discontinuity. This layer is commonly referred to as the internal boundary layer (IBL). The development of internal boundary layers over heterogeneities has been a subject of investigation using Large Eddy simulations for roughness transitions (Bou-Zeid et al. 2004) or other numerical techniques (Jozsa et al. 2007). In the case of a step change in surface humidity, an analytical approach has been described by Sutton (Sutton 1934) and further described in more suitable forms (Frost 1946; Brutsaert and Yeh 1970). This approach has been derived for a step change in humidity only. The degree of adjustment to the new surface is described by a boundary layer interface which depth is growing with distance downwind from the transition. A balance between horizontal advection and vertical turbulent diffusion is used in the derivation of the depth:

$$u\frac{dq}{dx} = -\frac{\partial}{\partial z}\left(\overline{w'q'}\right). \tag{33}$$

The turbulent flux is then closed using an eddy diffusivity, i.e.

$$\overline{w'q'} = -K_v \frac{\partial q}{\partial z}. \tag{34}$$

The diffusivity K_v is assumed to vary with height z following a power law of exponent n:

$$K_v = bz^n. \tag{35}$$

Using these assumptions, an expression is derived for the height of a layer of constant humidity difference. The power law assumption allows only for limited consideration of stability corrections.

We are observing the behavior of the IBL with a step change in only humidity first, and then with a transition between a dry hot surface and a wet cold surface as presented in the previous section. Fig. 28 shows the vertical profiles of sensible and latent heat fluxes above a domain with a homogeneous temperature, but the first half of the domain in the streamwise direction (4000 m) has a specific humidity set to 13 $g.kg^{-1}$ whereas the second half has a specific humidity set to 0 $g.kg^{-1}$. Even though the temperature is homogeneous, one can see that the sensible heat flux is larger over the wet surface, as a consequence of enhanced buoyancy coming from the moisture content of the air. The vertical profiles averaged over the wet surface show the influence of the penetration of dry air from the upstream plume, with a strong positive latent heat flux at the surface, but negative above 100 m. Fig. 29 and Fig. 30 show vertical slices of the temperature, specific humidity, sensible and latent heat fluxes where one can see the effect of the upstream source more clearly.

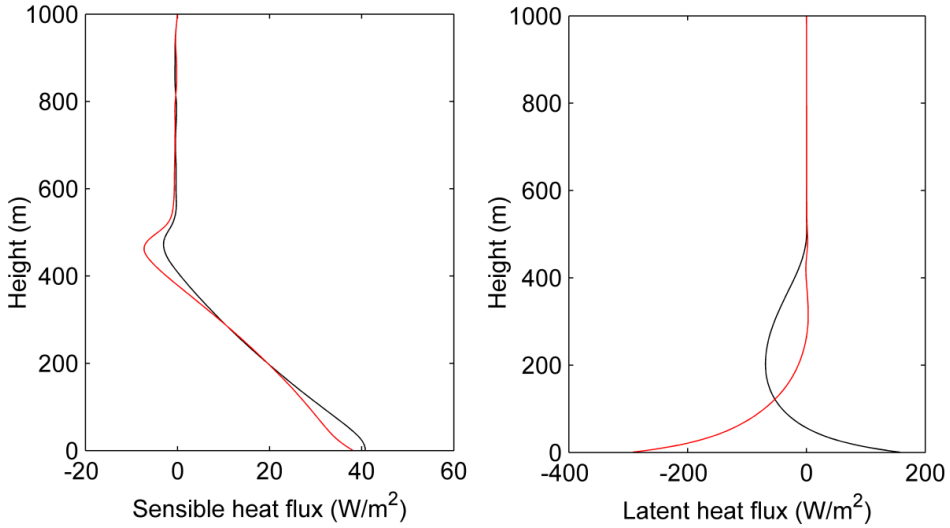

Fig. 28 Sensible and latent heat flux profiles. Red is averaged over the dry half of the domain, black over the wet half.

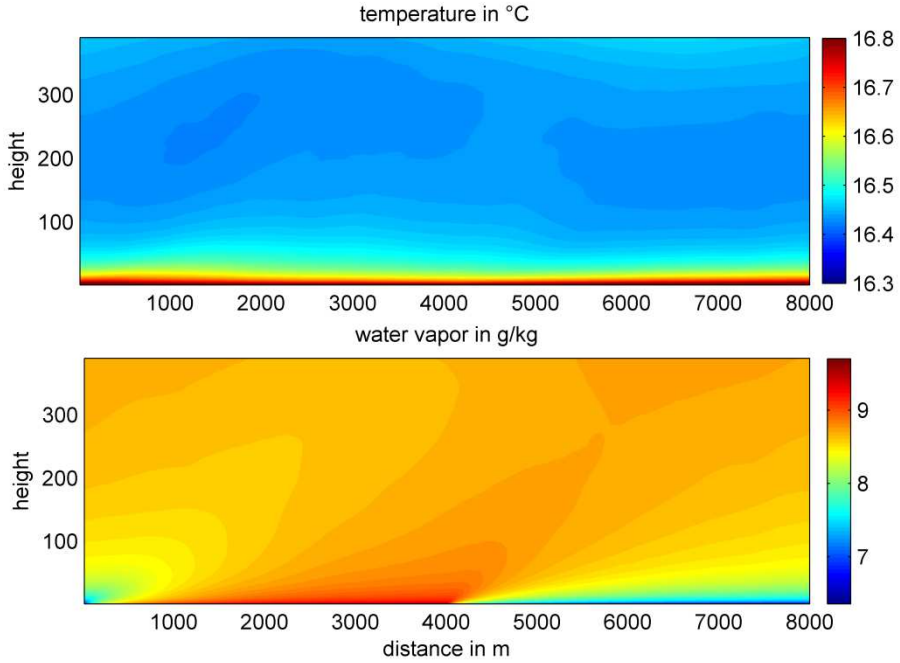

Fig. 29 Vertical slices of temperature and water vapor concentration. The left half is wet, the right half is dry.

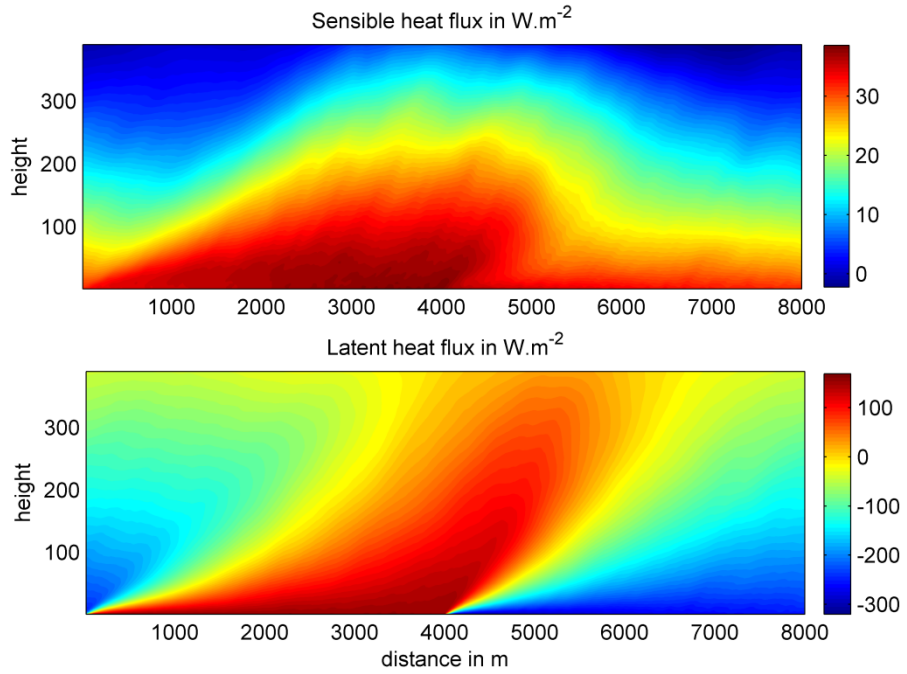

Fig. 30 Vertical slices of the sensible and latent heat fluxes.

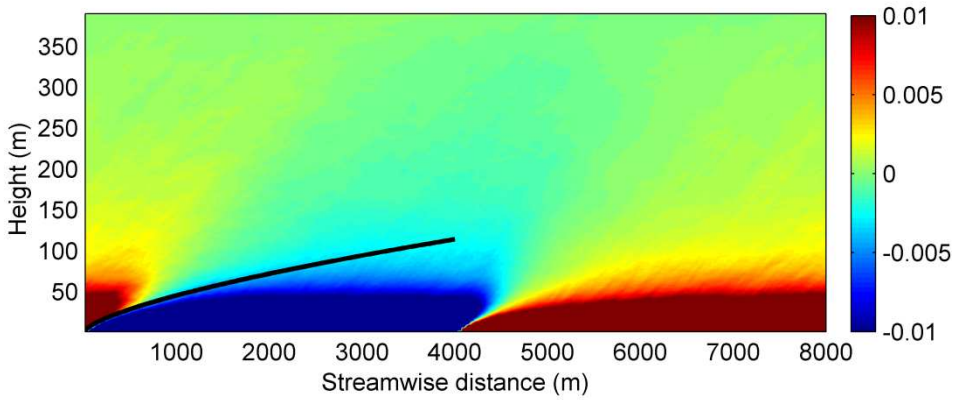

Fig. 31 Vertical slice of $\partial\langle q\rangle_{y,t}/\partial z - \partial\langle q\rangle_{x,y,t}/\partial z$ depicting the water vapor blanket forming above the wet surface. The black line shows Sutton's solution for the height of the blanket.

The IBL development is shown in Fig. 31 where the deviation of the local mean vertical humidity gradient from its value averaged over the wet and dry patches is plotted. Sutton's solution is added to the figure, with the exponent in the power law assumption for the vertical taken as n=1/2. Sutton's solution appears well validated, however the exponent had to be fitted

to reproduce the wind profile very close to the surface. This type of parameterization is not well defined and limits the use of the solution.

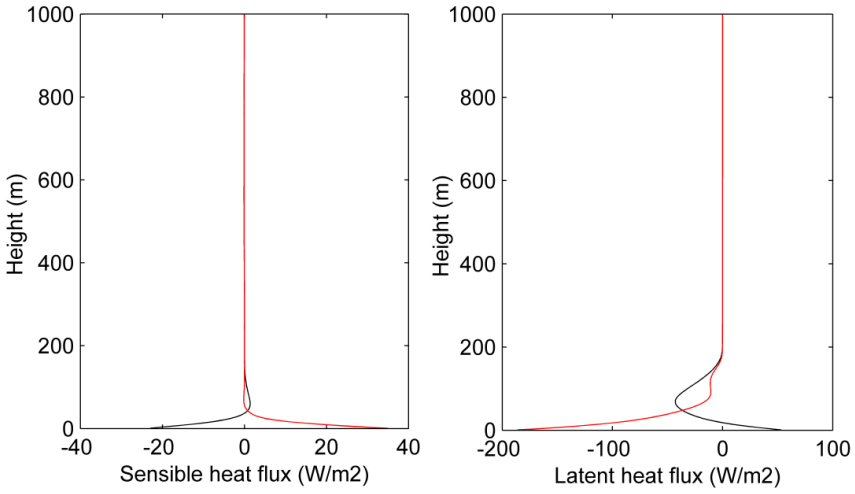

Fig. 32 Sensible and latent heat flux profiles. Red is averaged over the dry half of the domain, black over the wet half.

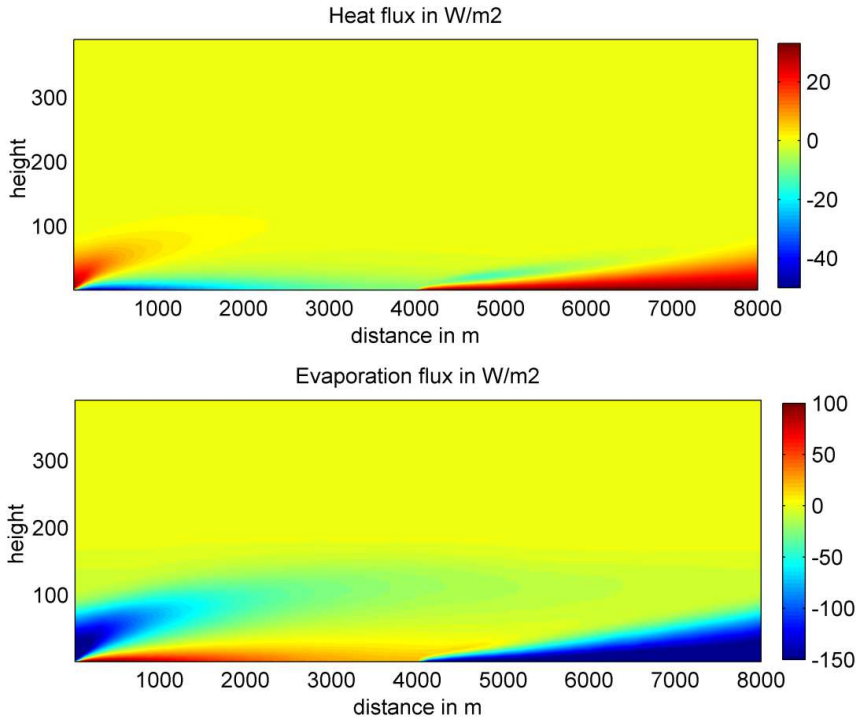

Fig. 33 Vertical slices of the sensible and latent heat fluxes.

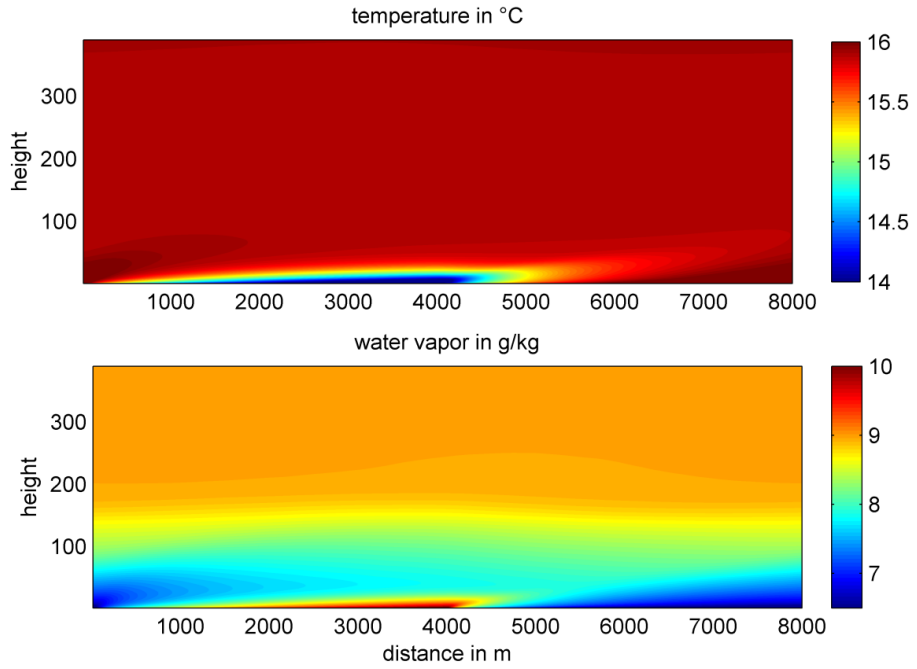

Fig. 34 Vertical slices of temperature and water vapor concentration. The left half is wet and cold, the right half is dry and hot.

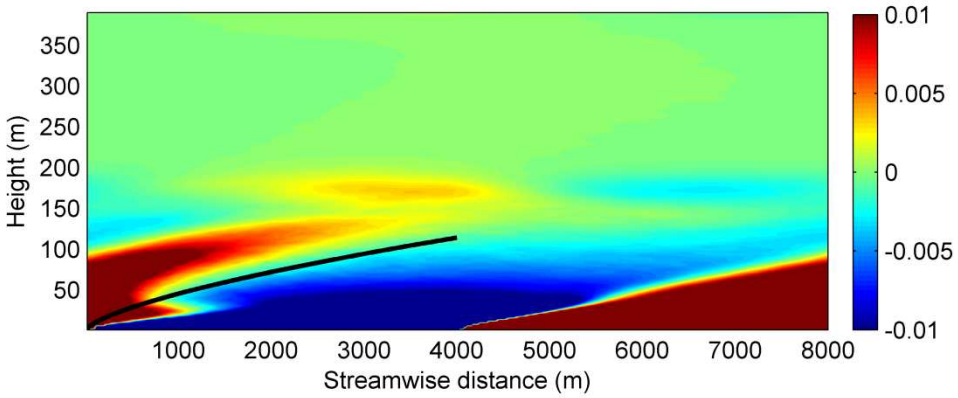

Fig. 35 Vertical slice of $\partial\langle q\rangle_{y,t}/\partial z - \partial\langle q\rangle_{x,y,t}/\partial z$ depicting the water vapor blanket forming above the wet surface. The black line shows Sutton's solution for the height of the blanket.

Fig. 32 to Fig. 34 show the results of the simulation with a wet and cold patch followed by a hot and dry patch. In this stable case, the surface layer is much shallower and Sutton's solution (Fig. 35) overestimates it.

Sutton's solution can work fine if one knows how to estimate the right power law to use for the wind profile. However, the choice of an exponent is not well defined, and the effect of atmospheric stability on the IBL depth can be very important as seen in the stable case. More advanced transition models like 1D footprint models include stability and are presented in the next chapter.

5.4 Relative transport efficiencies of water vapor and heat over varying surface transitions

A vertical slice of the correlation between T and q, R_{Tq}, is shown in Fig. 36 for the unstable simulation described in section 5.2. The figure shows a region of +1 correlation above the wet surface, and a region of -1 correlation above the dry surface. The transition zone between the two regions of unit correlation varies with the height, corresponding to the internal boundary layer of the wet surface. The ratio of transport efficiency of temperature and humidity is shown for the unstable simulation in Fig. 37. Similarly to R_{Tq}, the ratio has a unit value in the region above the wet surface and a value of -1 above the dry surface.

The transition zone between the dry surface and the wet surface can be observed in more details in Fig. 40 for two different heights. The fetch requirement for the ratio to go back to a unit value after the transition is similar to that found in the footprint analysis that is presented in the following chapter. The correlation R_{Tq} and the ratio of transport efficiencies between temperature and humidity are shown for the stable simulation in Fig. 38 and Fig. 39. In this case, R_{Tq} and the transport efficiency ratio have a value of -1 above the entire surface. However, a transition region where these values differ from unity still remain and can be observed in more details in Fig. 41. The fetch requirement to reach a unit value in this case is much shorter than the fetch estimated in the footprint analysis shown in the following chapter. Conditions of application of MOST are faster to reach than an equilibrium flux. The distance appears to be the same for the stable case as for the unstable case.

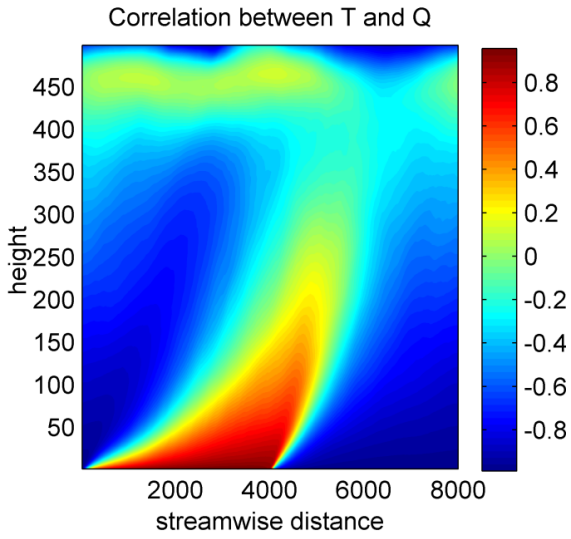

Fig. 36 Vertical slice of the correlation between temperature and humidity for the unstable simulation.

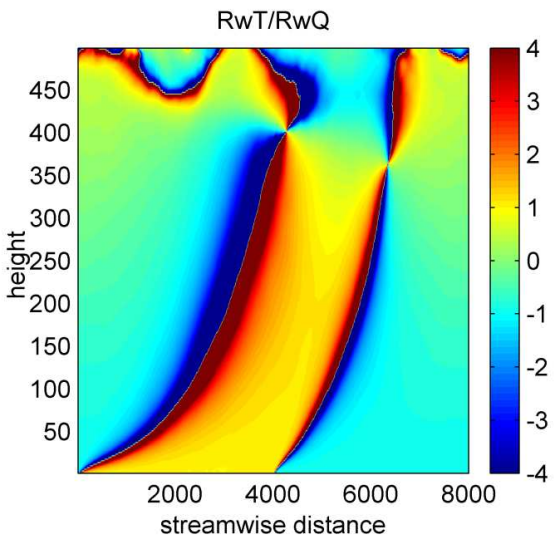

Fig. 37 Vertical slice of the ratio of temperature and water vapor transport efficiencies for the unstable simulation.

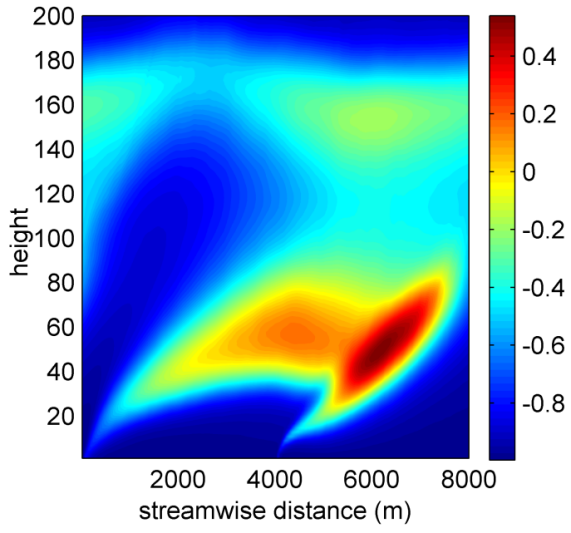

Fig. 38 Vertical slice of the correlation between temperature and humidity for the stable simulation.

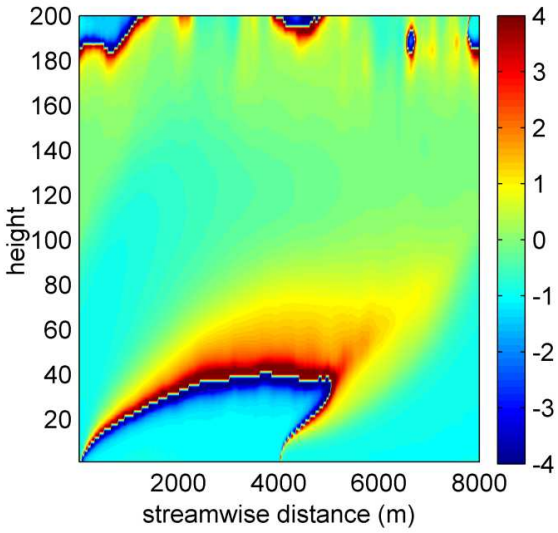

Fig. 39 Vertical slice of the ratio of temperature and water vapor transport efficiencies for the stable simulation.

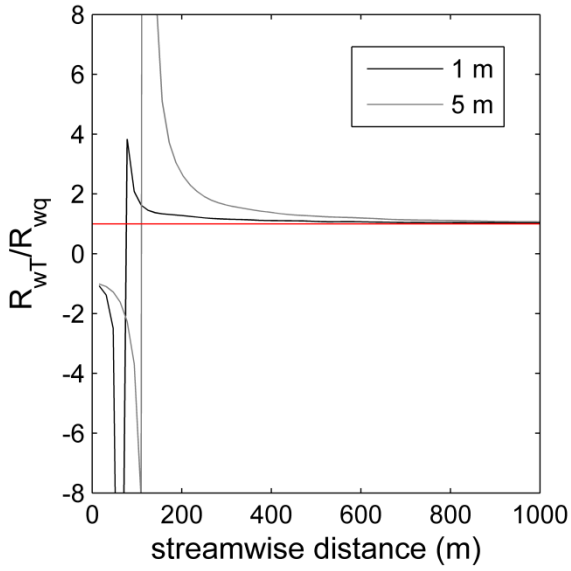

Fig. 40 Ratio of temperature and water vapor transport efficiencies for the unstable simulation at two different heights, averaged over the cross stream direction. The red line shows the 1 constant value.

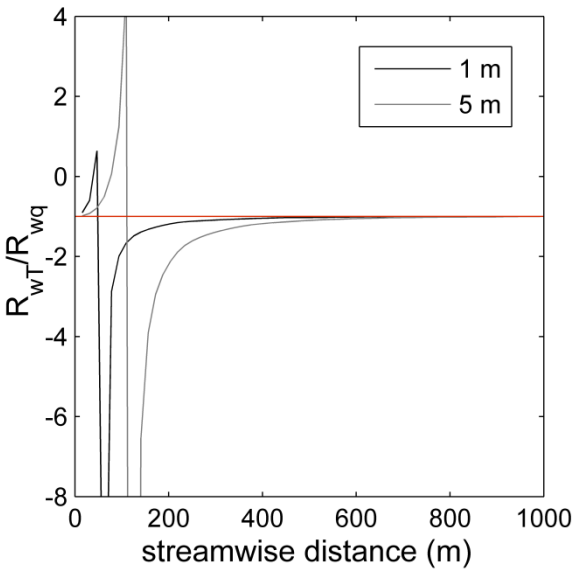

Fig. 41 Ratio of temperature and water vapor transport efficiencies for the stable simulation at two different heights, averaged over the cross stream direction. The red line shows the -1 constant value.

In their analysis over three different water bodies, Assouline et al. (2008) found that $R_{wT}/R_{wq} > 1$ above Lac Léman as part of the LATEX campaign (section 2.2), and $R_{wT}/R_{wq} < 1$ above a reservoir in a dry arid climate. They conclude that for Lac Léman, the advection is small and that the active role of temperature makes its transport be more efficient; for the reservoir, they claim that the advection is large and overcomes the active role of temperature. As mentioned earlier, the fetch above Lac Léman during the measurements was ensured to be a minimum of 10 km. That would correspond in our simulations to the region where the transport efficiencies are equal for temperature and humidity. For the case of the reservoir, we can compare the results of Assouline et al. for their afternoon measurements to the stable simulation. The fetch of their measurements is approximately 300 m. Our results only show $|R_{wT}|/|R_{wq}| < 1$ at the leading edge of the water surface, in the zone where the latent heat flux and the sensible heat flux still follow the gradients imposed by the dry surface. But

when the sign of the sensible and latent heat fluxes follows the gradients imposed by the wet surface under consideration, we see that $\left|R_{wT}\right|/\left|R_{wq}\right| > 1$ before reaching a steady state value of unity. The differences between the simulation results and the experimental data suggests that other causes could impact the transport efficiency ratio than advection and the active role of temperature.

5.5 Conclusions

Results of large eddy simulations using a dynamic Lagrangian scale-dependent subgrid scale model were analyzed in a situation of a transition from a dry to a wet surface. Questions to answer with this study were: how does the internal boundary layer develop over the transition? Is MOST valid over a moisture heterogeneity?

To answer the first question, we tested the theoretical derivation given by Sutton for the height of the water vapor blanket along the fetch. The solution successfully reproduced the LES result for an unstable simulation, however some tuning of the power law assumption of variation of the eddy diffusivity used in Sutton's derivation was necessary. Also in the stable case, Sutton's solution did not reproduce the LES results. The effect of non-neutral atmospheric stability is indeed not included in IBL development formulations.

We observed the ratio of transport efficiency of temperature and water vapor along the transition from a dry to a wet surface. Deviations from unity were observed but could not be compared to results from field experiments (Assouline et al. 2008). The effect of advection at the leading edge of the water surface was shown to perturb MOST scaling from idealized situations where the ratio of transport efficiency of temperature and water vapor has a unit value.

6 Scalar flux fetch analysis

6.1 Motivation and review of footprint models

The width, or fetch, of the water body affects the evaporation rate. As air moves from the land across an evaporating water body, water is gradually evaporated into the airflow causing the humidity to increase with distance downwind from the shore. Consequently, this process tends to cause evaporation rate to decrease with distance downwind from a shore (Weisman and Brutsaert.W 1973; Rao et al. 1974). Theoretical solutions for fetch-dependent evaporation are derived at the surface; however measurements that are used for potential evaporation modeling are never made at the surface but rather at a height between 2m and 10m. In advective situations, we can expect humidity to vary differently with height along the fetch above the wet surface as the vapor boundary layer develops. Attention should be paid to the height at which the local flux is measured as well as the downwind distance (Webster and Sherman 1995). Quantifying the effect of the vertical height of measurements combined with the effect of the downwind distance is rather complicated; field campaigns usually give information at one or few locations. Some new techniques such as scintillometry or scanning lidar allow spatial measurements and are promising tools to investigate transitions of surface conditions (Green et al. 2000; Froidevaux 2010).

When scalar flux measurements are carried out over heterogeneous surface, knowledge of the upwind fetch that influences the measured flux is necessary in order to have measurements representative of the area of interest. The required fetch will vary according to the stability conditions in the atmosphere, which control the development of the internal boundary layer. The flux footprint was defined to quantify these variations of the necessary fetch (Schuepp et al. 1990; Leclerc and Thurtell 1990). For practical application, scalar flux footprint models are generally used to quantify the area that contributes to scalar flux measurements or estimate the adequate fetch requirements (Horst 1999). Different types of models have been used until now, both Eulerian analytical models and Lagrangian stochastic models of different degrees of complexity. This problem was first addressed in the Eulerian sense by deriving approximate analytical solutions of the two dimensional diffusion equations for idealized surface boundary conditions. In the case of a moisture discontinuity at the surface, the work

originated from Sutton as presented in the previous chapter (Sutton 1934). Later solutions were based on Sutton's derivation first in neutral conditions (Pasquill 1972; Gash 1986). The model of Horst and Weil (1992) then included a treatment of atmospheric stability, but in an implicit way. The distance of adjustment of water vapor fluxes after a transition from a dry surface to a wet surface has later been investigated by means of Lagrangian stochastic models (Hsieh et al. 2000; Hsieh and Katul 2009). The authors give a review of the different Eulerian and Lagrangian methods used for footprint estimation. They compared eddy covariance measured and Lagrangian-model predicted water vapor fluxes as a function of downwind distance from a transition between a dry and a wet surface. Their findings show good comparison of the fluxes, however limited to a height of measurements of 4m. At this height, their model reproduces the distance needed to reach 90% of the equilibrium flux. Lagrangian models such as the one in this study are however simplified analytical models that are confined to the surface layer and that usually prescribe several parameters that are derived from field observations or numerical experiments.

Large eddy simulations can simulate both the turbulence characteristics of the flow and the scalar fluxes that results from those with a minimal degree of parameterization. Footprint of sources can then be analyzed based on LES outputs. The complexity and computational costs associated to LES does not allow them to be a realistic tool for footprint calculations. However they can be a diagnostic tool to assess the reliability of more simple models The use of LES to test footprint models in heterogeneous conditions has been recommended by Schmid (2002).

We will use LES to explore the fetch required to reach an equilibrium water vapor flux at different heights, and in different stability conditions. Indeed LES has the ability to estimate the fetch requirements in the entire boundary layer without an a priori knowledge of the velocity statistics that is required for the Lagrangian models used until now. The parameterization embedded in the LES model is minimized, since only the small, turbulent subgrid scales are parameterized. The current parameterization in the EPFL-LES described in section 1.4 uses a Lagrangian dynamic scale dependent model that adapts the subgrid scale model coefficients locally to the flow. The effect of spatial heterogeneities is thereby well represented.

6.2 Results

The EPFL-LES results are compared to the footprint model described in Hsieh et al (2000). The authors derived an explicit algebraic equation that considers the effect of non-neutral stability conditions on the footprint of a source. The authors used a Lagrangian stochastic model with a range of stabilities, roughness lengths and measurements heights and applied a regression technique in order to form non-dimensional groups with the results. Combining the simulation results with an analytical approach to get a flux footprint model, similarity parameters where derived to account for the stability of the atmosphere, leading to the footprint model

$$\frac{x_F}{|L|} = -\frac{1}{\kappa^2 \ln(F)} D \left(\frac{z_u}{|L|} \right)^P , \tag{36}$$

where x_F is the fetch requirement to achieve a desired scalar flux F, D and P are the similarity parameters fitted for each stability class (unstable, neutral and stable), $z_u = z_m \left(\ln\left(z_m / z_0\right) - 1 + z_0 / z_m \right)$ is a new length scale that includes the measurement height z_m and the roughness length z_u, L is Obukhov length and κ(=0.4) is Von Karman's constant. This model showed good comparison with measurements made over an irrigated bare soil and an irrigated potato field (Hsieh and Katul 2009), at one measurement height. In this type of approach, the turbulent mixing K and the velocity profile u are assumed to be horizontally homogeneous. Since the temperature and moisture content of the air both influence the stability, this is not necessarily the case when a step change in humidity or temperature is encountered at the surface. Further testing of the model at different heights is needed.

Scalar flux footprints have been investigated by means of LES previously, but the studies were limited to unstable conditions and to a very small domain (Leclerc et al. 1997). In the following, we investigate the fetch and height dependence of water vapor fluxes above a transition from dry to wet surface. The effect of atmospheric stability is also studied based on the two cases discussed in section 5.2 and 5.3. The first case in an unstable case with a homogeneous surface temperature. The second is stable on the wet surface. Fig. 42 and Fig. 44 show the latent heat flux simulated above the wet surface by the LES at several heights

above the ground, ranging from 1 m to 15 m every 2 m, respectively for the unstable case and for the stable case. In Fig. 42 (the unstable case), the enhanced evaporation at the leading edge of the wet surface can be observed at 1 m from the ground, but higher, the evaporation increases along the fetch until it reaches an equilibrium flux. In Fig. 44 (the stable case), the enhanced evaporation at the leading edge can be seen up to a height of 15 m, and the distance after which the maximum evaporation rate is observed increases with height.

We compare the fetch x_F required to reach 90% of the equilibrium flux to that given by the footprint model described in (Hsieh et al. 2000; Hsieh and Katul 2009),

$$\frac{x_F}{z_m} = \frac{D}{0.105\kappa^2} z_m^{-1} \left|L\right|^{1-P} z_u^P . \tag{37}$$

This distance is estimated with the LES results on the basis of Fig. 43 and Fig. 45. In the unstable case, Fig. 43 shows the normalized fraction of the equilibrium (downstream) latent heat flux computed by the LES along the fetch of the wet surface. The distances required to reach 90% of the equilibrium fluxes are summarized in Table 2. Two unstable simulations are shown in this table, with different roughness length such that the stability differs in both simulations. Close to the surface, the order of magnitude of the distance necessary to reach 90% of the equilibrium flux is similar between the LES and the Lagrangian footprint model. The fetch-to-height ratios $x_F \, z_m^{-1}$ are summarized in Table 3. The LES results show that the approximate 1/100 fetch-to-height ratio that is typically assumed as a rule of thumb for unstable conditions can be valid close to the ground. The main difference between the LES results and the results from the analytical model is that these ratios increase with height in the LES results but decrease with height in the footprint model.

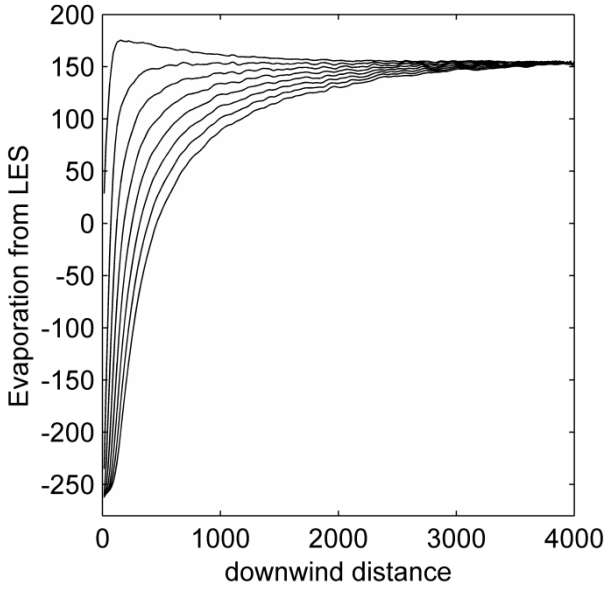

Fig. 42 Simulated evaporation along the wet surface at different heights. The highest curve is at 1m above the surface and the other lines show every 2m up to 15m.

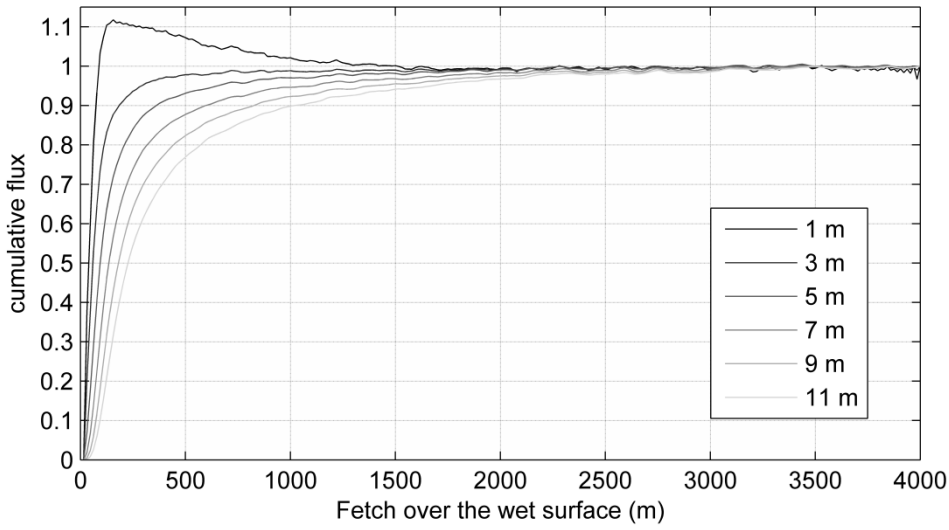

Fig. 43 Difference between the upstream flux and the LES modeled flux normalized by the difference between the upstream and the equilibrium (downstream) fluxes.

The latent heat fluxes at different heights are shown for the stable case in Fig. 44. In this case, the definition of the distance required to reach 90% of the equilibrium flux is ambiguous. In the stable atmosphere, the air passing over the wet surface becomes moist, but turbulent

mixing is minimal. The air quickly reaches saturation and the evaporation flux decreases drastically along the fetch after having had a maximum. Footprint models cannot capture the enhanced flux at the leading edge. The footprint estimation used in this study is derived imposing a flux as a source of moisture, and this flux is constant along the fetch. In our case, we impose a constant humidity and the flux is calculated based on MOST. This methods leads to a surface flux that decreases along the fetch as the air gets saturated and the lack of mixing prevents drier air from replacing saturated air. As we consider the fluxes higher above the ground surface, a certain fetch is necessary for the humidity to travel to the height considered, leading to a maximum flux that is displaced from the leading edge, and a certain fetch is necessary for the air to adjust to the surface with an equilibrium flux after that. In Fig. 45 we thus consider the normalized difference between the LES computed latent heat flux along the fetch and the maximal flux. By this mean, we can find the distance necessary to reach 90% of the equilibrium flux and compare it to the distance estimated by the footprint model.

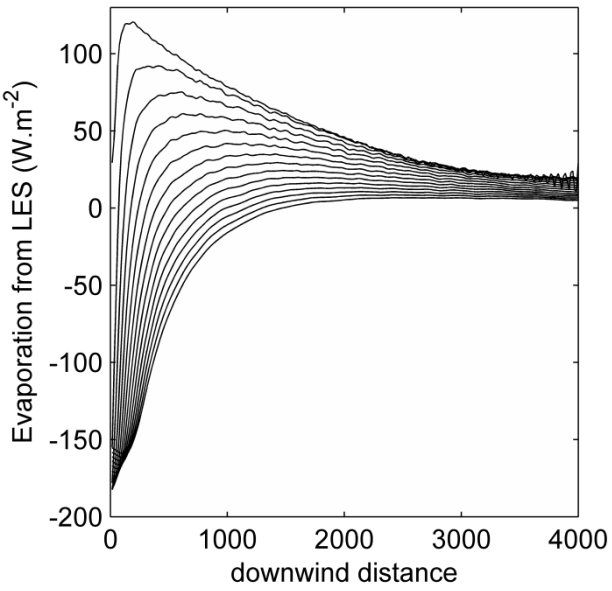

Fig. 44 Simulated evaporation along the wet surface at different heights. The highest curve is at 1m above the surface and the other lines show every 2m up to 27m.

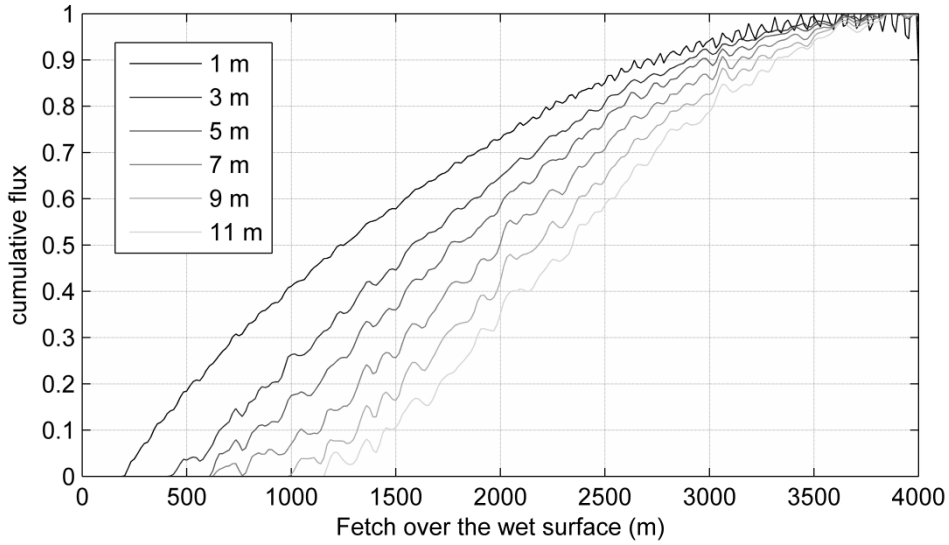

Fig. 45 Difference between the maximum flux and the LES modeled flux normalized by the difference between the maximum and the equilibrium (downstream) fluxes.

Table 2 Distance (m) to reach 90% of the equilibrium for LES versus analytical footprint model

	Unstable, z0 = 1 cm		Unstable, z0 = 10 cm		Stable, z0 = 1 cm	
	Fp_{LES}	$Fp_{analytical}$	Fp_{LES}	$Fp_{analytical}$	Fp_{LES}	$Fp_{analytical}$
2.9 m	190	340	65	250	2900	2000
4.9 m	375	490	125	385	3000	4000
6.8 m	625	630	219	498	3200	6000
8.8 m	830	760	344	604	3230	8000
10.7 m	1030	880	515	706	3300	9600

Table 3 Fetch to height ratio (m) for LES versus analytical footprint model

	Unstable, z0 = 1 cm		Unstable, z0 = 10 cm		Stable, z0 = 1 cm	
	$F2H_{LES}$	$F2H_{analytical}$	$F2H_{LES}$	$F2H_{analytical}$	$F2H_{LES}$	$F2H_{analytical}$
2.9 m	66	117	22	86	1000	690
4.9 m	77	100	26	79	612	816
6.8 m	92	93	32	73	470	882
8.8 m	94	86	39	69	367	909
10.7 m	96	82	48	67	308	900

The analytical footprint model relies on 1D assumptions such as a spatially homogeneous eddy diffusivity and homogeneous velocity statistics and is derived for the surface layer. However, the results shown on Fig. 46 for all stability situations obtained from the simulations show a reasonable performance of the analytical model. The next section analyses

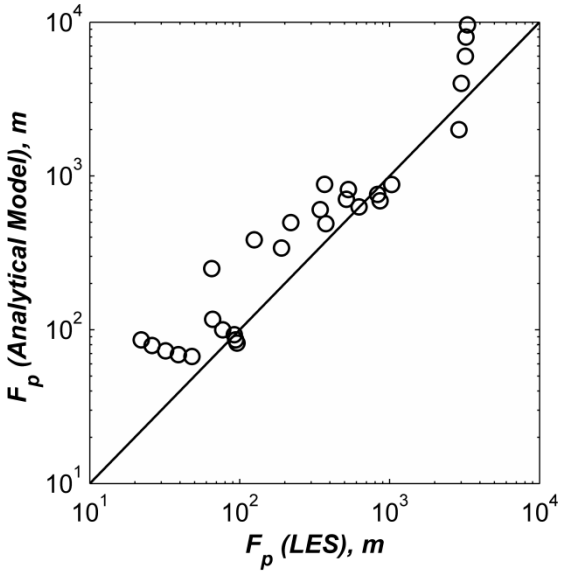

Fig. 46 Comparison between the footprint observed with LES and the analytical footprint model for all heights and stability range.

the deviations from MOST over the heterogeneity, which are part of the reason why footprint models do not reproduce the LES computed fetch requirement.

6.3 Fetch and evaporation

We compute evaporation models and compare to the simulation outputs for fetch dependent evaporation. The wet surface evaporation derived in chapter 3 is used. We include the effect of the stability in the wind function by determining the drying power of the air E_A in equation (19) from the Penman-Brutsaert model (Brutsaert 1982; Katul and Parlange 1992):

$$E_A = \kappa u_* \rho \left(q_a^* - q_a \right) \left[\ln\left(\frac{z_a}{z_{0v}} \right) - \psi_{sv}\left(\frac{z_a}{L} \right) \right]^{-1}, \tag{38}$$

where q_a and q_a^* are the specific humidity of the air and the saturation specific humidity of the air at air temperature respectively, κ is Von Karman constant, u_* is the friction velocity, ρ is the air density, z_a is the height above the surface, z_{0v} is the water vapor roughness length and L is Obukhov length. The function Ψ_{sv} is the Monin-Obukhov similarity stability correction function that depends on z/L and can be found in Brutsaert (2005), page 50.

Fig. 47 shows the comparison between the LES computed latent heat flux at 5 m above the wet surface and the flux obtained by the sensible heat flux based equation (19). The contribution of E_A is much larger than that of the sensible heat flux term (observation not shown). Its maximal value at the leading edge thus leads to a maximal evaporation estimate at the leading edge, which contradicts the simulation results. Indeed, the opposite transport direction between sensible and latent heat flux is not included in the model that is derived assuming that $R_{wT} / R_{wq} = 1$. This is not the case at the leading edge of the wet surface. We suggest to use the correlation between temperature and humidity to correct the sensible heat flux contribution to the evaporation formulation,

$$E = R_{Tq} \frac{\Delta}{\gamma} H + L_e E_A . \tag{39}$$

This is in fact correcting the Bowen ratio estimate of (16) by multiplying it by the correlation coefficient R_{Tq}. This will reflect the change of direction of transport that starts gradually as the

flow goes over the wet surface. The figure shows that the variation of the latent heat flux above the transition is well reproduced, even though there is a mismatch between the modeled and simulated evaporation probably due to an overestimation of E_A.

In the stable case shown in Fig. 48, the correction of the Bowen ratio estimate to take into account the opposite direction of transport of heat and water vapor is crucial to get an accurate evaporation estimation.

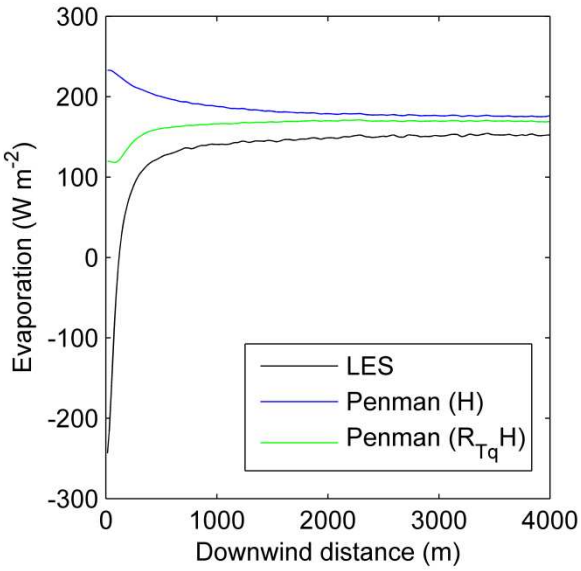

Fig. 47 Comparison of evaporation at 5m from LES and from evaporation model from chapter 0 for a roughness length of z0=0.01m. The green line uses H multiplied by R_{Tq}.

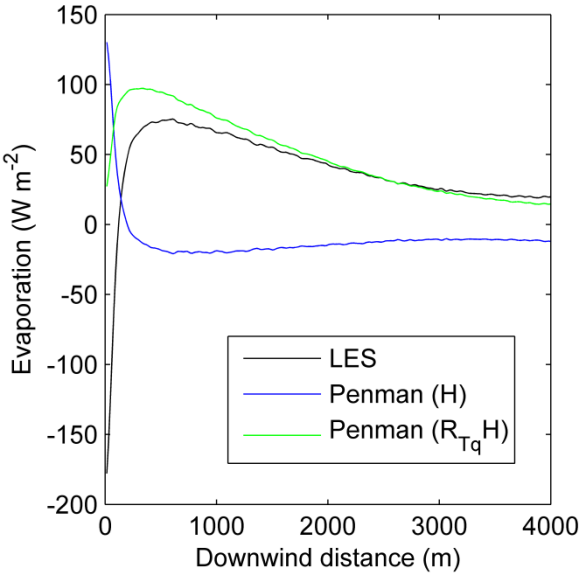

Fig. 48 Comparison of evaporation at 5m from LES and from evaporation model from chapter 0 for a roughness length of z0=0.01m in the stable case. The green line uses H multiplied by R_{Tq}.

If we were using the classical Penman formulation, the available energy Q_{ne} would not have dependence on the fetch, since the net radiation and the storage of energy do not vary along the fetch. This model would therefore not capture the increase of evaporation along the fetch that is observed in the simulations.

6.4 Conclusion

Results of large eddy simulations using a dynamic Lagrangian scale-dependent subgrid scale model were analyzed in a situation of a transition from a dry to a wet surface. Questions to answer with this study were: how long of a fetch is necessary for wet surface evaporation formulations to be applicable?

We analyzed results from source area footprint models that include stability corrections. The model of Hsieh et al. (2000) is such a model that has shown good comparison with field measurements. We compared the distance necessary to reach 90% of the equilibrium flux in the LES results to the distance estimated by the analytical model in different stability conditions. The footprint model gave reasonable comparison in a wide range of atmospheric stabilities, but the variation of the fetch-to-height ratio with height showed opposite trends between the analytical model and the LES.

We suggested that discrepancies in the modeled and simulated adjustment distances could be due to deviations from MOST in the heterogeneous surface context.

We finally tested the wet surface evaporation formulation derived in chapter 3 over the heterogeneous simulations. We observed a maximal evaporation rate at the leading edge of the water surface close to the surface, but as we moved to higher distance from the ground, the evaporation increased continually to reach an equilibrium value. For the unstable simulation, the maximal evaporation at the leading edge was only observed at 1 m from the water surface, whereas it persisted much higher in a stable simulation. The evaporation model predicts a maximal evaporation at the leading edge even when the simulations do not show it. We suggested that using the correlation R_{Tq} instead of assuming a ratio of transport efficiencies of temperature and water vapor of 1 as is done in the derivation of the evaporation formulation could improve the evaporation prediction for short fetches where MOST hypotheses are not yet applicable.

7 Summary and conclusions

This thesis investigated the exchanges of water vapor, heat and momentum over a lake and across the transition zone between the land surface and open water. On the basis of the LATEX field campaign carried out on Lac Léman (Lake Geneva) in 2006, we observed lake-specific surface exchanges. The transition zone between land surface and open water was analyzed by means of large eddy simulations.

Chapter 1 introduced the role of the atmospheric boundary layer and land-atmosphere exchanges on the dynamics of the atmosphere and the water cycle. We pointed out the importance of turbulence in the exchanges. We explained the specificities of lake surfaces compared to land surfaces, both in terms of the hydrologic cycle and of their effect on atmospheric dynamics. We then introduced the large eddy simulation technique for ABL flows as a tool to study ABL flow features, and reviewed field experiments designed to improve LES models.

In chapter 2, we used eddy covariance measurements to infer sensible and latent heat fluxes, and net radiation was provided by a net radiometer. We showed that the storage of energy derived from the previous measurements is a very important term in the energy budget of water surfaces. The dataset included a fiber optic measuring profiles of temperature in the water body that were used to compute the storage of energy in the lake. However methods to quantify this term, relying on the theory of conduction of heat, were unsuccessful (results not shown).

Subsequently, we revisited evaporation models in chapter 3 to derive a way to quantify evaporation from wet surfaces that relies on sensible heat flux measurements. We argued that sensible heat flux measurements could be more readily available using modern techniques like scintillometers or on the basis of flux variance methods, and that the characteristic spatial scales of all observed variables and the footprint captured by the instruments would be mutually compatible, leading to a better performance of the model. This technique proved successful with the LATEX dataset using the eddy covariance measurements of sensible heat flux.

We then investigated the effect of heterogeneity of the surface using large eddy simulations of the atmospheric boundary layer, with the goal of quantifying the effect of having a water surface of limited fetch on the performance of evaporation models. For this purpose, we analyzed parameterization embedded in LES, *i.e.* the dynamics of the subgrid scales, based on the LATEX dataset in chapter 0. The turbulent subgrid scale fluxes of water vapor were observed for the first time over a lake surface as part of this campaign. One of the questions raised in this chapter was whether the lake surface, which can react to the flow field as a moving interface, was responsible for different SGS dynamics compared to land surfaces that cannot adapt to the air aloft. We showed that the effect of the moving interface had very little effect on the SGS dynamics, which appeared to be very similar to observations over land surfaces made in the past. This is different from measurements made during OHATS over the ocean, where the swell waves were shown to affect the SGS significantly. The values found for the Schmidt number and the Prandtl number were very similar to values recorded above land surfaces.

We brought a particular attention to the similarity of transport characteristics of water vapor and heat across spatial scales. For the subgrid scales of importance in LES parameterization, the LATEX campaign showed in chapter 0 that the SGS dynamics of water vapor and heat were very well correlated. We suggested that the modeling of the SGS terms for water vapor and heat could be coupled in order to save computation time in LES including both scalars and relying on a dynamic computation of the SGS model coefficients. On larger scales, chapter 3 showed that evaporation and sensible heat are similar enough such that the suggested evaporation model based on sensible heat flux can perform very well above a large lake. In chapter 5, LES over homogeneous wet surfaces reproduced the high correlations between the transport of heat and water vapor. In this chapter, we raised the question of similarity of transport characteristics in the case of a non-homogeneous surface, and LES were used as a tool to investigate the dynamics of water vapor and heat over a transition from a dry to a wet surface. When the airflow passes above the transition zone between land and water, the scalars can typically go from a zone where they are transported the same way (a correlation coefficient of +1) to a zone where their transport goes in opposite directions (a correlation coefficient of -1), and there is a transition zone in which the correlation of heat and water vapor differs from unity (in absolute sense). Some fetch is necessary for the transport to

be similar again. After this fetch, the evaporation models derived for wet surfaces can perform well again. We observed the deviation from MOST and compared it to existing datasets. The fetch requirement of Bowen ratio measurements for evaporation models was determined with the results of the LES in chapter 6. We argued that simplified models were necessary in the field to determine fetch requirements in an non-computationally intensive way, and the performance of a source area footprint model taking into account atmospheric stability was tested against LES results. The performance of the footprint model in different stability conditions was reasonable. Reasons for mismatch between LES fetch requirements and the ones given by the footprint model were attributed to the deviation from MOST theory in a heterogeneous landscape.

Future work should naturally include the use of a scintillometer to quantify wet surface evaporation. This was in fact tested in a paper in review (McJannet et al. 2010) and shown to give very promising results, improving classical estimation techniques relying on scintillometry that are using the water storage term. The use of the sensible heat flux based model is thus recommended for open water surface where the estimation of the storage of energy is challenging.

It is also suggested that the modeling of water vapor and heat in LES that use a dynamic computation of the SGS model coefficients could be coupled in order to save computation time. However the relationships between the SGS fluxes of water vapor and heat should be observed over land or with different surface moisture conditions, to see how the amount of available water at the surface affects the correlation of the SGS. LES computing the heat and water vapor model coefficients dynamically could also be used to see how the relationship shown in chapter 0 holds when the surface moisture varies from a saturated surface to a wet surface progressively.

Bibliography

Albertson JD, Kustas WP, Scanlon TM (2001) Large-eddy simulation over heterogeneous terrain with remotely sensed land surface conditions. Water Resour Res 37 (7):1939-1953

Albertson JD, Parlange MB (1999a) Natural integration of scalar fluxes from complex terrain. Advances in Water Resources 23 (3):239-252

Albertson JD, Parlange MB (1999b) Surface length scales and shear stress: Implications for land-atmosphere interaction over complex terrain. Water Resour Res 35 (7):2121-2132

Albertson JD, Parlange MB, Katul GG, Chu CR, Stricker H (1995) Sensible Heat-Flux from Arid Regions - a Simple Flux-Variance Method. Water Resour Res 31 (4):969-973

Andreas EL (1991) Using scintillation at two wavelengths to measure path-averaged heat fluxes in free convection. Boundary-Layer Meteorology 54 (1):167-182

Aristotle (1952) Meteorologica / by Aristotle. With an English translation by H.D.P.Lee. Loeb classical library ; no. 397, vol Accessed from http://nla.gov.au/nla.cat-vn294469. Heinemann, Lond.

Asanuma J, Brutsaert W (1999) Turbulence variance characteristics of temperature and humidity in the unstable atmospheric surface layer above a variable pine forest. Water Resour Res 35 (2):515-521

Asanuma J, Tamagawa I, Ishikawa H, Ma Y, Hayashi T, Qi Y, Wang J (2007) Spectral similarity between scalars at very low frequencies in the unstable atmospheric surface layer over the Tibetan plateau. Boundary-Layer Meteorology 122 (1):85-103

Assouline S, Tyler SW, Tanny J, Cohen S, Bou-Zeid E, Parlange MB, Katul GG (2008) Evaporation from three water bodies of different sizes and climates: Measurements and scaling analysis. Advances in Water Resources 31 (1):160-172

Avissar R, Pielke RA (1989) A Parameterization of Heterogeneous Land Surfaces for Atmospheric Numerical-Models and Its Impact on Regional Meteorology. Monthly Weather Review 117 (10):2113-2136

Baldocchi DD, Rao KS (1995) Intra-field variability of scalar flux densities across a transition between a desert and an irrigated potato field. Boundary-Layer Meteorology 76 (1-2):109-136

Bardina J, Ferziger JH, Reynolds WC (1980) Improved subgrid scale models for large eddy simulation. American Institute of Aeronautics and Astronautics:Pap. 80-1357

Barrenetxea G, Ingelrest F, Schaefer G, Vetterli M, Couach O, Parlange M (2008) SensorScope: Out-of the-box environmental monitoring. 2008 International Conference on Information Processing in Sensor Networks, Proceedings:332-343

Beniston M (1986) The influence of water-surface on mesoscale dynamics as a function of atmospheric stability. Boundary-Layer Meteorology 36 (1-2):19-37

Bink NJ (1996) The ratio of eddy diffusivities for heat and water vapour under conditions of local advection. Physics and Chemistry of The Earth 21 (3):119-122

Bjerknes V (1904) Das Problem der Wettervorhersage, betrachtet vom Standpunkte der Mechanik und der Physik. vol 21. Meteorol. Z. ,

Bou-Zeid E (2002) Climate change and water resources in Lebanon and the Middle East. Journal of Water Resources Planning and Management 128 (5):343-355

Bou-Zeid E, Meneveau C, Parlange MB (2004) Large-eddy simulation of neutral atmospheric boundary layer flow over heterogeneous surfaces: Blending height and effective surface roughness. Water Resour Res 40 (2):W02505. DOI: 10.1029/2003WR002475

Bou-Zeid E, Meneveau C, Parlange MB (2005) A scale-dependent Lagrangian dynamic model for large eddy simulation of complex turbulent flows. Physics of Fluids 17 (2):025105. DOI: 10.1063/1.1839152

Bou-Zeid E, Parlange MB, Meneveau C (2007) On the parameterization of surface roughness at regional scales. Journal of the Atmospheric Sciences 64 (1):216-227

Bou-Zeid E, Vercauteren N, Parlange MB, Meneveau C (2008) Scale dependence of subgrid-scale model coefficients: An a priori study. Physics of Fluids 20 (11):115106-115106

Bradbrook KF, Lane SN, Richards KS, Biron PM, Roy AG (2000) Large eddy simulation of periodic flow characteristics at river channel confluences. Journal of Hydraulic Research 38 (3):207-215

Brocchini M, Peregrine DH (2001a) The dynamics of strong turbulence at free surfaces. Part 1. Description. Journal of Fluid Mechanics 449:225-254

Brocchini M, Peregrine DH (2001b) The dynamics of strong turbulence at free surfaces. Part 2. Free-surface boundary conditions. Journal of Fluid Mechanics 449:255-290

Brown AR, Derbyshire SH, Mason PJ (1994) Large-eddy simulation of stable atmospheric boundary-layers with a revised stochastic subgrid model. Q J R Meteorol Soc 120 (520):1485-1512

Brutsaert W (1982) Evaporation into the atmosphere: theory, history, and applications. Environmental fluid mechanics. Reidel, Dordrecht, Holland

Brutsaert W (1992) Stability correction functions for the mean wind-speed and temperature in the unstable surface-layer. Geophys Res Lett 19 (5):469-472

Brutsaert W (1998) Land-surface water vapor and sensible heat flux: Spatial variability, homogeneity, and measurement scales. Water Resour Res 34 (10):2433-2442

Brutsaert W (2005) Hydrology: an introduction. Cambridge Univeristy Press, Cambridge ; New York

Brutsaert W, Parlange MB, Gash JHC (1989) Neutral Humidity Profiles in the Boundary-Layer and Regional Evaporation from Sparse Pine Forest. Annales Geophysicae-Atmospheres Hydrospheres and Space Sciences 7 (6):623-630

Brutsaert W, Yeh G-T (1969) Evaporation from an Extremely Narrow Wet Strip at Ground Level. J Geophys Res 74 (13):3431-3433. doi:10.1029/JC074i013p03431

Brutsaert W, Yeh G-T (1970) Implications of a Type of Empirical Evaporation Formula for Lakes and Pans. Water Resour Res 6 (4):1202-1208. doi:10.1029/WR006i004p01202

Budyko M (1974) Climate and life : International geophysics series.

Bugbee B, Droter M, Monje O, Tanner B (1999) Evaluation and modification of commercial infra-red transducers for leaf temperature measurement. Advances in Space Research 22 (10):1425-1434

Businger JA, Wyngaard JC, Izumi Y, Bradley EF (1971) Flux-profile relationships in atmospheric surface-layer. J Atmos Sci 28 (2):181-&

Cabot W, Moin P (2000) Approximate wall boundary conditions in the large-eddy simulation of high reynolds number flow. Flow Turbulence and Combustion 63 (1-4):269-291

Chamecki M, Meneveau C, Parlange MB (2007) The local structure of atmospheric turbulence and its effect on the Smagorinsky model for large eddy simulation. Journal of the Atmospheric Sciences 64 (6):1941-1958

Chen TH, HendersonSellers A, Milly PCD, Pitman AJ, Beljaars ACM, Polcher J, Abramopoulos F, Boone A, Chang S, Chen F, Dai Y, Desborough CE, Dickinson RE, Dumenil L, Ek M, Garratt JR, Gedney N, Gusev YM, Kim J, Koster R, Kowalczyk EA, Laval K, Lean J, Lettenmaier D, Liang X, Mahfouf JF, Mengelkamp HT, Mitchell K, Nasonova ON, Noilhan J, Robock A, Rosenzweig C, Schaake J, Schlosser CA, Schulz JP, Shao Y, Shmakin AB, Verseghy DL, Wetzel P, Wood EF, Xue Y, Yang ZL, Zeng Q (1997) Cabauw experimental results from the project for intercomparison of land-surface parameterization schemes. Journal of Climate 10 (6):1194-1215

Choi TJ, Hong JY, Kim J, Lee HC, Asanuma J, Ishikawa H, Tsukamoto O, Gao ZQ, Ma YM, Ueno K, Wang JM, Koike T, Yasunari T (2004) Turbulent exchange of heat, water vapor, and momentum over a Tibetan prairie by eddy covariance and flux variance measurements. Journal of Geophysical Research-Atmospheres 109 (D21)

Clark RA, Ferziger JH, Reynolds WC (1979) Evaluation of sub-grid-scale models using an accurately simulated turbulent-flow. Journal of Fluid Mechanics 91 (Mar):1-16

Crago R, Brutsaert W (1996) Daytime evaporation and the self-preservation of the evaporative fraction and the Bowen ratio. Journal of Hydrology 178 (1-4):241-255

Crosman E, Horel J (2010) Sea and Lake Breezes: A Review of Numerical Studies. Boundary-Layer Meteorology 137 (1):1-29. doi:10.1007/s10546-010-9517-9

Crutzen PJ, Ramanathan V (2000) The Ascent of Atmospheric Sciences. Science 290 (5490):299-304

De Bruin HAR, Kohsiek W, Hurk BJJM (1993) A verification of some methods to determine the fluxes of momentum, sensible heat, and water vapour using standard deviation and structure parameter of scalar meteorological quantities. Boundary-Layer Meteorology 63 (3):231-257

De Bruin HAR, Van Den Hurk B, Kroon LJM (1999) On the temperature-humidity correlation and similarity. Boundary-Layer Meteorology 93 (3):453-468

Deardorff JW (1974) Three-dimensional numerical study of turbulence in an entraining mixed layer. Boundary-Layer Meteorology (Historical Archive) 7 (2):199-226

DeCosmo J, Katsaros KB, Smith SD, Anderson RJ, Oost WA, Bumke K, Chadwick H (1996) Air-sea exchange of water vapor and sensible heat: The humidity exchange over the sea (HEXOS) results. Journal of Geophysical Research-Oceans 101 (C5):12001-12016

Donelan MA, Dobson FW, Smith SD, Anderson RJ (1993) On the dependence of sea-surface roughness on wave development. J Phys Oceanogr 23 (9):2143-2149

Edson J, Crawford T, Crescenti J, Farrar T, Frew N, Gerbi G, Helmis C, Hristov T, Khelif D, Jessup A, Jonsson H, Li M, Mahrt L, McGillis W, Plueddemann A, Shen L, Skyllingstad E, Stanton T, Sullivan P, Sun J, Trowbridge J, Vickers D, Wang S, Wang Q, Weller R, Wilkin J, Williams AJ, Yue DKP, Zappa C (2007) The coupled boundary layers and air-sea transfer experiment in low winds. Bulletin of the American Meteorological Society 88 (3):341-356

Eichinger WE, Parlange MB, Stricker H (1996) On the concept of equilibrium evaporation and the value of the Priestley-Taylor coefficient. Water Resour Res 32 (1):161-164

Eltahir EAB, Bras RL (1996) Precipitation recycling. Rev Geophys 34 (3):367-378

Esau IN, Lyons TJ (2002) Effect of sharp vegetation boundary on the convective atmospheric boundary layer. Agric For Meteorol 114 (1-2):3-13

Figuerola PI, Berliner PR (2005) Evapotranspiration under advective conditions. International Journal of Biometeorology 49 (6):403-416. doi:10.1007/s00484-004-0252-0

Frisinger HH (1977) The history of meteorology to 1800 / H. Howard Frisinger. Historical monograph series (New York), vol Accessed from http://nla.gov.au/nla.cat-vn1157286. Science History Publications, New York :

Froidevaux M (2010) Land-Atmosphere Interactions Measured with Scanning Raman Lidar., Thèse EPFL, no 4768, Lausanne

Froidevaux M, Serikov I, Burgos S, Ristori P, Simeonov V, Van den Bergh H, Parlange MB (2009) A new lidar for water vapor and temperature measurements in the Atmospheric Boundary Layer. AsiaFlux Newsletter (28):p. 13-17

Frost R (1946) Turbulence and Diffusion in the Lower Atmosphere. Proceedings of the Royal Society of London Series A, Mathematical and Physical Sciences 186 (1004):20-35

Gao YH, Chen F, Barlage M, Liu W, Cheng GD, Li X, Yu Y, Ran YH, Li HY, Peng HC, Ma MG (2008) Enhancement of land surface information and its impact on atmospheric modeling in the Heihe River Basin, northwest China. J Geophys Res-Atmos 113 (D20). doi:D20s90

Garratt JR (1990) The Internal Boundary-Layer - a Review. Boundary-Layer Meteorology 50 (1-4):171-203

Garratt JR (1992) The atmospheric boundary layer. Cambridge atmospheric and space science series. Cambridge University Press, Cambridge ; New York :

Garratt JR (1993) Sensitivity of Climate Simulations to Land-Surface and Atmospheric Boundary-Layer Treatments - a Review. Journal of Climate 6 (3):419-449

Gash JHC (1986) A note on estimating the effect of a limited fetch on micrometeorological evaporation measurements. Boundary-Layer Meteorology 35 (4):409-413. doi:10.1007/bf00118567

Germano M, Piomelli U, Moin P, Cabot WH (1991) A dynamic subgrid-scale eddy viscosity model. Physics of Fluids A 3 (7):1760-1765

Giorgi F, Avissar R (1997) Representation of heterogeneity effects in earth system modeling: Experience from land surface modeling. Reviews of Geophysics 35 (4):413-437

Gleick PH, Palaniappan M (2010) Peak water limits to freshwater withdrawal and use. Proc Natl Acad Sci U S A 107 (25):11155-11162. doi:10.1073/pnas.1004812107

Green AE, Green SR, Astill MS, Caspari HW (2000) Estimating latent heat flux from a vineyard using scintillometry. Terrestrial Atmospheric and Oceanic Sciences 11 (2):525-542

Halldin S, Gottschalk L, van de Griend AA, Gryning SE, Heikinheimo M, Hogstrom U, Jochum A, Lundin LC (1998) NOPEX - a northern hemisphere climate processes land surface experiment. Journal of Hydrology 213 (1-4):172-187

Hechtel LM, Moeng CH, Stull RB (1990) The Effects of Nonhomogeneous Surface Fluxes on the Convective Boundary-Layer - a Case-Study Using Large-Eddy Simulation. Journal of the Atmospheric Sciences 47 (14):1721-1741

Heikinheimo M, Kangas M, Tourula T, Venalainen A, Tattari S (1999) Momentum and heat fluxes over lakes Tamnaren and Raksjo determined by the bulk-aerodynamic and eddy-correlation methods. Agricultural and Forest Meteorology 98-9:521-534

Held IM, Soden BJ (2000) Water vapor feedback and global warming. Annual Review of Energy and the Environment 25:441-475

Henderson-Sellers A, Irannejad P, McGuffie K (2008) Future desertification and climate change: The need for land-surface system evaluation improvement. Global and Planetary Change 64 (3-4):129-138. doi:10.1016/j.gloplacha.2008.06.007

Henderson-Sellers A, McGuffie K, Pitman AJ (1996) The Project for Intercomparison of Land-surface Parametrization Schemes (PILPS): 1992 to 1995. Climate Dynamics 12 (12):849-859

Higgins CW, Meneveau C, Parlange MB (2007) The effect of filter dimension on the subgrid-scale stress, heat flux, and tensor alignments in the atmospheric surface layer. Journal of Atmospheric and Oceanic Technology 24 (3):360-375

Higgins CW, Parlange MB, Meneveau C (2003) Alignment trends of velocity gradients and subgrid-scale fluxes in the turbulent atmospheric boundary layer. Boundary-Layer Meteorology 109 (1):59-83

Higgins CW, Parlange MB, Meneveau C (2004) The heat flux and the temperature gradient in the lower atmosphere. Geophys Res Lett 31 (22)

Hill RJ (1989) Implications of Monin–Obukhov Similarity Theory for Scalar Quantities. J Atmos Sci 46 (14):2236-2244. doi:10.1175/1520-0469(1989)046<2236:IOMSTF>2.0.CO;2

Horst TW (1999) The footprint for estimation of atmosphere-surface exchange fluxes by profile techniques. Boundary-Layer Meteorology 90 (2):171-188

Horst TW, Kleissl J, Lenschow DH, Meneveau C, Moeng CH, Parlange MB, Sullivan PP, Weil JC (2004) HATS: Field observations to obtain spatially filtered turbulence fields from crosswind Arrays of sonic anemometers in the atmospheric surface layer. Journal of the Atmospheric Sciences 61 (13):1566-1581

Horst TW, Weil JC (1992) Footprint estimation for scalar flux measurements in the atmospheric surface layer. Boundary-Layer Meteorology 59 (3):279-296. doi:10.1007/bf00119817

Hsieh CI, Katul G (2009) The Lagrangian stochastic model for estimating footprint and water vapor fluxes over inhomogeneous surfaces. Int J Biometeorol 53 (1):87-100. doi:10.1007/s00484-008-0193-0

Hsieh CI, Katul G, Chi T (2000) An approximate analytical model for footprint estimation of scaler fluxes in thermally stratified atmospheric flows. Adv Water Resour 23 (7):765-772

Jozsa J, Milici B, Napoli E (2007) Numerical simulation of internal boundary-layer development and comparison with atmospheric data. Boundary-Layer Meteorology 123 (1):159-175. doi:10.1007/s10546-006-9134-9

Kader BA, Yaglom AM (1990) Mean Fields and Fluctuation Moments in Unstably Stratified Turbulent Boundary-Layers. Journal of Fluid Mechanics 212:637-662

Katul G, Albertson J, Chu CR, Parlange M, Stricker H, Tyler S (1994) Sensible and Latent-Heat Flux Predictions Using Conditional Sampling Methods. Water Resour Res 30 (11):3053-3059

Katul GG, Hsieh CI (1999) A note on the flux-variance similarity relationships for heat and water vapour in the unstable atmospheric surface layer. Boundary-Layer Meteorology 90 (2):327-338

Katul GG, Parlange MB (1992) A Penman-Brutsaert Model for Wet Surface Evaporation. Water Resour Res 28 (1):121-126

Katul GG, Parlange MB (1994) On the Active Role of Temperature in Surface-Layer Turbulence. J Atmos Sci 51 (15):2181-2195. doi:10.1175/1520-0469(1994)051<2181:OTAROT>2.0.CO;2

Katul GG, Parlange MB (1995) Analysis of land-surface heat fluxes using the orthonormal wavelet approach. Water Resour Res 31 (11):2743-2749

Kays WM (1994) Turbulent Prandtl number - Where are we? Journal of Heat Transfer 116 (2):284-295

Keylock CJ, Hardy RJ, Parsons DR, Ferguson RI, Lane SN, Richards KS (2005) The theoretical foundations and potential for large-eddy simulation (LES) in fluvial geomorphic and sedimentological research. Earth-Science Reviews 71 (3-4):271-304

Kiely G, Albertson JD, Parlange MB, Eichinger WE (1996) Convective scaling of the average dissipation rate of temperature variance in the atmospheric surface layer. Boundary-Layer Meteorology 77 (3-4):267-284

Kleissl J, Gomez J, Hong SH, Hendrickx JMH, Rahn T, Defoor WL (2008) Large aperture scintillometer intercomparison study. Boundary-Layer Meteorology 128 (1):133-150

Kleissl J, Meneveau C, Parlange MB (2003) On the magnitude and variability of subgrid-scale eddy-diffusion coefficients in the atmospheric surface layer. Journal of the Atmospheric Sciences 60 (19):2372-2388

Kleissl J, Parlange MB, Meneveau C (2004) Field experimental study of dynamic Smagorinsky models in the atmospheric surface layer. Journal of the Atmospheric Sciences 61 (18):2296-2307

Kolmogorov A (1941a) The local structure of turbulence in incompressible viscous fluid for very large Reynolds numbers. C R Acad Sci URSS 30:301-305

Kolmogorov AN (1941b) Dissipation of energy in the locally isotropic turbulence. C R Acad Sci URSS 32:16-18

Kolmogorov AN (1962) A refinement of previous hypotheses concerning the local structure of turbulence in a viscous incompressible fluid at high Reynolds number. J Fluid Mech 13 (1):82-85

Kumar V (2007) Investigating the diurnal and spatial variability of flows in the atmospheric boundary layer: a Large Eddy Simulation study. PhD thesis, Johns Hopkins University,

Kumar V, Kleissl J, Meneveau C, Parlange MB (2006) Large-eddy simulation of a diurnal cycle of the atmospheric boundary layer: Atmospheric stability and scaling issues. Water Resour Res 42 (6):W06D09. DOI: 10.1029/2005WR004651

Kumar V, Svensson G, Holtslag AAM, Meneveau C, Parlange MB (2010) Impact of Surface Flux Formulations and Geostrophic Forcing on Large-Eddy Simulations of Diurnal Atmospheric Boundary Layer Flow. Journal of Applied Meteorology and Climatology 49 (7):1496-1516. doi:doi:10.1175/2010JAMC2145.1

Kustas WP (1990) Estimates of Evapotranspiration with a One-Layer and 2-Layer Model of Heat-Transfer over Partial Canopy Cover. Journal of Applied Meteorology 29 (8):704-715

Kustas WP, Albertson JD (2003) Effects of surface temperature contrast on land-atmosphere exchange: A case study from Monsoon 90. Water Resour Res 39 (6)

Kustas WP, Brutsaert W (1986) Wind-Profile Constants in a Neutral Atmospheric Boundary-Layer over Complex Terrain. Boundary-Layer Meteorology 34 (1-2):35-54

Lamaud E, Irvine M (2006) Temperature-humidity dissimilarity and heat-to-water-vapour transport efficiency above and within a pine forest canopy: The role of the Bowen ratio. Boundary-Layer Meteorology 120 (1):87-109. doi:10.1007/s10546-005-9032-6

Leclerc MY, Shen SH, Lamb B (1997) Observations and large-eddy simulation modeling of footprints in the lower convective boundary layer. Journal of Geophysical Research-Atmospheres 102 (D8):9323-9334

Leclerc MY, Thurtell GW (1990) Footprint prediction of scalar fluxes using a markovian analysis. Boundary-Layer Meteorology 52 (3):247-258

Leon LF, Lam DCL, Schertzer WM, Swayne DA, Imberger J (2007) Towards coupling a 3D hydrodynamic lake model with the Canadian Regional Climate Model: Simulation on Great Slave Lake. Environ Modell Softw 22 (6):787-796. doi:10.1016/j.envsoft.2006.03.005

Lilly DK The representation of small scale turbulence in numerical simulation experiments. In: IBM Scientific Computing Symposium on Environmental Sciences, White Plains, New York, 1967. pp 195-209

Liu SW, Meneveau C, Katz J (1994) On the properties of similarity subgrid-scale models as deduced from measurements in a turbulent jet. Journal of Fluid Mechanics 275:83-119

Lorenz EN (1983) A history of prevailing ideas about the general-circulation of the atmosphere. Bull Amer Meteorol Soc 64 (7):730-734

Lowe LD, Webb JA, Nathan RJ, Etchells T, Malano HM (2009) Evaporation from water supply reservoirs: An assessment of uncertainty. Journal of Hydrology 376 (1-2):261-274. doi:10.1016/j.jhydrol.2009.07.037

Lowe PR (1977) Approximating Polynomial for Computation of Saturation Vapor-Pressure. Journal of Applied Meteorology 16 (1):100-103

Lyons TJ, Halldin S (2004) Surface heterogeneity and the spatial variation of fluxes. Agricultural and Forest Meteorology 121 (3-4):153-165

Mahrt L, Sun JL, Vickers D, Macpherson JI, Pederson JR, Desjardins RL (1994) Observations of Fluxes and Inland Breezes over a Heterogeneous Surface. Journal of the Atmospheric Sciences 51 (17):2484-2499

Mason PJ (1989) Large-eddy simulation of the convective atmospheric boundary-layer. Journal of the Atmospheric Sciences 46 (11):1492-1516

Mason PJ (1994) Large-eddy simulation - a critical-review of the technique. Q J R Meteorol Soc 120 (515):1-26

Mason PJ, Brown AR (1999) On subgrid models and filter operations in large eddy simulations. Journal of the Atmospheric Sciences 56 (13):2101-2114

Mason PJ, Thomson DJ (1992) Stochastic backscatter in large-eddy simulations of boundary-layers. Journal of Fluid Mechanics 242:51-78

McJannet DL, Cook FJ, McGloin RP, McGowan HA, Burn S (2010) Estimation of evaporation and sensible heat flux from open water using a large aperture scintillometer. In review in Water Resources Research

McNaughton KG (1981) Net interception losses during sprinkler irrigation. Agricultural Meteorology 24:11-27

McNaughton KG, Laubach J (1998) Unsteadiness as a cause of non-equality of eddy diffusivities for heat and vapour at the base of an advective inversion. Boundary-Layer Meteorology 88 (3):479-504

Meijninger W, Beyrich F, Lüdi A, Kohsiek W, Bruin H (2006) Scintillometer-Based Turbulent Fluxes of Sensible and Latent Heat Over a Heterogeneous Land Surface – A Contribution to Litfass-2003. Boundary-Layer Meteorology 121 (1):89-110

Meneveau C (1994) Statistics of turbulence subgrid-scale stresses - necessary conditions and experimental tests. Physics of Fluids 6 (2):815-833

Meneveau C, Katz J (2000) Scale-invariance and turbulence models for large-eddy simulation. Annual Review of Fluid Mechanics 32:1-32

Mironov D, Heise E, Kourzeneva E, Ritter B, Schneider N, Terzhevik A (2010) Implementation of the lake parameterisation scheme FLake into the numerical weather prediction model COSMO. Boreal Environment Research 15 (2):218-230

Mitsuishi A, Hasegawa Y, Kasagi N Large eddy simulation of mass transfer across an air-water interface at high schmidt numbers. In: The 6th ASME-JSME Thermal Engineering Joint Conference, Hawai, USA, 2003. pp paper number TED-AJ03-231

Moeng CH (1984) A large-eddy-simulation model for the study of planetary boundary-layer turbulence. Journal of the Atmospheric Sciences 41 (13):2052-2062

Moeng CH, Sullivan PP, Stevens B (1999) Including radiative effects in an entrainment rate formula for buoyancy-driven PBLs. Journal of the Atmospheric Sciences 56 (8):1031-1049

Monin AS, Obukhov AM (1954) Basic laws of turbulent mixing in the ground layer of the atmosphere (in Russian). Trudy Geofizicheskogo Instituta, Akademiya Nauk SSSR 151:163-187

Nieuwstadt FTM (1984) Some aspects of the turbulent stable boundary-layer. Boundary-Layer Meteorology 30 (1-4):31-55

O'Sullivan PL, Biringen S, Huser A (2001) A priori evaluation of dynamic subgrid models of turbulence in square duct flow. Journal of Engineering Mathematics 40 (1):91-108

Ortega-Farias SO, Cuenca RH, English M (1995) Hourly Grass Evapotranspiration in Modified Maritime Environment. Journal of Irrigation and Drainage Engineering 121 (6):369-373

Palmer RN, Characklis GW (2009) Reducing the costs of meeting regional water demand through risk-based transfer agreements. J Environ Manage 90 (5):1703-1714. doi:10.1016/j.jenvman.2008.11.003

Pan HL, Mahrt L (1987) Interaction between soil hydrology and boundary-layer development. Boundary-Layer Meteorology 38 (1-2):185-202

Parlange MB, Brutsaert W (1989) Regional roughness of the Landes forest and surface shear-stress under neutral conditions. Boundary-Layer Meteorology 48 (1-2):69-81

Parlange MB, Eichinger WE, Albertson JD (1995) Regional-scale evaporation and the atmospheric boundary-layer. Reviews of Geophysics 33 (1):99-124

Parlange MB, Katul GG (1992) Estimation of the Diurnal-Variation of Potential Evaporation from a Wet Bare Soil Surface. Journal of Hydrology 132 (1-4):71-89

Parlange MB, Katul GG (1995) Watershed Scale Shear-Stress from Tethersonde Wind-Profile Measurements under near Neutral and Unstable Atmospheric Stability. Water Resour Res 31 (4):961-968

Pasquill F (1972) Some aspects of boundary-layer description. Q J R Meteorol Soc 98 (417):469-&

Patton EG, Sullivan PP, Moeng CH (2005) The influence of idealized heterogeneity on wet and dry planetary boundary layers coupled to the land surface. Journal of the Atmospheric Sciences 62 (7):2078-2097

Penman HL (1948) Natural Evaporation from Open Water, Bare Soil and Grass. Proceedings of the Royal Society of London Series A, Mathematical and Physical Sciences 193 (1032):120-145

Philip JR (1959) The theory of local advection .1. Journal of Meteorology 16 (5):535-547

Pielke RA, Uliasz M (1998) Use of meteorological models as input to regional and mesoscale air quality models - Limitations and strengths. Atmos Environ 32 (8):1455-1466

Piomelli U (1999) Large-eddy simulation: achievements and challenges. Progress in Aerospace Sciences 35 (4):335-362

Piomelli U, Balaras E (2002) Wall-layer models for large-eddy simulations. Annual Review of Fluid Mechanics 34:349-374

Pitsch H, Steiner H (2000) Large-eddy simulation of a turbulent piloted methane/air diffusion flame (Sandia flame D). Physics of Fluids 12 (10):2541-2554

Pope SB (2000) Turbulent flows. Cambridge University Press, Cambridge

Pope SB (2004) Ten questions concerning the large-eddy simulation of turbulent flows. New Journal of Physics 6:771

Porte-Agel F (2004) A scale-dependent dynamic model for scalar transport in large-eddy simulations of the atmospheric boundary layer. Boundary-Layer Meteorology 112 (1):81-105

Porte-Agel F, Meneveau C, Parlange MB (1998) Some basic properties of the surrogate subgrid-scale heat flux in the atmospheric boundary layer. Boundary-Layer Meteorology 88 (3):425-444

Porte-Agel F, Meneveau C, Parlange MB (2000a) A scale-dependent dynamic model for large-eddy simulation: application to a neutral atmospheric boundary layer. Journal of Fluid Mechanics 415:261-284

Porte-Agel F, Pahlow M, Meneveau C, Parlange MB (2001a) Atmospheric stability effect on subgrid-scale physics for large-eddy simulation. Advances in Water Resources 24 (9-10):1085-1102

Porte-Agel F, Parlange MB, Meneveau C, Eichinger WE (2001b) A priori field study of the subgrid-scale heat fluxes and dissipation in the atmospheric surface layer. Journal of the Atmospheric Sciences 58 (18):2673-2698

Porte-Agel F, Parlange MB, Meneveau C, Eichinger WE, Pahlow M (2000b) Subgrid-scale dissipation in the atmospheric surface layer: Effects of stability and filter dimension. Journal of Hydrometeorology 1 (1):75-87

Priestley CHB, Taylor RJ (1972) On the Assessment of Surface Heat Flux and Evaporation Using Large-Scale Parameters. Monthly Weather Review 100 (2):81-92

Rao KS, Wyngaard JC, Coté OR (1974) Local advection of momentum, heat, and moisture in micrometeorology. Boundary-Layer Meteorology 7 (3):331-348. doi:10.1007/bf00240836

Rider NE, Philip JR, Bradley EF (1963) The horizontal transport of heat and moisture - a micrometeorological study. Q J R Meteorol Soc 89 (382):507-531. doi:10.1002/qj.49708938207

Rind D, Rosenzweig C, Stieglitz M (1997) The role of moisture transport between ground and atmosphere in global change. Annual Review of Energy and the Environment 22:47-74

Rosenberry DO, Winter TC, Buso DC, Likens GE (2007) Comparison of 15 evaporation methods applied to a small mountain lake in the northeastern USA. Journal of Hydrology 340 (3-4):149-166

Rouse WR, Blyth EM, Crawford RW, Gyakum JR, Janowicz JR, Kochtubajda B, Leighton HG, Marsh P, Martz L, Pietroniro A, Ritchie H, Schertzer WM, Soulis ED, Stewart RE, Strong GS, Woo MK (2003) Energy and water cycles in a high-latitude, north-flowing river system - Summary of results from the Mackenzie GEWEX Study - Phase I. Bull Amer Meteorol Soc 84 (1):73-87. doi:10.1175/bams-84-1-73

Rouse WR, Oswald CJ, Binyamin J, Spence CR, Schertzer WM, Blanken PD, Bussieres N, Duguay CR (2005) The role of northern lakes in a regional energy balance. J Hydrometeorol 6 (3):291-305

Sagaut P (2003) Large eddy simulation for incompressible flows. 2nd edn. Springer-Verlag, Berlin

Schmid HP (2002) Footprint modeling for vegetation atmosphere exchange studies: a review and perspective. Agricultural and Forest Meteorology 113 (1-4):159-183

Schuepp PH, Leclerc MY, MacPherson JI, Desjardins RL (1990) Footprint prediction of scalar fluxes from analytical solutions of the diffusion equation. Boundary-Layer Meteorology 50 (1):355-373. doi:10.1007/bf00120530

Scotti A, Meneveau C, Lilly DK (1993) Generalized Smagorinsky model for anisotropic grids. Physics of Fluids A 5 (9):2306-2308

Sempreviva AM, Gryning SE (2000) Mixing height over water and its role on the correlation between temperature and humidity fluctuations in the unstable surface layer. Boundary-Layer Meteorology 97 (2):273-291

Shen L, Yue DKP (2001) Large-eddy simulation of free-surface turbulence. Journal of Fluid Mechanics 440:75-116

Shuttleworth WJ (2007) Putting the 'vap' into evaporation. Hydrology and Earth System Sciences 11 (1):210-244

Smagorinsky J (1963) General circulation experiments with the primitive equations: I. the basic experiment. Monthly Weather Review 91:99-164

Sodemann H, Wernli H, Schwierz C (2009) Sources of water vapour contributing to the Elbe flood in August 2002-A tagging study in a mesoscale model. Quarterly journal of the Royal Meteorological Society 135 (638):205-223

Stagnitti F, Parlange JY, Rose CW (1989) Hydrology of a Small Wet Catchment. Hydrological Processes 3 (2):137-150

Stannard DI, Rosenberry DO (1991) A comparison of short-term measurements of lake evaporation using eddy correlation and energy budget methods. Journal of Hydrology 122 (1-4):15-22

Stohl A, Forster C, Sodemann H (2008) Remote sources of water vapor forming precipitation on the Norwegian west coast at 60 degrees N - a tale of hurricanes and an atmospheric river. J Geophys Res-Atmos 113 (D5). doi:D05102

Stoll R, Porte-Agel F (2006) Dynamic subgrid-scale models for momentum and scalar fluxes in large-eddy simulations of neutrally stratified atmospheric boundary layers over heterogeneous terrain. Water Resour Res 42 (1)

Stull RB (1988) An introduction to boundary layer meteorology. Kluwer Academic Publishers, Dordrecht, the Netherlands

Sugita M, Brutsaert W (1992) Landsat Surface Temperatures and Radio Soundings to Obtain Regional Surface Fluxes. Water Resour Res 28 (6):1675-1679

Sullivan PP, Edson JB, Horst TW, Wyngaard JC, Kelly M Subfilter scale fluxes in the marine surface layer: Results from the Ocean Horizontal Array Turbulence Study (OHATS). In: 17th Symposium on Boundary Layers and Turbulence, San Diego, CA, 2006. doi:http://ams.confex.com/ams/pdfpapers/110884.pdf

Sullivan PP, Horst TW, Lenschow DH, Moeng CH, Weil JC (2003) Structure of subfilter-scale fluxes in the atmospheric surface layer with application to large-eddy simulation modelling. Journal of Fluid Mechanics 482:101-139

Sullivan PP, Mcwilliams JC, Melville WK (2007) Surface gravity wave effects in the oceanic boundary layer: large-eddy simulation with vortex force and stochastic breakers. Journal of Fluid Mechanics 593:405-452

Sullivan PP, McWilliams JC, Moeng CH (2000) Simulation of turbulent flow over idealized water waves. Journal of Fluid Mechanics 404:47-85

Sun JL, Vandemark D, Mahrt L, Vickers D, Crawford T, Vogel C (2001) Momentum transfer over the coastal zone. J Geophys Res-Atmos 106 (D12):12437-12448

Sutton GC (1934) Wind structure and evaporation in a turbulent atmosphere. Proceedings of the Royal Society of London Series a-Mathematical and Physical Sciences 146 (A858):0701-0722

Swayne D, Lam D, MacKay M, Rouse W, Schertzer W (2005) Assessment of the interaction between the Canadian Regional Climate Model and lake thermal-hydrodynamic models. Environmental Modelling & Software 20 (12):1505-1513

Szilagyi J, Katul GG, Parlange MB (2001) Evapotranspiration intensifies over the conterminous United States. Journal of Water Resources Planning and Management-Asce 127 (6):354-362

Tanner CB, Pelton WL (1960) Potential Evapotranspiration Estimates by the Approximate Energy Balance Method of Penman. Journal of Geophysical Research 65 (10):3391-3413

Tanny J, Cohen S, Assouline S, Lange F, Grava A, Berger D, Teltch B, Parlange MB (2008) Evaporation from a small water reservoir: Direct measurements and estimates. Journal of Hydrology 351 (1-2):218-229

Tao B, Katz J, Meneveau C (2002) Statistical geometry of subgrid-scale stresses determined from holographic particle image velocimetry measurements. Journal of Fluid Mechanics 457:35-78

Taylor PA (1970) A model of airflow above changes in surface heat flux, temperature and roughness for neutral and unstable conditions. Boundary-Layer Meteorology 1 (1):18-39. doi:10.1007/bf00193902

Tennekes H, Lumley JL (1972) A first course in turbulence. Cambridge: The MIT Press,

ter Heerdt G (2007) Climate change and the EU Water Framework Directive: how to deal with indirect effects of changes in hydrology on water quality and ecology? Water science and technology 56 (4):19-26

Tillman JE (1972) The Indirect Determination of Stability, Heat and Momentum Fluxes in the Atmospheric Boundary Layer from Simple Scalar Variables During Dry Unstable Conditions. Journal of Applied Meteorology 11 (5):783-792

Tjernstrom M, Zagar M, Svensson G, Cassano JJ, Pfeifer S, Rinke A, Wyser K, Dethloff K, Jones C, Semmler T, Shaw M (2005) Modelling the arctic boundary layer: An evaluation of six arcmip regional-scale models using data from the Sheba project. Boundary-Layer Meteorology 117 (2):337-381. doi:10.1007/s10546-004-7954-z

Tong CN, Wyngaard JC, Brasseur JG (1999) Experimental study of the subgrid-scale stresses in the atmospheric surface layer. Journal of the Atmospheric Sciences 56 (14):2277-2292

Tong CN, Wyngaard JC, Khanna S, Brasseur JG (1998) Resolvable- and subgrid-scale measurement in the atmospheric surface layer: Technique and issues. Journal of the Atmospheric Sciences 55 (20):3114-3126

Vercauteren N, Bou-Zeid E, Parlange MB, Lemmin U, Huwald H, Selker JS, Meneveau C (2008) Subgrid-scale dynamics of water vapour, heat, and momentum over a lake. Boundary-Layer Meteorology 128 (2):205-228

Vercauteren N, Huwald H, Bou-Zeid E, Selker JS, Lemmin U, Parlange MB, Lunati I (2011) Evolution of Superficial Lake Water Temperature Profile Under Diurnal Radiative Forcing. Under review in Water Resources Research

Veron F, Melville WK, Lenain L (2008) Wave-coherent air-sea heat flux. Journal of Physical Oceanography 38 (4):788-802

Vickers D, Mahrt L (2010) Sea-surface roughness lengths in the midlatitude coastal zone. Quarterly journal of the Royal Meteorological Society 136 (649):1089-1093. doi:10.1002/qj.617

Voller VR, Porte-Agel F (2002) Moore's law and numerical modeling. J Comput Phys 179 (2):698-703. doi:10.1006/jcph.2002.7083

Weaver HL (1990) Temperature and Humidity Flux-Variance Relations Determined by One-Dimensional Eddy-Correlation. Boundary-Layer Meteorology 53 (1-2):77-91

Webb EK, Pearman GI, Leuning R (1980) Correction of flux measurements for density effects due to heat and water-vapor transfer. Q J R Meteorol Soc 106 (447):85-100

Webster IT, Sherman BS (1995) Evaporation from fetch-limited water bodies. Irrig Sci 16 (2):53-64

Weisman RN, Brutsaert.W (1973) Evaporation and cooling of a lake under unstable atmospheric conditions. Water resources research 9 (5):1242-1257

Wesely ML (1988) Use of Variance Techniques to Measure Dry Air-Surface Exchange-Rates. Boundary-Layer Meteorology 44 (1-2):13-31

Wood N (2000) Wind flow over complex terrain: A historical perspective and the prospect for large-eddy modelling. Boundary-Layer Meteorology 96 (1-2):11-32

Wu YL, Nair US, Pielke RA, McNider RT, Christopher SA, Anantharaj VG (2009) Impact of Land Surface Heterogeneity on Mesoscale Atmospheric Dispersion. Boundary-Layer Meteorology 133 (3):367-389. doi:10.1007/s10546-009-9415-1

Yimer I, Campbell I, Jiang LY (2002) Estimation of the turbulent Schmidt number from experimental profiles of axial velocity and concentration for high-Reynolds-number jet flows. Canadian Aeronautics and Space Journal 48 (3):195-200

Yuge K, Haraguchi T, Nakano Y, Kuroda M, Anan M (2005) Quantification of soil surface evaporation under micro-scale advection in drip-irrigated fields. Paddy and Water Environment 3 (1):5-12. doi:10.1007/s10333-004-0058-z

Appendix A: An interesting moisture transport phenomenon

A.1 Motivation

In August 2008, the EPFL water vapor and temperature solar blind Raman Lidar (Froidevaux et al. 2009) was deployed on a field site in Seedorf, Switzerland for the TABLE-08 (Turbulent Boundary Layer Experiment) field campaign. The site is located on an old peat bog, converted into productive agricultural field. The lake is located between the agricultural land and is about 400 m wide. All the details about the field campaign can be found in (Froidevaux 2010). The deployment was designed to investigate several questions about turbulent fluxes, including the observation of a transition of surface conditions, with the agricultural field surrounding the lake (Fig. 49). The dataset also allowed for a study of stable boundary layers, having a site that often encountered stable conditions at nighttime. The EPFL Lidar is one of the first instruments capable of providing high-resolution spatial (1.25 m) and temporal (1 s) information on the water vapor concentration in the ABL. A laser beam is sent from the instrument, and the portion of the signal that travels back to the instrument is analyzed in order to get the water vapor mixing ratio and the temperature along the path of the beam. Interesting results from this field campaign cover the observation of coherent structures in the ABL, the formation of an internal boundary layer above the lake or an example of a layered stable atmosphere and can be found in (Froidevaux 2010).

Another goal of this field campaign was to gather a good dataset for the testing of Large Eddy simulations of the ABL. For this and other purposes, different types of instruments were installed along the path of the Lidar measurements. Among those, a Sodar/RASS system provided vertical profiles of horizontal and vertical wind speed, wind direction and potential temperature and was installed at one edge of the lake.

Fig. 49 Aerial view of the Seedorf field site.

We now focus on the night of August 29th, 2008. Clear sky and stable atmosphere were recorded this night and strong humidity stratification was observed. Lidar scans above the lake are shown in Fig. 50. In those measurements, the beam is rotated between the horizontal axis above the lake and the vertical axis. The rotation is done in 20-minute periods. The first scan in Fig. 50 is acquired between 22:12 and 22:33 on August 29th 2008 with a rotating movement from the horizontal axis to the vertical axis (upward motion), and the following are alternating upward and downward vertical scans. These vertical slices show an interesting phenomenon, which is the onset of humidity stratification. Around 22:30, a wet layer seems to get detached from the moist layer at the surface and brought upward to form a new wet layer. The following question naturally arises: what are the possible causes that lead to the stratification?

To assess this question, the temperature stratification of the atmosphere is observed (Fig. 51). The potential temperature vertical profile recorded at the beginning of the stratification event (22:45) shows a stable layer in the first 150 m above the ground, but an unstable layer remains in the layer above, between 150 m and 350 m approximately. At 350 m, an inversion is present and above this height is probably a free atmosphere. To confirm that, data from the Meteo Suisse radiosoundings taken in Payerne that day at 14:00, at a distance of about 10 km

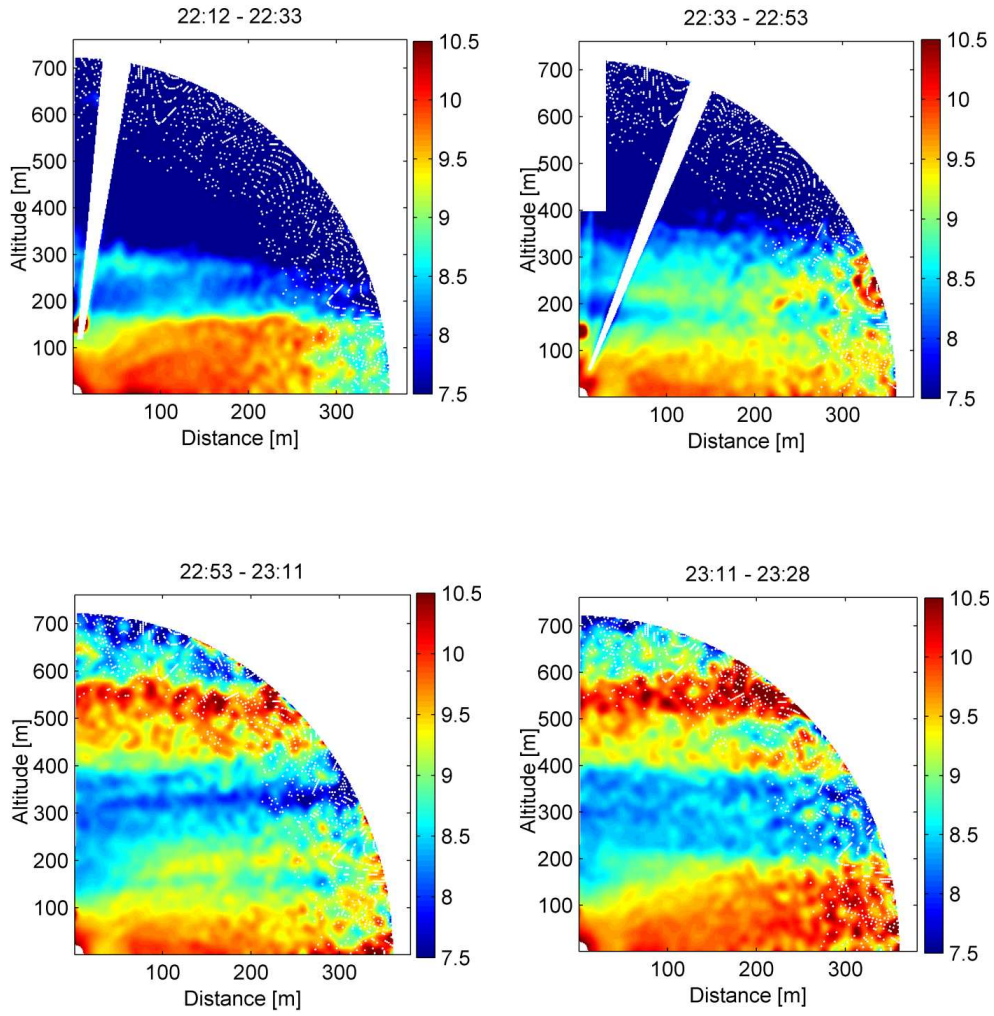

Fig. 50 Lidar scans of specific humidity (g.kg^{-1}) acquired with an angular scan. The time of scan is shown in each figure. The time evolution shows the onset of humidity stratification.

from the field site, are observed (Fig. 52). A convective boundary layer of a depth of approximately 500 m is deducted from the temperature profile. This depth is perfectly susceptible to have decreased in the late afternoon to reach the depth of 350 m shown in Fig. 51. If one looks at the specific humidity vertical distribution in Fig. 50 during the period between 22:12 and 22:33, a layer of higher concentration can be seen in the first 150 m above the ground. This height corresponds to the stable portion of the potential temperature profile. However, the unstable portion of the potential temperature aloft will tend to get reorganized. The subsequent question is: can stratification of humidity be formed by density

reorganization, forming a middle wet layer in altitude? This question will be assessed by use of the Large Eddy Simulation code presented in section 1.4.

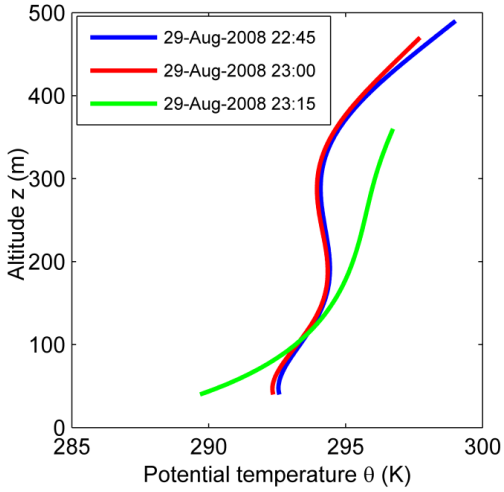

Fig. 51 Potential temperature profiles given by the Sodar/RASS system during the beginning of the layering event.

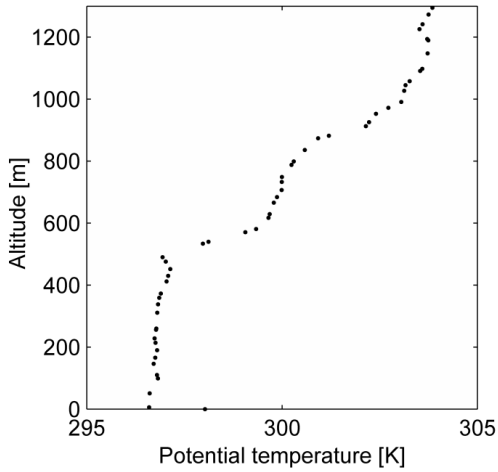

Fig. 52 Potential temperature profile obtained from a radiosounding in Payerne on August 29 at 14:00.

A.2 LES reproducing the initial conditions

Large Eddy Simulations are used to investigate the layering of humidity happening on the night of August 29. For this, the code uses an approximation of the measured temperature and specific humidity shown in Fig. 50 and Fig. 51 as initial condition. The subsequent modifications of humidity profiles are then recorded every minute. The simulated domain is 2100 m^2 in the horizontal directions and 600 m in the vertical. The numerical resolution used is 128^3, leading to a spatial resolution of approximately 16 m in the horizontal and 4.7 m in the vertical direction, with the first vertical node at 2.3 m. The bottom boundary is fixed at a constant temperature (293 K) and a constant specific humidity (12 g kg^{-1}), and a roughness height of 1 cm is defined. Monin-Obukhov similarity theory is then used to compute the gradients and stress at the first vertical level. A rate of entrainment is imposed for temperature and humidity at the top boundary.

The initial temperature profile shows an unstable layer between 150 m and 300 m (Fig. 51). This instability leads to unstable density stratification, and thus the initial profile is rearranged with time into a stable temperature profile, as shown in Fig. 51 for the measurements and Fig. 53 for the simulation. Because of the importance of humidity in the present study, the virtual potential temperature is shown for the simulation. Potential temperature and specific humidity are computed from the LES, and the virtual potential temperature is computed as $\theta_v = \theta(1+0.61q)$ where θ is the potential temperature and q is the specific humidity in kg.kg^{-1}.

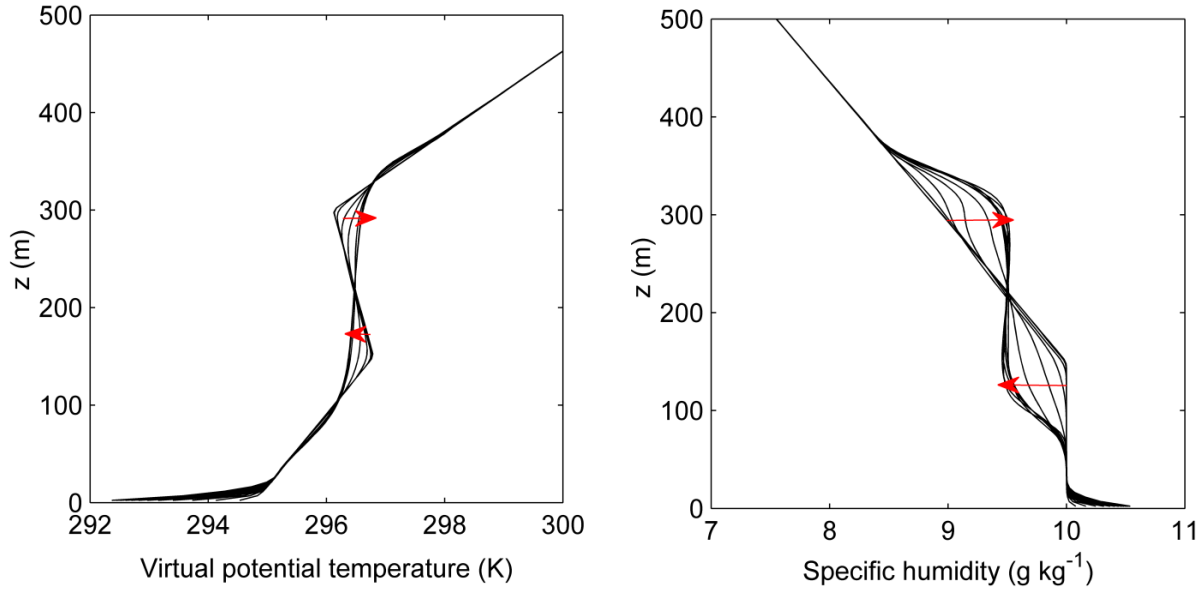

Fig. 53 Evolution of the virtual potential temperature and specific humidity profiles averaged over the horizontal domain. The total time is 30 minutes and a profile is shown every 5 minutes. The arrows show the direction of the time evolution of the profiles.

The initial specific humidity profile presents a mixed layer that reaches 150 m (Fig. 50). As can be seen in Fig. 53, while the temperature parcels get reordered to form a stable profile, air charged with humidity is transported upward. The effect is an entrainment of humid air that is then replaced by dryer air coming from above. The replacement of moist air by dryer air can be observed in more details in Fig. 54: the initial layering of humidity is homogeneous in the horizontal direction, but after 13 minutes one can observe the initiation of a Rayleigh-Bénard type of instability. Fingers of denser air penetrate into the homogeneous layer while fingers of

wet air are moving upwards. Finally after 23 minutes, the wet air that was carried upwards is trapped under the strong temperature inversion and two detached wet layers can be observed. During the detachment process, strong vertical velocities are observed (Fig. 55), showing the vortices present in the flow.

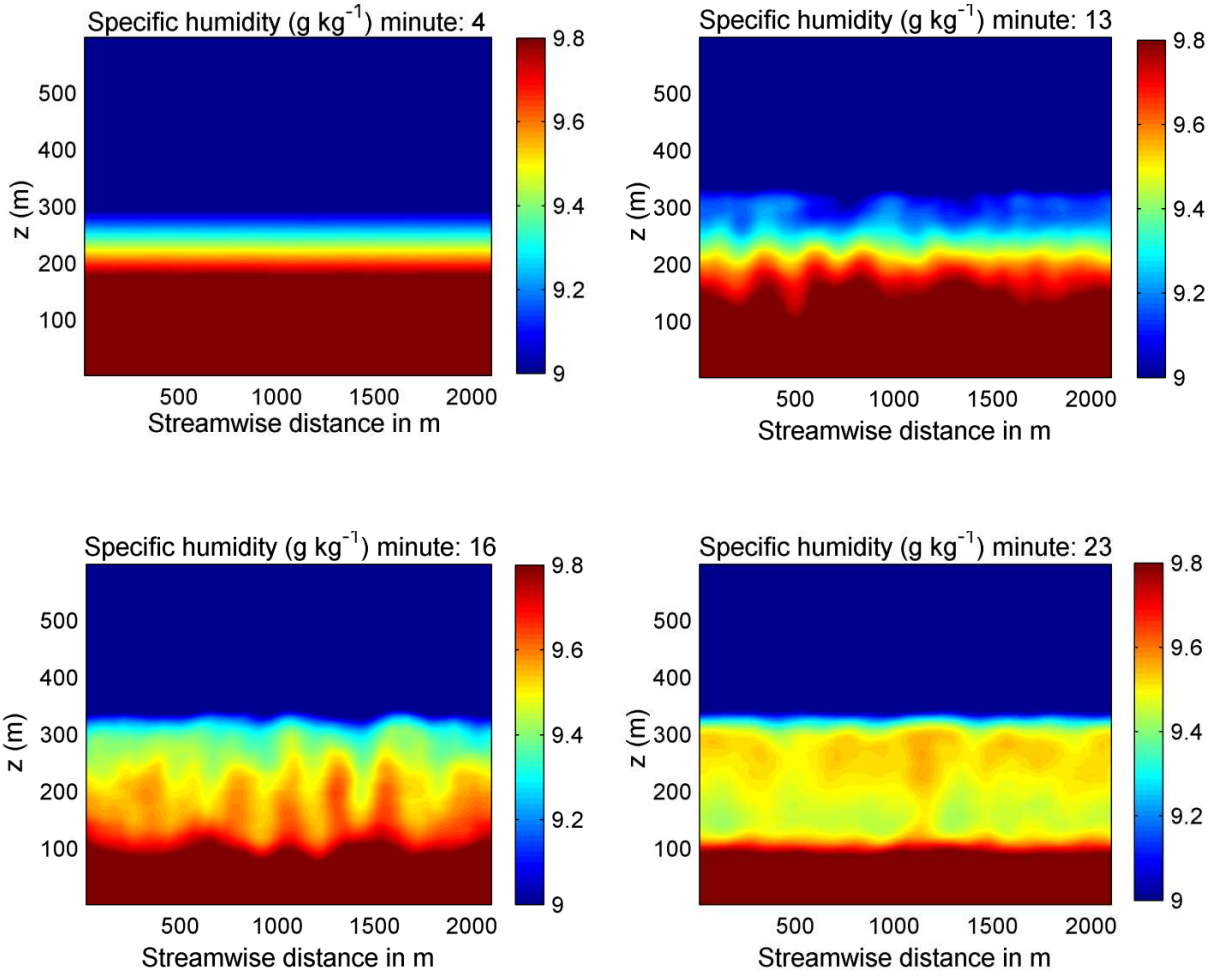

Fig. 54 Evolution of vertical slices of specific humidity averaged over the horizontal domain and over one minute. The time is given in minute after the beginning of the simulation.

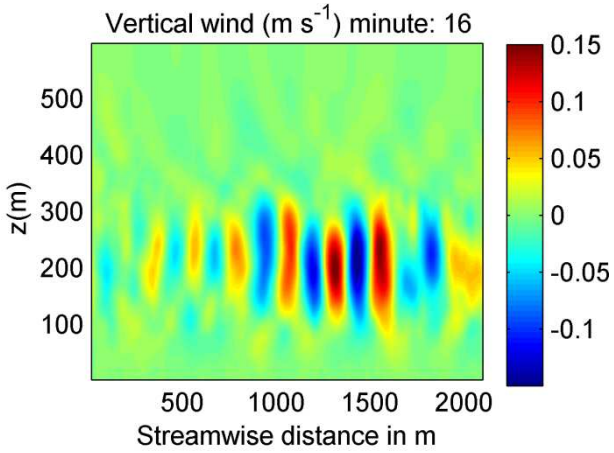

Fig. 55 Vertical wind component averaged over 1 minute, 16 minutes after the initial situation in the simulation.

A.3 Conclusion

These results suggest that density reordering due to an instability in the potential temperature profile is a possible cause for the lifting of humidity. Even though the initial situation for the specific humidity was a situation presenting equilibrium, the reorganization of the air particles due to the initial temperature profile leads to a counterintuitive positioning of the water vapor. The final situation with two detached layer that are more humid than the rest of the atmosphere remains stable for some time, both in the observations and in the simulation. Many other possible causes exits, such as advection of a wet layer from surrounding atmosphere for example, and are not investigated here.

Nikki Vercauteren

nikki.vercauteren@a3.epfl.ch
French and Belgian. 28 years old

Education

2007-2010 :	***PhD in environmental engineering***, EPFL Heat and water vapor exchange over lakes. Advisor: M. B. Parlange	**Lausanne**
2005-2006 :	***Master's In applied Mathematics,*** **EPFL** Thesis supervised by J.H. Maddocks and C.Schütte, Freie Universitet	**Berlin**
2004-2005 :	First year of *Master's in applied mathematics,* EPFL	**Lausanne**
2003-2004 :	ERASMUS exchange programm, KTH, Sweden. Bachelor.	**Stockholm**
2001-2003 :	First two years of applied Mathematics, Ecole Polytechnique Fédérale de Lausanne (EPFL).	**Lausanne**

Professional summary

2011-present	**Post doctoral research fellow, Stockholm university**: ecohydrology research
2003-2010	**Teaching assistant at EPFL**: several courses, master projects supervision including snow transport modelling, ecohydrological studies in Burkina Faso.
2006:	**Research engineer, CEREA, Ecole Nationale des Ponts et Chaussées, France.** Network design for the monitoring of accidental radionuclide dispersion for the French radioprotection and nuclear safety institute (**IRSN**).

Publications

- Vercauteren N., Bou-Zeid E, Parlange M.B., and Brutsaert W. (2009).
  Estimation of wet-surface evaporation from sensible heat flux measurements.
  Water Resources Research, 45, W06424, doi:10.1029/2008WR007544.
- Bou-Zeid E, Vercauteren N., Parlange M.B., and Meneveau C. (2008).
  Scale dependence of subgrid-scale model coefficients: an a-priori study.
  Physics of Fluids, 20(11), 115106.
- Rachid Abida, Marc Bocquet, Nikki Vercauteren, Olivier Isnard (2008).
  Design of a monitoring network over France in case of a radiological accidental release.
  Atmospheric Environment, 42: 5205-5219.
- Vercauteren N., E. Bou-Zeid, M.B. Parlange, U. Lemmin, H. Huwald, J. Selker, C. Meneveau (2008).
  Subgrid-Scale Dynamics of Water Vapour, Heat and Momentum over a Lake.
  Boundary-Layer Meteorology, 128: 205-228.
- M. Sc Thesis: ***Numerical investigation of solutions of Langevin equations.*** (2006)

Computer skills

MATLAB, Fortran, C++, MPI, Python programming. Statistical programming tool R.

Summer Schools

- *Inverse problem theory and model parameter estimation* (Swiss doctoral program, 1 week)
- *Atmospheric Boundary Layer: Concepts, Observations and Numerical Simulations* (organized by Utrecht and Wageningen universities, 2 weeks)
- *Pathways to environmental sustainability* (Istituto Veneto di Scienze, Lettere ed Arti, 1 week)

Reviewer

Water Resources Research, Advances in Water Resources, Swiss National Science Foundation

Languages

French, English, German, Dutch, Swedish

Interests

Rowing (competition and teaching). Reading, travelling, art.